**Der Autor**

Adrian Heger, geboren 1991 in Hamburg, studierte Geowissenschaften mit Vertiefungsrichtung Bodenkunde an der Universität Hamburg. Schwerpunkte seiner Abschlussarbeiten waren der Kohlenstoff- und Wasserhaushalt von Hochmooren in Norddeutschland sowie die Energiebilanzen von Mooren auf Feuerland, Argentinien. Währenddessen war er als Tutor und als studentische Hilfskraft im Institut für Bodenkunde der Universität Hamburg tätig. In seiner Promotion untersuchte er den prozessbasierten Boden-Kohlenstoff-Haushalt von Hartholz-Auenwäldern der unteren Mittelelbe. Dabei fokussierte er auf den Einfluss von Auen-Hydrologie und -Vegetation auf die Kohlenstoff-Speicherung und -Freisetzung des Bodens.

Adrian Heger

Process-based characterization of the soil carbon balance in hardwood floodplain forests of the lower middle Elbe River

A. Heger
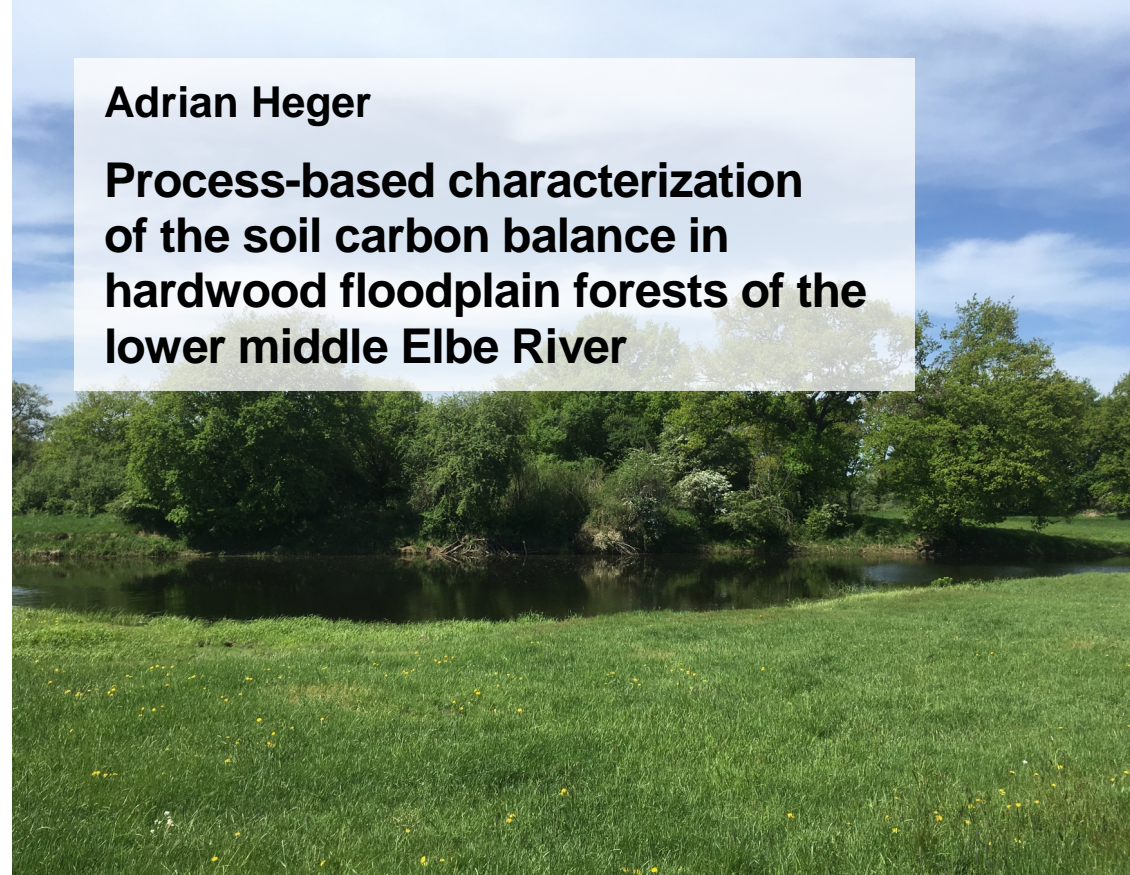
Verein zur Förderung der Bodenkunde Hamburg

c/o Institut für Bodenkunde - Universität Hamburg

https://www.geo.uni-hamburg.de/de/bodenkunde.html

Band 103

Hamburger Bodenkundliche Arbeiten

HBA

Process-based characterization of the soil carbon balance in hardwood floodplain forests of the lower middle Elbe River

Dissertation

with the aim of achieving a doctoral degree

at the Faculty of Mathematics, Informatics and Natural Sciences

Department of Earth System Sciences

at Universität Hamburg

submitted by

Adrian Heger

Hamburg

2022

Contents

List of figures

List of tables

Journal articles published or under review

Parts of this thesis have been previously published or are under review in international journals:

Heger, A., Becker, J. N., Vásconez Navas, L. K., & Eschenbach, A. (2021). *Factors controlling soil organic carbon stocks in hardwood floodplain forests of the lower middle Elbe River.* Geoderma, 404. https://doi.org/10.1016/j.geoderma.2021.115389. **Article I**

- Author Contributions: Adrian Heger: Conceptualization; Methodology; Software; Data curation; Formal analysis; Validation; Visualization; Investigation; Writing - original draft. Joscha N. Becker: Conceptualization; Methodology; Validation; Formal analysis; Writing - review & editing. Lizeth K. Vásconez: Conceptualization; Writing - review & editing; Methodology; Formal analysis; Data curation; Investigation. Annette Eschenbach: Supervision; Conceptualization; Writing - review & editing; Validation.

Heger, A., Becker, J. N., Vásconez Navas, L. K., & Eschenbach, A. (under review). *Drivers for soil organic carbon stabilization in Elbe River floodplains.* Under review at European Journal of Soil Science. **Article II**

- Author Contributions: Adrian Heger: Conceptualization; Methodology; Software; Data curation; Formal analysis; Validation; Visualization; Investigation; Writing - original draft. Joscha N. Becker: Conceptualization; Methodology; Validation; Formal analysis; Writing - review & editing. Lizeth K. Vásconez: Writing - review & editing. Annette Eschenbach: Supervision; Conceptualization; Writing - review & editing; Validation.

Heger, A., Becker, J. N., Vásconez Navas, L. K., Holl, D., & Eschenbach, A. (under review). *Soil texture and pH affect soil CO_2 efflux in hardwood floodplain forests of the lower middle Elbe River.* Under review at European Journal of Soil Science. **Article III**

- Author Contributions: Adrian Heger: Conceptualization; Methodology; Software; Data curation; Formal analysis; Validation; Visualization; Investigation; Writing - original draft. Joscha N. Becker: Conceptualization; Methodology; Validation; Formal analysis; Writing - review & editing. Lizeth K. Vásconez: Writing - review & editing; Methodology; Formal analysis; Data curation. David Holl: Writing - review & editing. Annette Eschenbach: Supervision; Conceptualization; Writing - review & editing; Validation.

Heger, A., Kleinschmidt, V., Gröngröft, A., Kutzbach, L., & Eschenbach, A. (2020). Application of a low-cost NDIR sensor module for continuous measurements of in situ soil CO2 concentration. Journal of Plant Nutrition and Soil Science, 183, 557–561. https://doi.org/10.1002/jpln.201900493. **Article IV**

- Author Contributions: Adrian Heger: Conceptualization; Methodology; Software; Data curation; Formal analysis; Validation; Visualization; Investigation; Writing - original draft. Volker Kleinschmidt: Conceptualization; Methodology; Investigation; Writing - review & editing. Alexander Gröngröft: Writing - review & editing; Methodology. Lars Kutzbach: Conceptualization; Formal analysis; Writing - review & editing; Validation. Annette Eschenbach: Supervision; Conceptualization; Writing - review & editing; Validation.

Abstract

I assessed key drivers for processes in the soil carbon (C) balance of hardwood floodplain forests at the lower middle Elbe River. Floodplains play a significant role in the global C cycle, particularly due to their soil organic carbon (SOC) storage potential in hardwood floodplain forests. In floodplains, C input occurs from deposition of dead plant debris and fluviatile sediments. C losses are mainly driven by flood-induced soil erosion and SOC mineralization. These processes vary by relief position and vegetation type. However, anthropogenic landscape modifications have affected the natural flooding regime and the vegetation composition. The interaction between natural conditions and anthropogenic modifications complicate the understanding of processes in the C balance of hardwood floodplain forests. To determine the driving mechanisms for these processes, I selected 50 floodplain study sites along the lower middle Elbe River and categorized them into hydrologic situation (low and high relief position; active and former flooding zone) and vegetation type (forest and grassland; old and young forest). The aim of my dissertation is to understand the processes controlling the soil C balance of hardwood floodplain forests.

To characterize the processes controlling the soil C balance of hardwood floodplain forests, I related SOC stocks, SOC stability, and soil CO_2 efflux (through autotrophic and heterotrophic soil respiration) to vegetation (e.g., forest age, basal area) and soil characteristics, particularly pedological traits (e.g., hydromorphic features, soil texture, pH, C/N ratio). SOC stocks were determined up to a depth of 1 m and compared to topsoil SOC stocks. SOC density fractions, SOC mineralizability and microbial biomass in top- and subsoils were analyzed to identify drivers for SOC stability. Soil CO_2 effluxes were measured over a full year using the closed-chamber method. Based on the response of soil CO_2 efflux to soil moisture and temperature, annual rates were determined. Additionally, the applicability of a low cost CO_2 sensor (K33SOIL) for *in situ* soil measurements was tested to improve the spatial and temporal resolution of soil CO_2 flux studies.

Abstract

SOC stocks were unaffected by vegetation type (grassland and forest) but greatest in low relief position and in the active flooding zone. SOC stocks ranged between 99–149 t ha^{-1} and were thereby similar to other temperate hardwood floodplain forest but also larger than terrestrial forests. SOC stocks in low lying forests of the active flooding zone were 50% greater compared to high elevated forests and to hardwood floodplain forests of the former flooding zone. Fine soil texture (< 6.3 µm) was the most important univariate predictor for SOC stocks, followed by flooding duration. A multiple linear regression showed that fine texture, pH, C/N ratio and forest age explain 86% of variance in SOC stocks. Consequently, fine texture was the most important driver for SOC stabilization to organomineral complexes, explaining 43–64% of variance in mineralizable C and the heavy density fraction (HF) of SOC. The HF was the most important SOC pool (contributing > 64% in top- and subsoil) and further confirmed the importance of fine texture for SOC storage. Thus, SOC stocks and SOC stabilization were strongly controlled by proxies for floodplain relief and sedimentation processes, such as flooding duration and fine soil texture.

Soil CO_2 efflux ranged between 1006–2209 gC m^{-2} y^{-1} (corresponding to 10–22 t ha^{-1} y^{-1}) and was also closely related to fine texture and soil pH (R^2 = 0.75), confirming a close relationship between the C balance and relief-affected features. Soil CO_2 efflux was decreased at high pH (i.e., close to neutral). This result fits with the finding that SOC stocks were greatest at high pH. The largest total soil CO_2 efflux occurred on sites, with highest fine texture content. This seems to contradict with the finding, that fine texture is the main driver for SOC storage. However, this effect was related to an indirect positive effect of fine texture on soil moisture and SOC content, which are important for microbial mineralization and root vitality. Total soil CO_2 efflux occurred thereby partly in amounts comparable to tropical forests. Relative soil CO_2 efflux (in gCO_2-C gSOC^{-1} y^{-1}) revealed that the smallest efflux occurred in low lying sites, where largest SOC stocks and fine texture contents occur. These sites where also represented by greatest pH and hydromorphic features appearing close to the soil surface. These results again suggest that SOC is protected by oxygen scarcity and stabilization to fine soil particles in low lying forests. To cover further CO_2 flux measurements

with high spatial and temporal resolution, I approved the applicability of a low cost CO_2 sensor module in precision and accuracy in floodplain soils.

To sum up, the process-based soil C balance in hardwood floodplain forests of the lower middle Elbe River was mainly controlled by properties representing the hydrologic situation, such as fine soil texture, soil pH and C/N ratio, the depth of hydromorphic features, and flooding duration. These findings indicated that oxygen scarcity, allochthonous C input, and SOC stabilization through the accumulation of fine soil particles are the main processes contributing to SOC preservation and mitigation of C loss through soil CO_2 efflux in hardwood floodplain forests. Thus, hardwood floodplain forests act as more efficient C sinks once located in the active flooding zone where flooding and sedimentation processes occur.

My dissertation thereby provides important information that should be considered during floodplain management. Furthermore, my studies underline the importance of hardwood floodplain forests as a considerable SOC reservoir but also highlight the relevance of the hydrologic situation for future climate change scenarios.

Zusammenfassung

Ich habe die wesentlichen Treiber für Prozesse im Bodenkohlenstoff-Haushalt von Hartholz-Auenwäldern an der unteren Mittelelbe untersucht. Auen spielen eine wichtige Rolle im globalen Kohlenstoffkreislauf, insbesondere aufgrund ihres Speicherpotenzials für organischen Bodenkohlenstoff (SOC) in Hartholz-Auenwäldern. In den Auen erfolgt der Eintrag von Kohlenstoff (C) durch die Ablagerung von abgestorbenen Pflanzenresten und fluviatilen Sedimenten. Die C-Verluste werden hauptsächlich durch hochwasserbedingte Bodenerosion und SOC-Mineralisierung verursacht. Diese Prozesse variieren je nach Reliefposition und Vegetationstyp. Allerdings haben anthropogene Landschaftsveränderungen das natürliche Überflutungsregime und die Vegetationszusammensetzung beeinflusst. Die Wechselwirkung zwischen den natürlichen Bedingungen und den anthropogenen Veränderungen erschwert das Verständnis der Prozesse im C-Haushalt von Hartholz-Auenwäldern. Um die treibenden Mechanismen für diese Prozesse zu ermitteln, habe ich 50 Auenstandorte an der unteren Mittelelbe ausgewählt und sie nach hydrologischer Situation (tiefe und hohe Relieflage; aktive und ehemalige Aue) und Vegetationstyp (Wald und Grünland; alter und junger Wald) kategorisiert. Ziel meiner Dissertation ist es, die Prozesse zu verstehen, die den C-Haushalt des Bodens in Hartholz-Auenwäldern steuern.

Um die Prozesse zu charakterisieren, die den C-Haushalt des Bodens in Hartholz-Auenwäldern steuern, habe ich die SOC-Vorräte, die SOC-Stabilität und die CO_2-Freisetzung des Bodens (durch autotrophe und heterotrophe Bodenatmung) mit der Vegetation (z. B. Alter des Waldes, Bestandsgrundfläche) und den Bodeneigenschaften, insbesondere den pedologischen Merkmalen (z. B. hydromorphe Merkmale, Bodentextur, pH-Wert, C/N-Verhältnis), in Beziehung gesetzt. Die SOC-Vorräte wurden bis zu einer Tiefe von 1 m bestimmt und mit den SOC-Vorräten des Oberbodens verglichen. SOC-Dichtefraktionen, SOC-Mineralisierbarkeit und mikrobielle Biomasse in Ober- und Unterböden wurden analysiert, um Faktoren für die SOC-Stabilität zu ermitteln. Die CO_2-Freisetzungen des Bodens wurden über ein ganzes Jahr hinweg mit der Methode der geschlossenen Haube gemessen. Auf der Grundlage der

Reaktion der CO_2-Freisetzung des Bodens auf die Bodenfeuchtigkeit und -temperatur wurden jährliche Raten bestimmt. Darüber hinaus wurde die Anwendbarkeit eines kostengünstigen CO_2-Sensors (K33SOIL) für *in situ*-Bodenmessungen getestet, um die räumliche und zeitliche Auflösung von Untersuchungen von Boden-CO_2-Flüssen zu verbessern.

Die SOC-Vorräte waren unabhängig von der Vegetationsart (Grünland und Wald), aber am größten in tiefer Relieflage und in der aktiven Überflutungszone. Die SOC-Vorräte lagen zwischen 99-149 t ha^{-1} und waren damit ähnlich wie bei anderen Hartholz-Auenwäldern der gemäßigten Breiten, aber auch größer als in terrestrischen Wäldern. Die SOC-Vorräte in den tief liegenden Wäldern der aktiven Überflutungszone waren um 50 % höher als in den hoch gelegenen Wäldern und in den Hartholz-Auenwäldern der ehemaligen Aue. Die feine Bodentextur (< 6,3 µm) war der wichtigste univariate Prädiktor für den SOC-Vorrat, gefolgt von der Überflutungsdauer. Eine multiple lineare Regression zeigte, dass die feine Bodentextur, der pH-Wert, das C/N-Verhältnis und das Waldalter 86 % der Varianz der SOC-Vorräte erklären. Folglich war die feine Bodentextur der wichtigste Treiber für die Stabilisierung des SOC zu organomineralischen Komplexen und erklärte 43-64 % der Varianz des mineralisier-baren C und der schweren Dichtefraktion (HF) des SOC. Die HF war der wichtigste SOC-Pool (mit einem Anteil von > 64 % im Ober- und Unterboden) und bestätigte die Bedeutung der feinen Bodentextur für die SOC-Speicherung. Somit wurden die SOC-Vorräte und die SOC-Stabilisierung in starkem Maße durch Proxies für das Auenrelief und Sedimentationsprozesse, wie z. B. die Überflutungsdauer und die feine Bodentextur, gesteuert.

Die CO_2-Freisetzung des Bodens lag zwischen 1006-2209 gC m^{-2} y^{-1} (entspricht 10-22 t ha^{-1} y^{-1}) und war ebenfalls eng mit der feinen Bodentextur und dem pH-Wert des Bodens verbunden (R^2 = 0,75), was eine enge Beziehung zwischen dem C-Haushalt und reliefbedingten Merkmalen bestätigt. Die CO_2-Freisetzung des Bodens war bei hohem pH-Wert (d. h. nahe dem neutralen Wert) geringer. Dieses Ergebnis deckt sich mit der Feststellung, dass die SOC-Vorräte bei hohem pH-Wert am größten waren. Die größte Gesamt-CO_2-Freisetzung des Bodens trat an Standorten mit dem höchsten Gehalt an feiner Bodentextur auf. Dies scheint im Widerspruch zu der Feststellung zu stehen, dass die feine

Bodentextur die treibende Kraft für die SOC-Speicherung ist. Jedoch stand dieser Effekt im Zusammenhang mit einer indirekten positiven Wirkung der feinen Bodentextur auf die Bodenfeuchtigkeit und den SOC-Gehalt, welche wichtig für die mikrobielle Mineralisierung und Wurzelvitalität sind. Die Gesamt-CO_2-Freisetzung des Bodens erfolgte dabei teilweise in Mengen, die mit denen tropischer Wälder vergleichbar sind. Die relative CO_2-Freisetzung des Bodens (in gCO_2-C $gSOC^{-1}$ y^{-1}) zeigte, dass die geringste Freisetzung an tiefliegenden Standorten auftrat, wo SOC-Vorräte und Gehalte der feinen Bodentextur am höchsten sind. Diese Standorte wiesen auch die höchsten pH-Werte und hydromorphen Merkmale nahe der Bodenoberfläche auf. Diese Ergebnisse deuten erneut darauf hin, dass der SOC in tiefliegenden Wäldern durch Sauerstoffmangel und Stabilisierung an feinen Bodenpartikeln geschützt ist. Um weitere CO_2-Flussmessungen mit hoher räumlicher und zeitlicher Auflösung abzudecken, habe ich die Anwendbarkeit eines kostengünstigen CO_2-Sensormoduls hinsichtlich Präzision und Genauigkeit in Auenböden anerkannt.

Zusammenfassend lässt sich sagen, dass der prozessbasierte Boden-C-Haushalt in Hartholz-Auenwäldern der unteren Mittelelbe hauptsächlich durch Eigenschaften gesteuert wurde, die die hydrologische Situation repräsentieren, wie z. B. die feine Bodentextur, der pH-Wert und das C/N-Verhältnis des Bodens, die Tiefe der hydromorphen Merkmale und die Überflutungsdauer. Diese Ergebnisse deuten darauf hin, dass Sauerstoffmangel, allochthoner C-Eintrag und SOC-Stabilisierung durch die Anhäufung feiner Bodenpartikel die wichtigsten Prozesse sind, die zur Speicherung des SOC und zur Minderung des C-Verlusts durch CO_2-Freisetzung des Bodens in Hartholz-Auenwäldern beitragen. Hartholz-Auenwälder fungieren also als effizientere C-Senken, wenn sie in der aktiven Überflutungszone liegen, in der Überflutungs- und Sedimentationsprozesse stattfinden.

Meine Dissertation liefert somit wichtige Informationen, die bei der Bewirtschaftung von Auenwäldern berücksichtigt werden sollten. Darüber hinaus unterstreichen meine Unter-suchungen die Bedeutung von Hartholz-Auenwäldern als beachtlicher SOC-Speicher, aber auch die Relevanz der hydrologischen Situation für zukünftige Klimawandelszenarien.

1 General introduction

Floodplains play a significant role in the global carbon (C) cycle, particularly due to their soil organic carbon (SOC) storage potential in hardwood floodplain forests (Battin et al., 2009; Cole et al., 2007; Dybala et al., 2019). Estimates suggest that up to 8% of the global SOC stocks occur in floodplains, with temperate hardwood floodplain forests storing about 177 t SOC ha^{-1} (Scholz et al., 2012; Sutfin et al., 2016). The main processes in the soil C balance of hardwood floodplain forests are C input by deposition of dead plant debris and fluviatile sediments as well as soil C loss by erosion and soil CO_2 efflux (Battin et al., 2009). In hardwood floodplain forest soils, allochthonous and autochthonous C input—from river and vegetation—is mainly controlled by flood induced sedimentation and the vegetation composition (Giese et al., 2003; Swinnen et al., 2020) (Fig. 1). Floodplain relief affects flooding, sedimentation and soil erosion, and thereby local soil properties and moisture conditions, which influence the activity and vitality of microorganisms and plants (Cierjacks et al., 2011; Wilson et al., 2011). Their temperature dependent respiration activity control C loss through soil CO_2 efflux (Fan & Han, 2018; Lininger et al., 2018). SOC can be stabilized and protected from microbial mineralization due to progressed soil development and oxygen scarcity (Graf-Rosenfellner et al., 2016; Hennings et al., 2021). However, C input, loss, and stabilization processes vary dynamically due to a natural heterogeneous relief and seasonal variation in temperature (Swinnen et al., 2020). Additionally, anthropogenic landscape modifications, e.g., channelization, clearing, and dike building, have affected many natural ecosystem functions of hardwood floodplain forests, such as biodiversity, C retention and flood risk regulation (Hornung et al., 2019). Thus, the natural heterogeneous relief as well as the interaction with anthropogenic landscape modifications, make soil C balance estimation in hardwood floodplain forests a complex challenge where different factors have to be taken into account. Understanding the processes in the soil C balance can help to infer the impact of hardwood floodplain forests on climate change (Scharlemann et al., 2014; Sutfin et al., 2016).
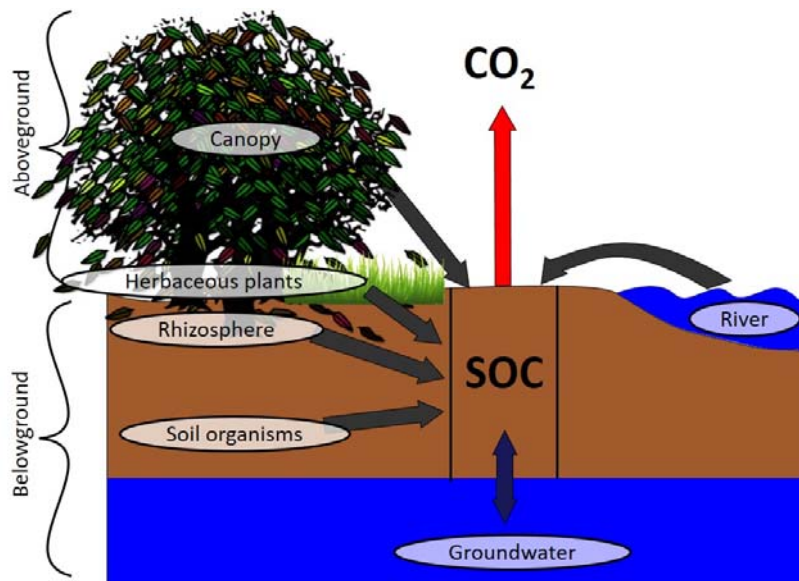
Fig. 1. The input fluxes of soil organic carbon (SOC) in hardwood floodplain forests are displayed with black arrows, whereby the translocation of dissolved organic carbon in groundwater is assigned with a double-sided arrow. Ellipses mark the input sources. The red arrow shows soil carbon dioxide (CO_2) efflux as a product of aerobic SOC mineralization. The connection of the groundwater to the river water table as well as the output flux of SOC by soil erosion was neglected for simplification.

SOC has been acknowledged to be the most important organic C pool in floodplains (Sutfin et al., 2016). Natural mechanism that affect SOC stocks in floodplains usually depend on standing vegetation and relief, which control autochthonous and allochthonous soil C input (Cierjacks et al., 2011). Oxygen scarcity in low relief position can preserve SOC (Hennings et al., 2021). SOC stocks can increase by flooding and with forest age due to organic C sedimentation and leaf litter input (Giese et al., 2003). However, dike building and clearing in the past centuries have changed natural C input mechanisms drastically. Hence, today, many hardwood floodplain forests are situated behind a dike (former floodplain) and the natural floodplain area (active floodplain) is dominated by grasslands (Brunotte et al., 2009). A projection on floodplain soils of the Elbe River showed that hardwood floodplain forests in the diked area store about 60 t ha^{-1} less SOC than their counterpart in the active flooding zone (Scholz et al., 2012). Thus, relief position (low or high), flooding zone (active or former) as well as the vegetation type (grassland or forest) and forest age, can affect SOC stocks in hardwood floodplain forests dynamically, which complicates the understanding of differences in SOC stocks between river systems.

Stabilization and mineralization of SOC is controlled by the activity of microorganisms, which is affected from physical and chemical soil properties, such as pH, salinity, oxygen supply, soil moisture, SOC and nutrient content (Basile-Doelsch et al., 2020). Soil microorganisms are able to stabilize SOC to more complex and stable structures, i.e., mainly organomineral associations, represented by the heavy density fraction (HF) of SOC. The light density fractions—dominated by plant detritus originated particulate organic matter—can be differentiated into a physically unprotected free light fraction (fLF) and an occluded light fraction (oLF) where organic matter is protected within aggregates (Wagai et al., 2009). The knowledge about stable soil aggregates and organomineral associations, and their drivers, can help to identify SOC mineralization and stabilization processes in floodplains (Schrumpf et al., 2013). However, microbial activity varies strongly with local soil properties and SOC availability, which strongly depend on relief- and vegetation-driven allochthonous and autochthonous C input (Wilson et al., 2011). Understanding the processes contributing to SOC stabilization and mineralization in floodplains would help to infer their SOC storage potential.

Soil CO_2 efflux—consisting of heterotrophic SOC mineralization from soil and litter and autotrophic root respiration—is the most important process for C loss in forests (Fan & Han, 2018). Soil CO_2 efflux is mainly controlled by seasonal changes in temperature and soil moisture (Davidson et al., 1998). Also local soil properties, such as soil pH, oxygen supply and SOC availability, control the activity of microorganisms and roots (Chen et al., 2014). However, the heterogeneous micro-relief and anthropogenic landscape modifications affect these soil properties dynamically. Thus, soil CO_2 effluxes comparable to deserts up to those comparable to tropical forests can occur in a single floodplain ecosystem (Doering et al., 2011). Understanding the processes contributing to spatial and temporal differences in soil CO_2 efflux would help to estimate C losses in hardwood floodplain forests.

Continuous measurements of *in situ* soil CO_2 concentration is costly, work-intensive, and therefore, limited regarding spatial and temporal coverage (Luther-Mosebach et al., 2018; Zhang et al., 2015). The low cost CO_2 sensor module K33 ICB (Senseair, Sweden) (referred to as "K33SOIL"), is known in the scientific community (Bastviken et al., 2015; Harmon et al.,

2015; Martin et al., 2017; Yasuda et al., 2012) but has not been used for *in situ* soil measurements yet. The application of K33SOIL in floodplains could improve the spatial and temporal resolution of CO_2 flux studies.

SOC stocks, their stability pools as well as soil CO_2 effluxes are important parameters of the soil C balance. To examine the processes that control these parameters in hardwood floodplain forests of the lower middle Elbe River, my journal articles I–IV aim to answer the following overriding research questions:

I.   What factors control SOC stocks in Elbe River hardwood floodplain forests?

II.   What mechanisms drive SOC stabilization in Elbe River floodplains?

III. How do soil properties affect C losses through soil CO_2 efflux in hardwood floodplain forests?

IV.   Is the low cost CO_2 sensor module K33 ICB suitable for *in situ* soil CO_2 measurements?

To answer these questions, I selected 39 hardwood floodplain forests and 11 floodplain grasslands along the lower middle Elbe River (Fig. 2).
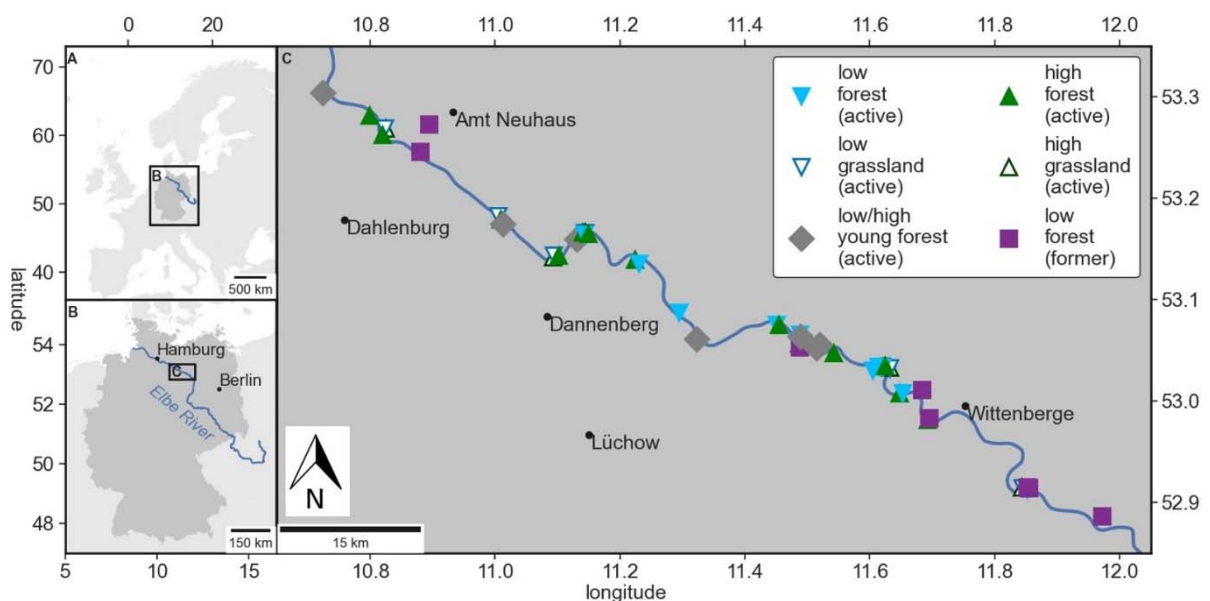
Fig. 2. Location of 50 hardwood floodplain forest and grassland study sites along the lower middle Elbe River region. Low and high are height indications of the study sites. The age of the young forests ranges from 15 to 30 years and that of the forests from 80 to 200 years. River connection of the floodplain is indicated in parentheses.

The study sites were categorized into forest age (forest and young forest), vegetation type (grassland and forest), and hydrologic situation. The hydrologic situation was separated into low and high relief position in the active and former (i.e., situated behind the dike) flooding zone. I selected 49 study sites (11x low forest (active), 13x high forest (active), 6x low grassland (active), 5x high grassland (active), 7x low/high young forest (active), 7x low forest (former)) for the study on factors controlling SOC stocks; 8 study sites (2x low forest (active), 3x high forest (active), 2x low grassland (active), 1x high grassland (active)) for the study on the effects on SOC stabilization; and 6 forest sites (2x low forest (active), 2x high forest (active), 2x low forest (former)) for the study on the effects on soil CO_2 efflux. I integrated the K33SOIL in a newly developed probe for *in situ* soil measurements and tested its applicability for measurements in floodplains at sites in the urban area of Hamburg and in laboratory experiments.

2 Article I: Factors controlling soil organic carbon stocks in hardwood floodplain forests of the lower middle Elbe River

2.1 General introduction

Riparian ecosystems play a significant role in the global carbon cycle (Battin et al., 2009; Cole et al., 2007). In these ecosystems, soil organic carbon (SOC) has been acknowledged to be the largest organic carbon pool (Sutfin et al., 2016). The size and stability of this SOC pool are largely dependent on the local relief (Swinnen et al., 2020). Floodplain soils with strong flooding and sedimentation dynamics are characterized by strong horizontal layering, often coarse textured and poor in organic matter. Floodplain soils with low flooding and sedimentation dynamics often have fewer but thicker, organic matter-enriched, and fine-textured horizons (Cierjacks et al., 2011; Drouin et al., 2011). Furthermore, SOC stocks in forested floodplains can increase with tree age due to stronger litter input and a higher abundance of deep fine roots (Giese et al., 2003; Lal, 2005). Lowland hardwood floodplain forest SOC stocks of mineral soils can thereby be as high as in German forests (Cierjacks et al., 2010; Ricker & Lockaby, 2015; Wellbrock et al., 2017). The ability to store large amounts of allochthonous and autochthonous carbon highlights the SOC sequestration potential of hardwood floodplain forests soils (Graf-Rosenfellner et al., 2016). However, the importance of these SOC input sources as well as SOC losses, e.g., from erosion (Bai et al., 2005), varies by ecoregion and geological setting, so that no significant pattern has yet emerged (Sutfin et al., 2016). Empirical data may help to identify the factors controlling SOC stocks in floodplains and to understand differences in SOC stocks between river systems, which could eventually improve estimates for Earth System Models (Scharlemann et al., 2014; Sutfin et al., 2016).

The main natural drivers of tree vegetation composition and SOC stocks in a floodplain are small elevation changes (Cierjacks et al., 2011; Giese et al., 2000; Pinay et al., 1992), as well as soil moisture and clay content (Graf-Rosenfellner et al., 2016; Hennings et al., 2021;

Hoffmann et al., 2009; Pinay et al., 1992; Wigginton et al., 2000). However, the heterogeneous micro-relief of floodplains can affect soil formation through periodic flooding and sedimentation processes (Gallardo, 2003). In addition to the natural floodplain relief, anthropogenic landscape modifications such as channelization and dike construction can alter hydrologic features (e.g., smaller flooding frequency) and vegetation composition of the floodplain, which affects the organic carbon dynamics in the system (Cierjacks et al., 2010; Sutfin et al., 2016). A projection on floodplain soils of the Elbe River revealed that SOC stocks of the active floodplain can be 60 t ha^{-1} higher than those of the former floodplain (Scholz et al., 2012). Though this effect could be the result of the stopped allochthonous carbon inputs, even higher SOC stocks in diked forests compared to forests of the active flooding zone have been found at the Danube River (Rieger et al., 2014). This was related to long-term processes, mainly input from autochthonous carbon sources, such as undisturbed biomass production, e.g., fine roots (Rieger et al., 2013) and litter fall. Thus, changes in the hydrologic situation of the floodplain can affect autochthonous as well as allochthonous carbon input.

Hardwood floodplain forests can be the largest reservoir of carbon in floodplain ecosystems (Cierjacks et al., 2010), and SOC sequestration can be substantially greater than on unforested floodplains (Dybala et al., 2019). At the lower middle Elbe River, hardwood floodplain forests can be found under sand-dominated high-elevated embankments as well as on loam-dominated low-lying floodplain (Schwartz et al., 2003). Thus, the relief and parent material can be very heterogeneous, which affects flooding exposure and soil biochemical processes (Hughes, 1997; Pinay et al., 1992). However, studies focusing on the influence of hydrologic features on SOC stocks usually compare micro-relief indices in combination with different floodplain forest types (e.g., Marks et al. (2020)) and not within one floodplain forest type. Soil hydromorphic features, observed in the field, can be used to indicate high SOC content, but can also be contradictory due to an effect of differences in vegetation type (Bullinger-Weber et al., 2014). At the Elbe River, clearing and river engineering practices in past centuries have affected the vegetation, and forests are often replaced by grasslands (Brunotte et al., 2009). Anthropogenic modifications (e.g., dikes and change from forest to

grassland) and features of the natural landscape (e.g., micro-relief and vegetation) as well as their interaction seem to affect SOC storage in hardwood floodplain forest soils. To understand the controlling effect on SOC stocks, we aim to answer (1) how much SOC is stored at different depth intervals, (2) what effect vegetation has on these stocks, and (3) what effect the hydrologic situation has on SOC stocks and how those effects are reflected by pedological traits. Our investigation was conducted at selected hardwood forests and grasslands of the active floodplain as well as at diked hardwood forests of the former floodplain along the lower middle Elbe River.

2.2 Material and methods

2.2.1 Study sites, soil types, and categorization

Our study area is located at the lower middle Elbe River in northern Germany (Fig. 3). In 21 forests found along the lower middle Elbe River, 38 hardwood floodplain forest study sites have been integrated. The tree species composition is dominated by *Quercus robur*. All forests but one are managed forests. This includes wood harvesting and deadwood removal due to safety measures for the Elbe River shipping traffic. Located beside corresponding forest study sites, we selected 11 floodplain grasslands sites.

Every study site has a defined area of 2,500 m^2. While defining the boundaries of each study site, we took care to exclude border effects (avoiding anthropogenic disturbance and minimizing closeness between sites) and to ensure homogenous relief, vegetation, and soil characteristics. By taking into account the latter aspects, each study site measured 50 m x 50 m or 25 m x 100 m.

The study sites were differentiated by six categories. The category classes were divided into hydrologic situation and vegetation classes. Hydrologic separation was based on height-indicated low-lying (low) and high elevated (high) classes. In low sites, more frequent flooding was to be expected. High sites are usually sites found on embankments or are higher than the surrounding area. Of the study sites, 6 grasslands are located in low and 5 in high areas; 11 forests are located in low and 12 in high areas. Seven low forests are situated behind

the dike (former) and are affected hydrologically by the Elbe River through seepage inflow, whereas the other study sites are all located in the active flooding zone (active). The forests have ages between 80 and 200 years. Seven forests of the active floodplain are young plantings with ages between 15 and 30 years. The young forests are the only young forests found in our study area. The hydrologic situation within these sites is mixed; therefore they are categorized as low and high.
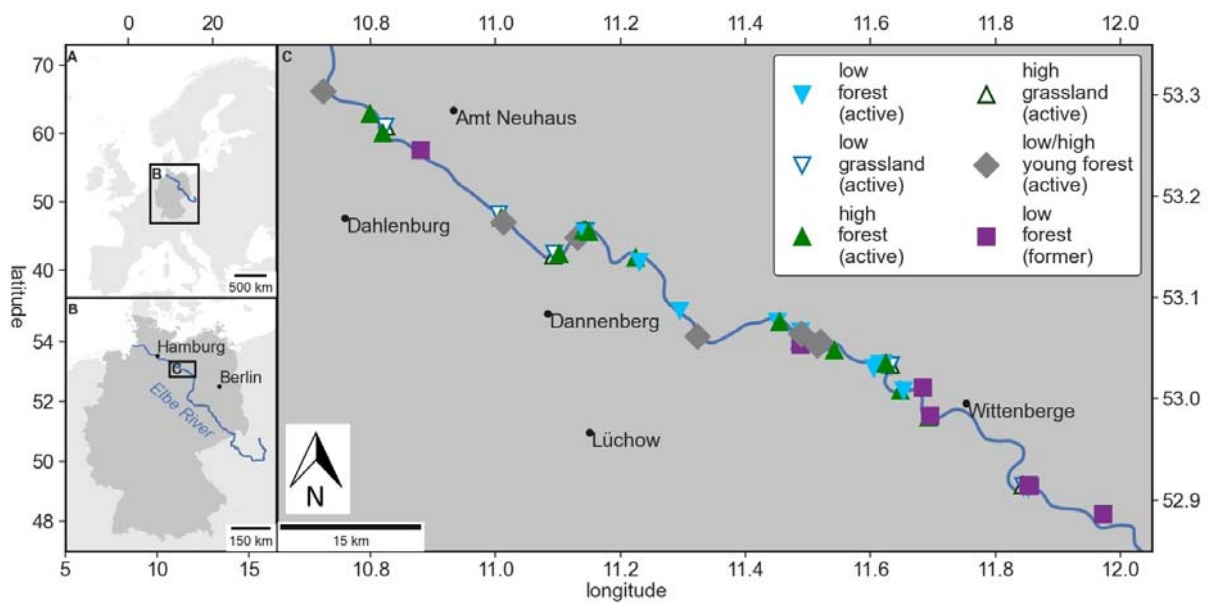
Fig. 3: Location of the hardwood floodplain forest and grassland study sites along the lower middle Elbe River region. Low and high are height indications of the study sites. The age of the young forest ranges from 15 to 30 years and that of the forests from 80 to 200 years. River connection of the floodplain is indicated in parentheses.

The fluviatile parent material consists of a sand and gravel component originating from northern glacial meltwater consisting of crystalline rocks, flint stones, limestones, sand stones, and quarzites as well as a southern component originating from the present catchment area consisting of Thuringian Forest Porphyrys, brown sandstones, lydites, quarzites, and milky quartz (Schröder, 1988). Additionally, loess-rich sediments originating from the Saale River catchment might be a component of the Holocene fluviatile parent material (Rennert et al., 2018). We characterized floodplain soils in the low active and former zone as Gleyic or Fluvic Cambisols, Fluvic Gleysols, or Gleyic Fluvisols (Table A 1). The texture was loam, sandy loam, or loamy sand. Floodplain soils found in the active high zone were often sand-dominated Fluvic Arenosols or Fluvic Cambisols.

2.2.2   Field sampling and laboratory analyses

At each of the 49 study sites, one composite topsoil sample (10 cm below mineral surface) was collected from 12–13 random locations, using a topsoil auger. Ten study sites in each of the high and low active floodplain forest categories and 5 in each of the other categories were selected for soil profile characterization and analyses. The criteria for the selection of these sites were (i) to have sites covering the complete lower middle Elbe River region and (ii) safety measures for fieldwork, as we were not able to perform time-intensive drillings or create soil pits in forests that had a too high concentration of the allergenic oak processionary caterpillar (*Thaumetopoea processionea*). We characterized soil profile*s* (n ≥ 3 per study site) using Ad-hoc-AG Boden (2005) and IUSS Working Group WRB (2015). We sampled 120 soil profile*s* using an Edelmann auger at defined depth intervals (0–5 cm, 5–10 cm, 10–30 cm, 30–60 cm, and 60–100 cm). Sixteen profiles were sampled horizon specific by creating soil pits. To study the effects of hydromorphic features, we noted the depth up to 2 m below the surface of each soil profile with the first appearance of hydromorphic mottling, i.e., where redoximorphic features covered an area of > 5% of the soil horizon according to Ad-hoc-AG Boden (2005), and calculated a mean depth per study site, referred to as "hydromorphy" (m).

The soil samples were air-dried and sieved to < 2 mm. pH was measured in 0.01 M $CaCl_2$ solution using a pH meter (MP230 GLP, Mettler Toledo, Germany). SOC and N content (in $g\,kg^{-1}$) was determined using a carbon and nitrogen analyzer (vario MAX cube, Elementar, Germany). Samples with pH ≥6.5 were additionally tested for inorganic carbon content using a total organic carbon analyzer (soli TOC cube, Elementar, Germany). In all samples exceeding this limit (29% of total soil samples), the total inorganic carbon content was below $0.5\,g\,kg^{-1}$. The ratio of SOC to N is referred to as the C/N ratio. The grain size distribution was determined for topsoil samples. According to DIN ISO 11277, the sand fraction (63 µm–2000 µm) was analyzed by a vibratory sieve shaker (Vibro, Retsch GmbH, Germany), and the fine fraction (< 2 µm – < 63 µm) was analyzed using the sedimentation approach with Sedimat 4-12 (Umwelt-Geräte-Technik GmbH, Germany). For all topsoil samples, a categorical mean was calculated (Table A 2).

2.2.3   Bulk density and stock calculation

Undisturbed samples with volume-specified cylinders (100 cm^3) were taken from the soil pits. Bulk density (ρ), in dry mass (g) per volume (cm^3), was determined following the method after DIN 19683 with 5 replicates per soil horizon. In total, we determined the bulk density of 93 different soil horizons along the lower middle Elbe River. For remaining horizons (n = 755), ρ was calculated using a pedotransfer function fitted to the measured data as well as to additional bulk density values from our institute's soil database with ρ values that have been studied from 1993 to 2005 and in 2017 in soils of Elbe River floodplains close to Lenzen, Germany. With the combined data, 173 ρ values were used to select the best fitting pedotransfer function by performing a 10-fold cross validation (Kohavi, 1995) for selected pedotransfer functions known from the literature (De Vos et al., 2005; Steinicke et al., 2016). The best fitting function for our study was a model by Tamminen and Starr (1994) (Fig. A 1):

$$\rho_{forest} = 1.591 - 0.176 \times LOI^{0.5} \tag{1}$$

$$\rho_{grassland} = 1.595 - 0.197 \times LOI^{0.5} \tag{2}$$

LOI is the loss on ignition (%), which was calculated from the SOC according to Craft et al. (1991). The R^2 and MSE for ρ_{forest} and $\rho_{grassland}$ were 0.71 and 0.85 and 0.012 g cm^{-3} and 0.017 g cm^{-3}, respectively ($p < 0.001$). We calculated SOC stocks (in t ha^{-1}) using the following equation (Hiederer & Köchy, 2011; Kobal et al., 2011):

$$SOC\ stock = SOC \times thic \times \rho \times ston \tag{3}$$

where thic is the thickness of the soil horizon (in m) and ston is a correction factor of stoniness which indicates the volumetric content of mineral components > 2 mm in the soil horizon. Depth-specific SOC stock was summed to the depth of interest. A study site mean and categorical mean was evaluated for all analytical soil profile data (Table A 3).

2.2.4   Vegetation and flooding data sources

We used vegetation data comprising mean tree age (age, in years), basal area (BA, in m^2 ha^{-1}), and mean leaf litter carbon stock (litter-C, in t ha^{-1}) per forest study site from Shupe et al. (2021). Modelled flooding duration per study site (flooding, in days year^{-1}) based on the

years 1990 to 2016 (DEM1, digital elevation model with 1 m solution) from Weber and Hatz (2020) and Weber and Rosenzweig (2020) was used.

2.2.5 Gap handling

For the multivariate analyses, we set vegetation parameters (age, litter-C, BA) for the grassland sites as well as flooding duration in the former floodplain to zero (except for one site near Popelau, Lower Saxony, where the modelled flooding duration was 2.7 days year^{-1}). Other data gaps were filled after testing for difference of vegetation or flooding duration parameter between the categories. In case of significant differences, the categorical median was used; otherwise the overall median was used to fill single gaps. Gap filling was performed in the same way for study sites with no description of the depth of the hydromorphic features (e.g., where we only retrieved topsoil samples). At described sites where we did not find hydromorphic features until 2 m, we set the depth to 2 m, assuming that processes that contribute to hydromorphic mottling starts close to this depth.

2.2.6 Statistical analyses

We used Python v3.7.9 (Van Rossum & Drake, 2009) for one-way analysis of variance (ANOVA) (with post-hoc tests) and univariate regression analyses (with Spearman (r_s) and Pearson (r_p) correlation). For ANOVA, Tukey HSD post-hoc comparison was used to identify significant differences between floodplain categories. Variance homogeneity was tested using Levene's test ($p < 0.05$), and residuals were checked for normality using the Shapiro-Wilk test ($p < 0.05$). In case of heteroscedasticity, a Welch-ANOVA was performed instead, and category comparisons were conducted using pairwise t-tests with Bonferroni-Holm p-adjustment. Differences were considered significant for $p < 0.05$.

We used R v4.0.3 (R Core Team, 2020) for nonmetric multidimensional scaling (NMDS) and multiple linear regression (MLR) analysis. NMDS was conducted with Bray-Curtis dissimilarity. Vector fitting and significance testing ($p < 0.05$) of the variables was done using the envfit() function of vegan. MLR was performed with a stepwise selection of predictors, based on the Akaike Information Criterion (AIC). The model with smallest AIC was selected.

Residuals were checked for normality using the Shapiro-Wilk test ($p < 0.05$). Spearman

correlation was used to identify correlations between the variables. Variance of inflation factor

(VIF, with factors below 3) was used to estimate collinearity between the predicting variables.

2.3 Results

2.3.1 Effect of hardwood floodplain forest category on SOC stocks

Mean SOC stocks in the topsoil (0–10 cm, Fig. 4 A) of low forests were 51% greater

than in active high forests and in low grasslands 66% greater than their high counterpart. SOC

stocks in the active low grasslands and forests combined were 58% greater than in the high

sites. Active forests combined stored 38 t ha^{-1} and grasslands 34 t ha^{-1} SOC, respectively.

SOC stocks in active forests were thereby about 12% greater than in grasslands. Mean SOC

stocks of the active young forests were 34% smaller than those of active low forests and thus

similar to SOC stocks of active high forests (< 1% smaller). In the former low forests, mean

SOC stocks were 33% smaller than in their active low counterpart.
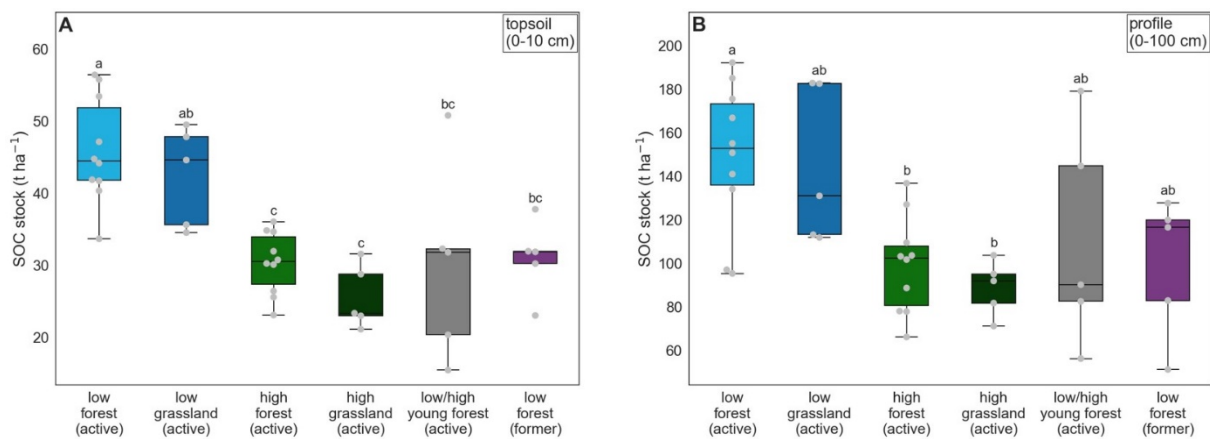
Fig. 4: SOC stocks in topsoil (0–10 cm, A) and 1 m profile (B) for 6 hydrologic situation and vegetation categories. Active floodplains are separated into low and high grassland, low and high hardwood floodplain forest, and low/high young hardwood floodplain forest. Former floodplain is represented by low hardwood floodplain forest. Dots indicate individual sample values (n = 40); significant differences according to ANOVA with Tukey post-hoc comparison are annotated with letters.

In the profile (0–100 cm, Fig. 4, B), low forests of the active floodplain stored 50% more

SOC than their high counterparts. Low grasslands stored 63% more SOC than their high

counterparts. Active low forests and grasslands together stored 56% more SOC than their high

counterparts. Mean SOC stocks for all active forests were 124 t ha^{-1}, and 116 t ha^{-1} for

grasslands. The stocks in forests were thereby 7% greater than in the grasslands. Young forest

SOC stocks were 26% smaller than in the active low forests and 11% greater than in the active high forests. SOC stocks in the low forests of the former floodplain were 33% smaller than the low forests of the active floodplain.

At both depth intervals, SOC stocks of the active low floodplains (forests and grasslands) were more than 50% greater than their high counterparts (in grasslands even > 60% more). Forest and grassland SOC stocks of the same hydrologic situation were not significantly different from another. In the topsoil, SOC stocks in young forests were smaller than in low forests of the active floodplain. At both depth intervals, mean SOC stocks of the former floodplain forest amounted to about two-thirds of those of their active counterpart.

2.3.2   Depth distribution of SOC stocks

To inspect the distribution of SOC in different depth intervals within the top 1 m of soil, we calculated a categorical mean for each depth using the profile samples (Fig. 5 and Table A 3). Mean forest (young and old) SOC stocks with decreasing depth were 38 t ha^{-1} (0–10 cm), 33 t ha^{-1} (10–30 cm), 22 t ha^{-1} (30–60 cm) and 22 (t ha^{-1}). At 0–10 cm, maximum SOC was stored in low grasslands, followed by low forests of the active floodplain. Smallest stocks were stored in active high grasslands. At 10–30 cm, maximum SOC stocks were stored in active low grasslands and active low forests, and minimum stocks were in the former low forests. Below 30 cm, we always found maximum SOC stocks in active low forests. At 30–60 cm depth, the smallest SOC stocks were found in active high as well as in former low forests. At 60–100 cm depth, active high grasslands had the smallest stocks.
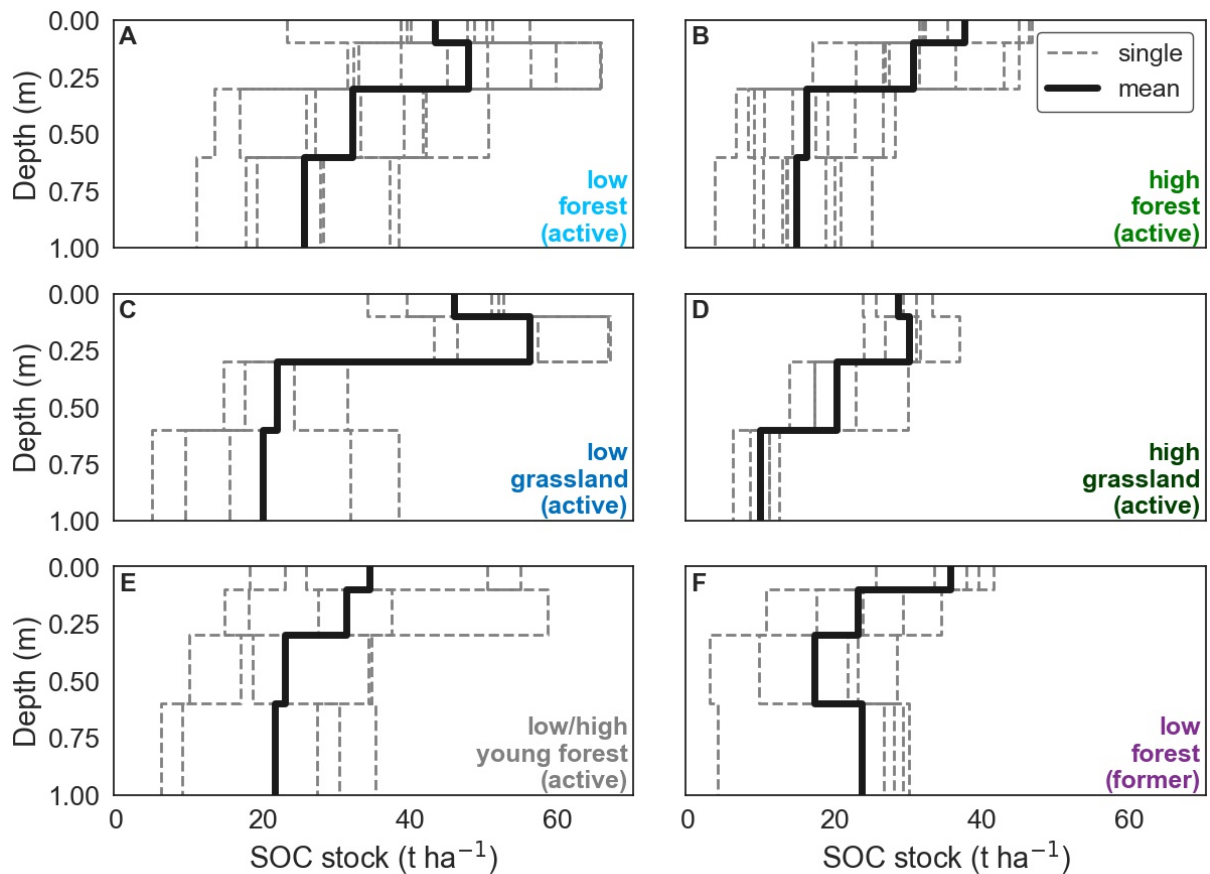
Fig. 5: SOC stocks in defined depths up to 1 m from the mineral surface (0–10 cm, 10–30 cm, 30–60 cm, 60–100 cm). The depth-dependent stocks are displayed as single mean of each study site (dashed, gray) or the mean (line, black) of the respective category. A and B: SOC stocks of the active low and high hardwood floodplain forests. C and D: SOC stocks of the active low and high floodplain grasslands. E: SOC stocks of active low and high young hardwood floodplain forests. F: SOC stocks of former low hardwood floodplain forests.

2.3.3 Environmental variables interacting in hardwood floodplain forests

Because category effects on SOC stocks were similar at all depth intervals, we extended our data set with additional topsoil samples to increase spatial representativeness. NMDS was conducted to identify (inter-)relationships between SOC stocks at 0–10 cm depth and other variables (Fig. 6 and Table A 4). The NMDS variable input comprised soil analytical data variables—SOC stock, SOC, C/N ratio, pH, fine texture ($\sum$(clay, finesilt) or < 6.3 µm, in %)—and hydrologic characteristics: depth of hydromorphic features (hydromorphy); flooding duration (flooding); and vegetation characteristics—basal area (BA), mean leaf litter carbon stock (litter-C), and mean forest age (age).
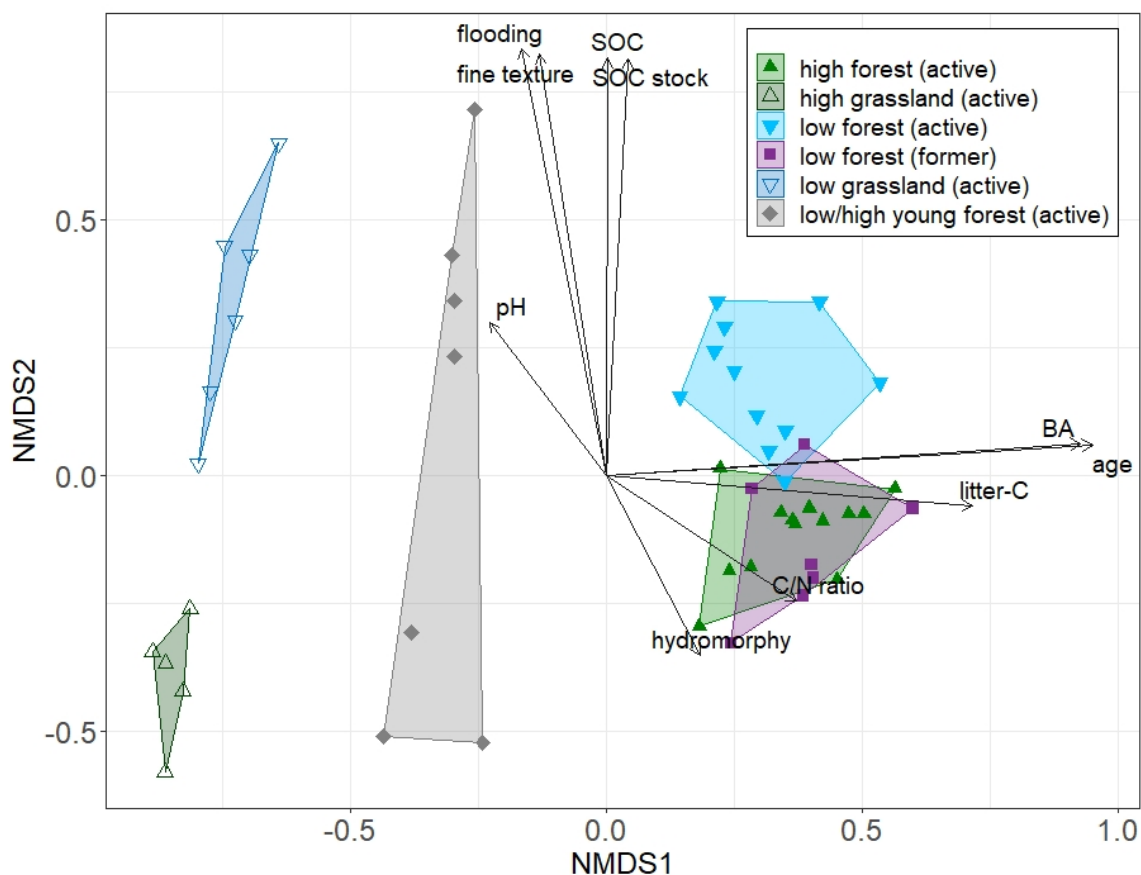
Fig. 6: The NMDS variable input comprised soil analytical data variables (SOC stock, SOC, C/N ratio, pH, fine texture (< 6.3 μm)), hydrologic characteristics (depth of hydromorphic features, flooding duration), and vegetation variables (basal area, leaf litter carbon stock, and age). Clustering on the NMDS1 mainly represents vegetation effects. Clustering on the NMDS2 mainly represents soil characteristics and hydrologic effects.

All environmental variables scored significantly. NMDS1 mainly clustered vegetative variables and successional forest stages of the categories (grassland, young forest, forest). The vegetative variables forest age, BA, and litter-C as well as the C/N ratio reached maximum scores in NMDS1. NMDS2 clustered low and high sites of the active floodplain with soil analytical data variables and hydrologic characteristics. Highest predictors were flooding, fine texture, and SOC and SOC stock, followed by hydromorphy and pH. Flooding was inversely related to hydromorphy and showed a strong connection to fine texture and SOC stocks. Therefore, the depth of the hydromorphic features could be expected to be smaller the more flooding days occur during the year. Only one forest of the former floodplain, which penetrates the cluster of active low forests, had a flooding duration of 2.7 days year^{-1}, whereas the other categorical sites were zero and predominately clustered within the active high forest cluster.

2.3.4 Factors controlling SOC stocks

As indicated by NMDS, flooding duration showed a positive relationship to SOC stocks, univariately explaining nearly 40% of the response variance (Fig. 7, A). Although the depth of hydromorphic features was inversely dependent on the flooding duration, no relationship between SOC stocks and hydromorphy was found (Fig. 7, B). However, SOC was negatively related to hydromorphy once only active forests were considered (Fig. A 2, $R^2 = 0.47$, $p = 0.01$). Fine texture was the strongest predictor for SOC stocks with $R^2 = 0.63$ (Fig. 7, C). Other predictors, particularly vegetation-related variables such as age appeared to have no effect on SOC stocks (Fig. 7, D).
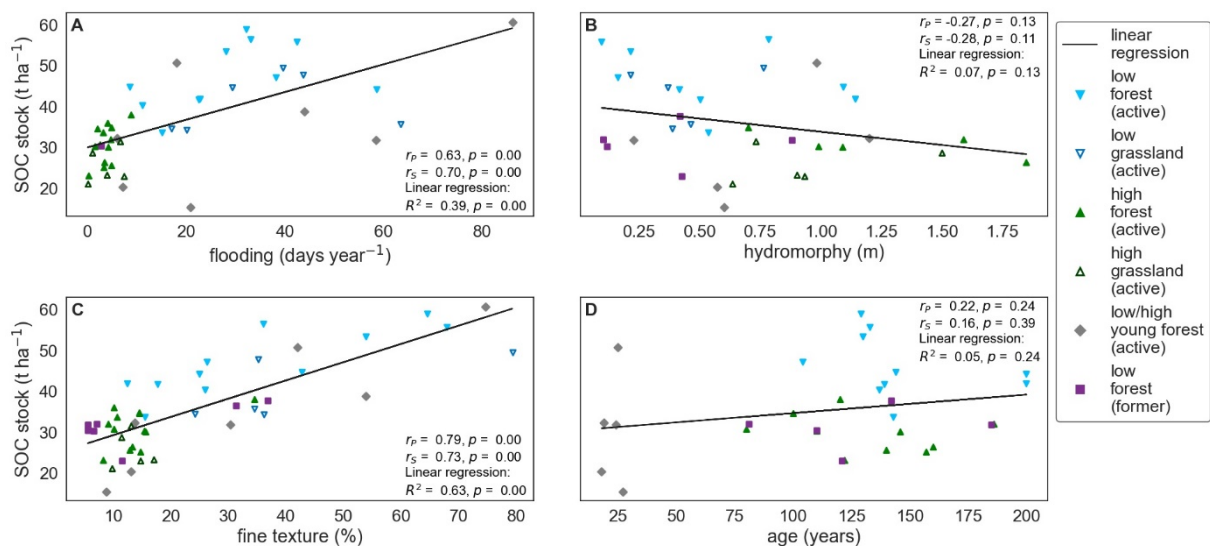
Fig. 7: SOC stocks on the y axis vs. flooding duration (A), the depth of the hydromorphic features below the mineral soil surface (B), fine texture (< 6.3 μm) (C), and mean forest age (D). The black line indicates linear regression between variables in x and y.

To inspect the most important factors that explain variance in SOC stocks, we conducted stepwise multiple linear regression analysis. Grasslands have been excluded for this analysis because their vegetation parameters valued zero. The best performing model included soil pH, C/N ratio, fine texture, and age as predictors (Eq. (4)), and it explained 86% (p < 0.001, AIC = 111.81) of the variance in SOC stocks (Table A 5). This shows that hardwood floodplain forests' SOC stocks strongly relate positively to soil fine texture, pH, and the C/N ratio as well as to the mean forest age.

$$SOC\ stock = 5.96 \times pH + 3.39 \times C/N\ ratio + 0.04 \times age + 0.56 \times fine\ texture \qquad (4)$$

2.4 Discussion

2.4.1 SOC stocks in hardwood floodplain forests of the lower middle Elbe River

We quantified SOC stocks in Elbe River hardwood floodplain forests at different depth intervals up to 1 m. SOC stocks in the topsoil (0–10 cm) ranged between 30 and 46 t ha^{-1} and between 99 and 149 t ha^{-1} in the profile (0–100 cm) (Fig. 4). Mean forest SOC decreased with depth from 38 (top, 0–10 cm) to 22 t ha^{-1} (bottom, 60–100 cm) (Fig. 5).

Topsoil and profile SOC stocks of floodplain forests of the active floodplain are in the same range as SOC stocks in hardwood floodplain forests at the Danube River of 48 t ha^{-1} and up to 186 t ha^{-1}, respectively (Cierjacks et al., 2010). In periodically flooded flats and levees from a lowland hardwood floodplain forest at Congaree River, which are similar to our forests of the active floodplain, comparative SOC stocks of up to 109 t ha^{-1} were found (Ricker & Lockaby, 2015). At more frequently flooded sites, SOC stocks up to 193 t ha^{-1} were found. Thus, SOC stocks are similar to those of temperate and lowland hardwood floodplain forests.

In all hydrologic and vegetation floodplain categories, the vertical distribution of SOC decreased with depth. In southeast Asian riparian forests, stocks of the first 10 cm of 23.4 t ha^{-1} are smaller compared to stocks in our study (of 38 t ha^{-1}) but are similar at greater depth (10–30 cm), where stocks of 32.7 t ha^{-1} have been found (Hennings et al., 2021). In German forests, SOC stocks are estimated to be 55.6 t ha^{-1} up to 30 cm in depth and up to 99.1 t ha^{-1} at 90 cm (Wellbrock et al., 2017). In our study, the stocks of the first 30 cm (71 t ha^{-1}) and of

the first meter (114 t ha^{-1}) are slightly greater. Though SOC stocks in our study are generally decreasing with depth, in the former floodplain forest category it seems to increase at 60–100 cm (Fig. 5, F). This could be attributed to either long-term processes, mainly input from autochthonous carbon sources, such as undisturbed biomass production, e.g., fine roots and litter fall (Rieger et al., 2013; Rieger et al., 2014) or to buried surface horizons (e.g., Ricker et al. (2012)). However, in general, in the current study SOC stocks of former floodplain forests were more in the range of active and high floodplain forests, which was also reflected by similar site properties (Fig. 6).

Global wetland SOC stocks are usually much greater (> 375 t ha^{-1}), which is mostly due to the inclusion of peatlands (Mitra et al., 2005). Soils of our study were solely mineral soils where increasing pH with greater depth indicates the natural acidification during pedogenesis, which is common for German forest soils (Meesenburg et al., 2019). Similarly, decreasing C/N ratio with greater depth (Table A 3) throughout all categories indicates the presence of highly processed soil organic matter with depth. Decreasing C/N ratio might be more a feature of terrestrial soils (Rumpel & Kögel-Knabner, 2011) but have also been found in floodplain soils that have a 5% to 50% chance of flooding on an annual basis (Ricker & Lockaby, 2015), which is characteristic of our study sites. Thick, organic-rich soil horizons (e.g., mollic), that are not uncommon in the upstream lying middle Elbe River region (Rennert et al., 2018), have not been found. Considerable amounts of organic muds ("Gyttja") and peat, found at the Rhine River (Hoffmann et al., 2007; Hoffmann et al., 2009), also did not appear in our study. However, in Germany, approximately 10% of the active floodplain area is covered by peatlands (Scholz et al., 2012). Precise measurements of the area coverage of hardwood floodplain forests along the lower middle Elbe River must be included to estimate a total stock value (as mass unit). Nonetheless, hardwood floodplain forests of the lower middle Elbe River store considerable amounts of SOC, as the comparison between similar floodplain ecosystems has shown.

Further studies should also consider deeper-lying SOC stocks up to 3 m, as forest SOC stocks in the second and the third meter can be found in amounts of up to 56% of those in the first meter (Jobbágy & Jackson, 2000). On floodplains, subsoil SOC stocks can even be larger

than in the first meter, due to buried organic rich horizons, which have been deposited before human modifications to the river system have been made and are today preserved by inundation (Appling et al., 2014; D'Elia et al., 2017). We did not find such buried surface horizons within 1 m of depth, but they could be important for studies focusing on deeper-lying sediments.

2.4.2 Effects of vegetation

Vegetation type and forest age had no effect on SOC stocks, neither in topsoil nor in the whole profile (Fig. 4). However, age may play a role locally, where other influencing factors are less variable (Eq. (4)).

While deforestation and forest management are commonly considered to affect SOC stocks (Guo & Gifford, 2002), we found no effects of vegetation type or vegetation change. Similar to our study, no differences in SOC stocks were found between young floodplain forests (> 20 years) and adjoined grasslands in New Zealand (Davis & Condron, 2002), or between forest and grasslands on Danube River floodplains (Cierjacks et al., 2010). This absence of land-use effects on SOC stocks in floodplains can be attributed to an overprinting effect of hydrologic and geomorphic conditions (Hennings et al., 2021), as well as potentially low effect strength and value range of vegetation and management variables because vegetation carbon stocks did not differ among different hydrologic situations in our study sites (Shupe et al., 2021).

Reforestation and forest aging are commonly expected to increase SOC stocks due to higher litter input and a higher abundance of deep fine roots in old forests (Lal, 2005; Rasse et al., 2005). This relationship has also been reported for hardwood floodplain forests (Giese et al., 2003). Though no significant difference was found, the finding that SOC stocks of forests are about 7% greater compared to grasslands might support the importance of forest age for SOC sequestration, which also appeared in the stepwise MLR analysis together with C/N ratio, pH, and fine texture when these confounding variables were kept constant (Eq. (4)). Whereas fine texture is mainly driven by sedimentation processes, soil C/N ratio is affected through

autochthonous input from lower-story vegetation and litter fall because the chemical composition of litter can affect decomposition rates (McClaugherty et al., 1985). Higher C/N ratio in forest compared to grassland (Table A 2) is probably caused by the permanent input of particulate organic carbon from fresh litter. Usually, pH is negatively correlated to C/N ratio and SOC due to the accumulation of organic matter during carbon stabilization processes and microbial activity (Cao et al., 2016; Zhou et al., 2019). These effects have also been found on floodplains (Yin et al., 2019). However, these effects were not found in our study, which was probably due to the overlaying effect caused by flooding duration and fine texture content (Fig. 6). However, higher soil pH, found at active sites, could have a positive feedback on net primary productivity due to higher nutrient availability as a consequence of high soil cation exchange capacity (Härdtle et al., 2004). Thus, higher pH could contribute to an enhanced autochthonic SOC input in active hardwood floodplain forests.

2.4.3 Effects of hydrologic situation

Inundation and floodplain relief lead to large spatial variability of biogeochemical processes, depending on elevation, micro-relief, and flooding exposure (Hughes, 1997; Naiman et al., 2010; Wilson et al., 2011), which in the current study had a driving effect on SOC stocks in lower middle Elbe River hardwood floodplain forests. Flooding duration and fine texture were the strongest predictors for SOC stocks (Fig. 7). Soils with deep-lying hydromorphic features in the soil profile were characterized by low flooding frequency, low SOC stocks, and low percentage of fine texture, and they occurred in high active as well as in former floodplains (Fig. 6). Hydrologic control on SOC stocks in floodplains can be driven by restricted SOC decomposition due to waterlogged conditions, direct allochthonous carbon input through sedimentation, and indirect accumulation of stabilized carbon due to the deposition of fine-textured sediments (Bechtold & Naiman, 2009; Bechtold & Naiman, 2006; Swinnen et al., 2020; Yin et al., 2019).

Periodic flooding partly controls soil respiration in wetland forests (Yoon et al., 2014), and oxygen scarcity in low-lying wetlands can reduce aerobic carbon mineralization, resulting in the preservation of SOC (Hennings et al., 2021; Yin et al., 2019). Long-term inundation also

lowers the soil redox potential, which can initiate methane emissions due to microorganisms that reduce Fe under the consumption of soil organic matter (Moore et al., 2018). Also, the strong denitrification potential on floodplains at long inundation periods—turnover to N_2 and N_2O (Dee & Tank, 2020; Korol et al., 2019) with pH close to 5 (Van Den Heuvel et al., 2011), as characteristic pH of sites in our study area—should be considered. However, oxygen-limited conditions can decrease decomposition of soil organic matter (Gurwick et al., 2008), and reactive allochthonic dissolved organic matter can be processed by aquatic bacteria, which would increase carbon sequestration potential in active floodplains (Sieczko & Peduzzi, 2014).

Groundwater fluctuations, induced by periodic flooding, also control dissolution and precipitation of Fe and Mn, which can be involved in metal organic complexes. Also, in wetlands, Fe oxides are able to protect SOC under aerobic conditions (Wang et al., 2017). The correlation of hydromorphy as an indicator for SOC stocks, once former floodplains were excluded (Fig. A 2), could imply that hydromorphic features on former floodplains are relict as a result of dike construction. However, former floodplain forests are largely affected by Elbe River hydrologic conditions due to seepage water inflow (Schwartz et al., 2003). Nevertheless, our study showed that the characterization of hydromorphic features in the soil can be used as a helpful indicator for large SOC stocks in hardwood floodplain forests in the active flooding zone.

Besides the controlling effect of flooding on chemical dissolution and precipitation processes as well as on soil microbial activity, floodplain relief also controls the accumulation of allochthonous SOC (through flood-induced sedimentation), which can be 6 times more abundant than the long-term (> 50 years) accumulation of autochthonous SOC in floodplain forest soils (González et al., 2014). While inundation and sedimentation are able to reduce nutrient release from litter (Baker III et al., 2001), sedimentation of fresh and nutrient-rich material can also accelerate the net primary productivity of the standing vegetation, which supports autochthonic carbon input (Zehetner et al., 2009). These effects could explain the 33% smaller SOC stocks in former floodplain forests compared to active floodplain forests. This implies that an active connection to the river could be an indicator for high SOC stocks in

hardwood floodplain forest soils due to SOC preservation in low sites and flooding-induced sedimentation. The strong hydrologic effect on environmental parameters was also reflected within the young forest category, as the high elevated sites within this category are also the sites with smallest SOC stocks and fine texture content (Fig. 6). The indirect relation of fine texture (which was also the strongest univariate predictor for SOC) to flooding duration and its strong effect on SOC stocks became apparent from stepwise MLR analysis (Eq. (4)), which indicated that the importance of flooding duration for SOC prediction was reflected in fine texture. The direct relationship of fine texture to SOC in floodplains can be explained by the adsorption of organic matter to clay minerals and the incorporation within clay and silt aggregates, which can protect SOC against microbial degradation (Deiss et al., 2017; Skjemstad et al., 1993; Sollins et al., 1996). A strong relation of SOC storage and stabilization to clay and silt has also been found at upper humic layers of Rhine River floodplains (Bullinger-Weber et al., 2014). Our study shows that in hardwood floodplain forests, relief, hydromorphic features, and the sedimentation of fine-textured material, as typical proxies for SOC sequestration on floodplains, are important controlling factors for the spatial distribution of SOC stocks.

Spatial distribution of fine-textured sediments in floodplains is characterized by high variability in soils and soil horizon distribution (Gallardo, 2003; Mendonça Santos et al., 2000). Soil texture information in this study is limited to topsoil samples. Soils of riparian hardwood forests have been found to be enriched with fine-textured material up to 1 m and more, where SOC in the heavy fraction can dominate with 90% as a consequence of sedimentation and progressed soil development (Graf-Rosenfellner et al., 2016). How much carbon is stabilized on mineral surfaces within low-lying and high elevated hardwood floodplain forests remains to be studied.

However, as we found a strong relation between SOC stocks and floodplain relief, we showed that basic field data such as spatial information on topsoil texture, height indices (low and high), and soil hydromorphic features can serve as significant predictors for SOC stocks in lower middle Elbe River hardwood floodplain forests. With the additional inclusion of soil

parameters C/N ratio and pH as well as the vegetation parameter age (Eq. (4)), the model
quality for SOC prediction can be increased.

2.5   Conclusion

SOC stocks in hardwood floodplain forests of the lower middle Elbe River were strongly
related to relief-affected features such as flooding duration and fine texture. Topsoil (0–10 cm)
and profile (0–100 cm) SOC stocks (30 to 46 t ha^{-1} and 99 to 149 t ha^{-1}) as well as stocks of
different depth intervals up to 1 m were within the range of mineral hardwood floodplain forest
soils in the temperate region reported in the literature. SOC stocks decreased with depth. SOC
stocks were not related to vegetation type (grassland, young forest, old forest) but rather
affected by the hydrologic situation of the floodplain (low, high, active, former). Occurrence of
hydromorphic features close to the mineral soil surface indicated large SOC stocks in forests
of the active floodplain. An active connection to the river increased SOC sequestration
potential compared to diked sites, and within the active floodplains, low sites stored
significantly more SOC than high sites. This effect was mainly controlled by proxies for
floodplain relief and sedimentation processes (i.e., hydromorphic features, flooding duration,
soil texture, C/N ratio, and pH). Both can be related to allochthonous carbon inputs, local SOC
stabilization through the accumulation of fine soil particles, and reducing aerobic carbon
mineralization potential through oxygen scarcity. Our study highlights the importance of relief,
flooding regime, and soil texture for SOC stock estimates and hardwood floodplain forest
management.

3 Article II: Drivers for soil organic carbon stabilization in Elbe River floodplains

3.1 Introduction

Floodplain ecosystems play a significant role in the global carbon (C) cycle (Battin et al., 2009; Cole et al., 2007). In these ecosystems, soil organic carbon (SOC) makes up for the largest organic C pool (Sutfin et al., 2016). Due to stabilization by fine soil particles and preservation by oxygen scarcity, the amount of SOC can be remarkably high in temperate floodplain grasslands and forests (Graf-Rosenfellner et al., 2016; Mayer et al., 2019; Rennert et al., 2018). SOC stabilization processes are mainly driven by the activity of microorganisms (fungi and bacteria), which are affected by local soil properties (Basile-Doelsch et al., 2020; Goenster et al., 2017). The heterogeneous floodplain relief, flooding and sedimentation processes affect soil properties, and thus microbial activity dynamically (Wilson et al., 2011). Today, many natural floodplains have lost their natural ecosystem functions such as C retention and biodiversity due to anthropogenic landscape modifications, e.g. by clearing and channelization (Brunotte et al., 2009; Hornung et al., 2019; Sutfin et al., 2016). Because of these reasons, estimating SOC stabilization processes in floodplains is difficult. Understanding the processes for SOC stabilization and mineralization in floodplains, may provide inferences about their SOC storage potential and implications for climate change (Sutfin et al., 2016).

Soil microorganisms are involved in organic matter mineralization during oxidative degradation or the conversion to more stabilized compounds (e.g., aggregates, organomineral associations, supramolecular interactions) (Basile-Doelsch et al., 2020). A separation to these compounds through density fractionation can help to identify the stability of this SOC pool (Cerli et al., 2012; Golchin et al., 1994). The SOC pool is composed of a heavy density fraction (HF), which are mainly organomineral associations, and light density fractions (LF). LFs are composed of particulate organic matter, mainly originating from plant detritus, and can be differentiated into a free light fraction (fLF) and an occluded light fraction (oLF), which is

45

physically protected within soil aggregates (Wagai et al., 2009). The contribution of the respective fraction to SOC varies with soil depth, generally with decreasing contribution of the LF to SOC as a consequence of progressed soil development (Graf-Rosenfellner et al., 2016). The structure (biodegradability) and size of SOC—as well as other soil properties, such as water content, oxygen supply, soil texture, poorly crystalline minerals, soil pH, available N, P, and S—control the community size and activity of soil microorganisms (Richter et al., 2018).

In the active flooding zone of the lower middle Elbe River, the vegetation cover is dominated by grasslands and hardwood floodplain forests (Brunotte et al., 2009; Jungmann et al., 2009). SOC storage in Elbe River floodplains is primarily driven by proxies for relief and sedimentation, such as soil texture (Heger et al., 2021). However, it is unclear to what extend fine texture also relates to stabilization of SOC to organomineral complexes. To determine the predominant drivers for SOC stabilization in Elbe River floodplain soils, we want to answer (1) what are the contributions of respective density fractions to SOC and (2) how soil properties affect SOC stabilization and mineralization. We used a simplified study design (with 8 floodplain study sites differing in micro-relief and vegetation cover) to answer these questions for a general perspective on soils of the active flooding zone of the lower middle Elbe River.

3.2 Material and methods

3.2.1 Study area

The study area is located at the lower middle Elbe River in northern Germany (Fig. 8). We selected 8 study sites in the active flooding zone of the lower middle Elbe River, of which 5 are located inside hardwood floodplain forests and 3 grasslands adjacent to these forests. The tree species composition of the forests is dominated by *Quercus robur*. Each study site covers an area of 625 m^2. To cover different hydrologic situations, the study sites were categorized into high and low relief position. Of the study sites, 2 grasslands are located in low and 1 in a high area; 2 forests (age: 104 and 144 years) are located in low and 3 (age: 18 to 186 years) in high areas. Floodplain soils in low areas are Gleyic or Fluvic Cambisols, Fluvic Gleysols, or Gleyic Fluvisols, usually fine textured with loam, sandy loam, or loamy sand.

Floodplain soils found in high areas are mostly sand-dominated Fluvic Arenosols or Fluvic Cambisols (Heger et al., 2021).
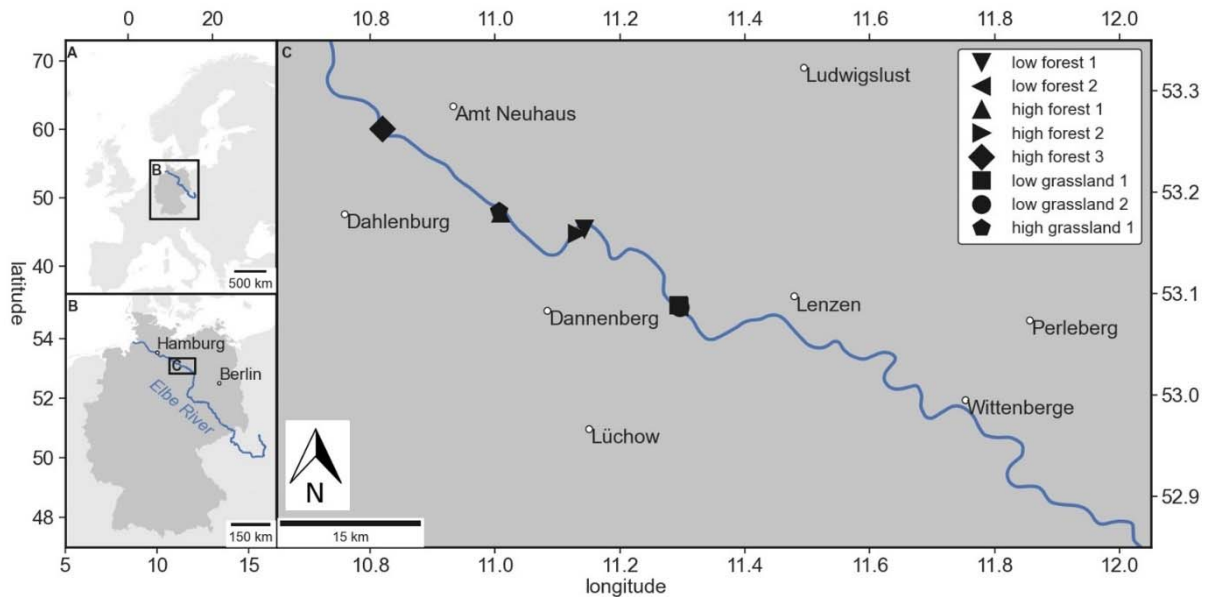
Fig. 8. Black markers indicate the 8 study sites locations in the active flooding zone of the Elbe River. Low and high are height indications of the study sites. The age of the forests ranged from 18 to 186 years.

3.2.2   Field sampling and laboratory analyses

At each study site, composite samples from 0–10 cm (topsoil) and from 10–30 cm (subsoil) were collected at 17 locations using a gouge auger. All samples were taken between March 4 and March 6, 2019, and were stored at -18°C until the analysis.

An aliquot of each soil sample was air-dried and sieved to < 2 mm. The pH was measured in 0.01 M $CaCl_2$ solution using a pH meter (MP230 GLP, Mettler Toledo, Germany). Electric conductivity (EC) was measured in a solid to solution ratio of 1:2.5. SOC content, organic carbon (OC) content of the fractions, nitrogen (N) content (in g kg^{-1}), and the ratio (C/N ratio) was determined using an elemental analyzer (vario MAX cube, Elementar, Germany). Samples with pH ≥ 6.5 were additionally tested for inorganic C content using a total organic carbon analyzer (soli TOC cube, Elementar, Germany). The sand fraction (63 μm–2000 μm) was analyzed by a vibratory sieve shaker (Vibro, Retsch GmbH, Germany), and the fine fraction (< 2 μm – < 63 μm) was analyzed using the sedimentation approach with Sedimat 4–12 (Umwelt-Geräte-Technik GmbH, Germany), according to DIN ISO 11277. The fine texture content is defined as the sum of clay and fine silt (< 6.3 μm, in %) (Table 1).

Table 1. Soil characteristics of the study sites.

	SOC (g kg^{-1})		N (g kg^{-1})		C/N ratio		pH[a]		EC[b] (µS cm^{-1})		fine texture[c] (%)	
	Mean	SD	Mean	SD	Mean	SD	Mean	SD	Mean	SD	Mean	SD
topsoil	41.86	24.55	3.55	2.13	11.9	0.6	5.2	0.3	72.88	45.37	28.33	18.67
subsoil	16.22	11.56	1.45	1.01	11.2	0.8	5.3	0.5	46.63	27.89	23.38	18.77

[a] measured in 0.01 M CaCl$_2$
[b] measured in a solid to solution ratio of 1:2.5
[c] sum of clay and fine silt fraction (< 6.3 µm)

3.2.3 Carbon mineralization and microbial parameters

For each sample, 3 analytical replicates were set to approximately 55% water holding capacity and weighed to 20 g dry mass in 500 cm^3 glasses fitted with a rubber stopper. The samples were stored in the dark at 22°C and were measured daily during the first 5 days and then with decreasing frequency. The total incubation time (t) comprised 258-259 days (start April 3, 2019). The CO_2 concentration was measured using a gas chromatograph (Agilent 6890 Gaschromatograph, Aglient, USA). If the CO_2 concentration inside an incubation glass exceeded 3%, the glass was flushed with synthetic air. The amount of produced CO_2 was corrected by the share in dissolved in water based on the Henry's law constant (Sander, 2015).

The potentially mineralizable C (C0, in % SOC) and the mineralization rate constant for SOC (k, in day^{-1}) were evaluated by applying a one-component exponential function to the cumulative mineralization (Zhang & Zhou, 2018):

$$C_{min}(t) = C_0 \times (1 - e^{-k \times t}) \tag{5}$$

Where C_{min} is the cumulative mineralized SOC after time t. The k shows the C proportion released per day (e.g., 0.005 day^{-1} = 0.5% C day^{-1}).

Initial respiration (basal respiration) and substrate induced respiration (SIR) rates were determined using a respirometer (BSBdigi Selutec GmbH, Deutschland) according to DIN 14240-2 by using the amount of effluent CO_2, which was precipitated as CO_3^{2-} with NaOH inside the absorbers after 24 hours. The amount of effluent CO_2-C was converted with the used HCl during titration and unneutralization of $NaCO_3^{2-}$ with $BaCl_2$ (Wildung et al., 1975).

Soil microbial biomass (absolute C_{mic}, in g kg dry soil^{-1}; relative C_{mic}, in % SOC) and metabolic quotient (qCO_2, in µg CO_2-C d^{-1} mg C_{mic}^{-1}) were evaluated according to the methods described in DIN 14240-2 and DIN 16072: absolute C_{mic} was evaluated from SIR with constants according to Kaiser et al. (1992). The qCO_2—the ratio of basal respiration rate to C_{mic}— indicates mineralization efficiency of microorganisms (Anderson & Domsch, 1993; Wardle & Ghani, 1995).

3.2.4 Density fractionation

A density fractionation was conducted following Golchin et al. (1994) and Viret and Grand (2019) using sodium polytungstate (SPT-2, TC-Tungsten Compounds, Germany) with a density of 1.62 g cm^{-3}. 50 ml SPT was added to 10 g dry soil sample and then centrifuged to separate the free light fraction (fLF) from the sample. The floating fLF was decanted, filtered (filter size 0.45 µm) under vacuum, and washed with deionized water until the electric conductivity was below 50 µS. To separate the oLF and HF, another 50 ml SPT were added to the sedimented material and sonicated with 280 J m^{-1}. After this step, the sample was centrifuged and the oLF could be retrieved following the method described above for the fLF. The remaining sample was then centrifuged until the supernatant was clear. The sedimented material—containing the HF—was washed with deionized water and centrifuged until the conductivity was < 50 µS. The fLF, oLF, and HF masses were weighed and OC and N contents were analyzed.

3.2.5 Statistical analyses

We used Python v3.7.9 (Van Rossum & Drake, 2009) for univariate regression analyses, one-way analysis of variance (ANOVA) (with post-hoc tests), and t-tests as well as Pearson (r_P) and Spearman (r_S) correlation. For ANOVA, Tukey HSD post-hoc comparison was used to identify significant differences between the density fractions. Variance homogeneity was tested using Levene's test ($p < 0.05$) and residuals were checked for normality using the Shapiro-Wilk test ($p < 0.05$). In case of heteroscedasticity, a Welch-ANOVA was performed instead, and comparisons were conducted using pairwise t-tests. For the pairwise t-test, pair differences were checked for normality using the Shapiro-Wilk test

(p < 0.05). In case of significance, a Wilcoxon pairwise t-test was performed instead. Significance codes are ' *** ' for p < 0.001, ' ** ' for p < 0.01, ' * ' for p < 0.05, and ' . ' for p < 0.1.

3.3 Results

3.3.1 Contributions of density fractions to SOC

The recovery of the contributions of density fractions to SOC was 93.46 ± 13.53%. The HF was the most important SOC pool at both depth intervals (Fig. 9). In the topsoil, the contribution of each fraction to SOC decreased in the order HF > oLF > fLF (Table 2). In the subsoil, the contributions of fLF and oLF to SOC did not differ (p > 0.05). From top- to subsoil, the contribution of the oLF to SOC decreased (p < 0.01) by 63% and the contribution of the HF to SOC increased weakly (p < 0.1) by 19%. Depth-differences of the fLF were not significant (p = 1.00).
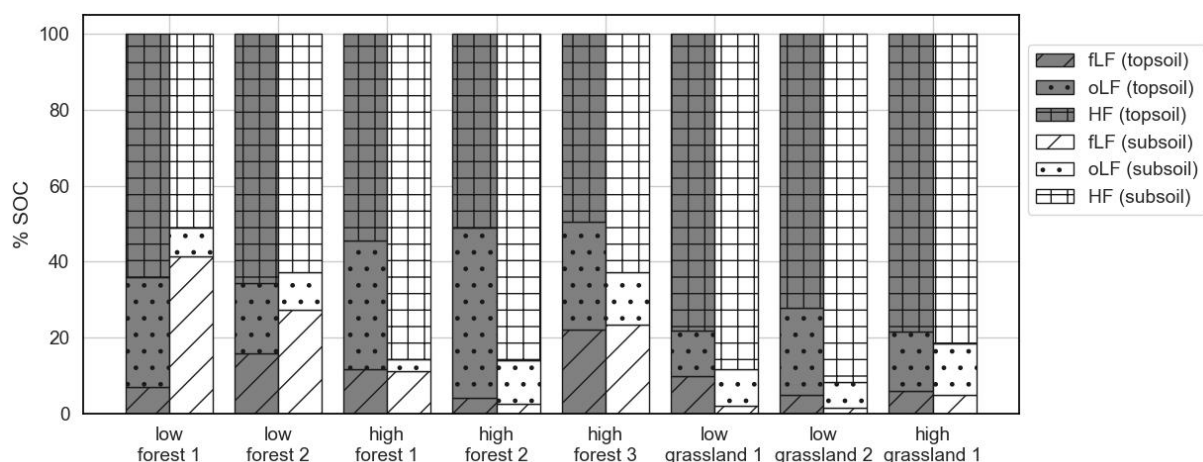
Fig. 9. Contributions the free light fraction (fLF), occluded light fraction (oLF), heavy fraction (HF) to total SOC (in % SOC) in top- (0–10 cm) and subsoil (10–30 cm). Depth differences were not significant for fLF, significant for oLF (p < 0.01), and weakly significant for HF (p < 0.1).

The average mass recovery of the samples after density fractionation was 97.94 ± 2.56%. Differences between the SOC contents of recovered SOC and total soil SOC where not significant at both depth intervals. Total SOC content decreased by 61% with depth (p < 0.01) (Table B 1). The OC contents of the fractions differed significantly between both depths only in the HF, where it decreased (p < 0.01) by 55% with depth. The OC content of the HF was smallest at both depth intervals (Table 2). In the topsoil, OC content of the oLF

fraction was largest. The C/N ratios of the fLF and oLF increased ($p < 0.001$) by 26% and 22% but did not change for the HF.

The absolute contribution (g kg^{-1} soil) of the HF to SOC was largest at both depth intervals (Table 2). The absolute fractions sizes decreased with depth.

Table 2: OC and N content (in g kg^{-1} fraction), and C/N ratio in fraction as well as absolute (in g kg^{-1} soil) and relative (in %) contribution of fraction to SOC. Depth specific (topsoil: 0–10 cm; subsoil: 10–30 cm) significant differences according to ANOVA with Tukey post-hoc comparison are annotated with letters.

Depth (cm)		OC (g kg^{-1})		N (g kg^{-1})		C/N		SOC (g kg^{-1})		SOC (% SOC)	
		Mean	SD	Mean	SD	Mean	SD	Mean	SD	Mean	SD
top-soil	fLF	234.35a	29.67	13.91a	2.55	17.1a	1.9	3.66a	2.28	10.24a	6.23
	oLF	305.36b	46.69	21.14b	2.58	14.5b	1.8	8.81a	4.27	25.64b	10.66
	HF	26.24c	16.75	2.58c	1.73	10.2c	1.2	25.39b	15.52	64.12c	11.61
sub-soil	fLF	204.65a	43.14	9.67a	2.39	21.5a	2.9	1.84a	2.14	14.32a	14.80
	oLF	307.06a	137.77	14.13a	6.20	21.0a	4.7	1.40a	0.81	9.53a	3.65
	HF	12.13b	10.06	1.31b	1.13	9.6b	1.8	11.97b	10.00	76.15b	15.12

3.3.2 Contributions of mineralizable C and microbial biomass to SOC

The mineralizable carbon (C0) correlated ($p < 0.05$) to mineralized carbon after 258 and 259 days (C_{min}) at both depth intervals (Fig. B 1). C_{min} was 5.4 ± 0.72% in the topsoil and 4.38 ± 0.80% in the subsoil. C0 (% SOC) was 13% larger ($p < 0.05$) in the topsoil compared to subsoil. C_{mic} ranged between 0.98 to 5.26% (corresponding to 0.6 to 2.83 g kg^{-1}) in the topsoil and between 1.42 and 8.82% (corresponding to 0.23 and 0.84 g kg^{-1}) in the subsoil (Fig. B 2 and Table 3). The mineralization rate constant (k), C_{mic} (in % SOC), and qCO_2 did not differ between both depth intervals. The absolute contributions of C0 and C_{mic} (g kg^{-1} soil) were greater ($p < 0.05$) in the topsoil compared to the subsoil (Table B 1).

Table 3. Mineralizable carbon (C0) and microbial biomass (C_{mic}) in relative (per SOC) and absolute (per soil) amount. k is the mineralization rate constant and qCO_2 is the metabolic quotient for both studied depths.

	C0 (g kg^{-1})		C_{mic} (g kg^{-1})		C0 (% SOC)		C_{mic} (% SOC)		k (day^{-1})		qCO_2 (mg CO_2-C day^{-1} gC_{mic}^{-1})	
	Mean	SD	Mean	SD	Mean	SD	Mean	SD	Mean	SD	Mean	SD
top-soil	2.67	1.27	1.48	0.87	6.75	1.33	3.66	1.22	0.006	0.002	28.22	20.15
sub-soil	0.88	0.49	0.53	0.23	5.97	1.49	4.11	2.29	0.005	0.001	17.44	11.13

3.3.3 Effects of soil properties on SOC density fractions

Fine texture had a positive effect on the HF of SOC in the topsoil (Fig. 10, G). The contribution of oLF to SOC was negatively related to fine texture at this depth interval (Fig. 10, D), showing that occlusion of the LF decreases fine texture. The contribution of C_{mic} to SOC and the C/N ratio had no direct effect on the SOC density fractions. In the topsoil, the contribution of the HF to SOC was weakly positively related to the absolute C_{mic} contents ($p < 0.1$) according to r_P (Fig. B 3). The absolute contributions (g kg^{-1} soil) of HF to SOC were positively related ($p < 0.05$) to fine texture, SOC content and SOC stocks and negatively related ($p < 0.05$) to bulk density (Fig. B 3 and Fig. B 4).
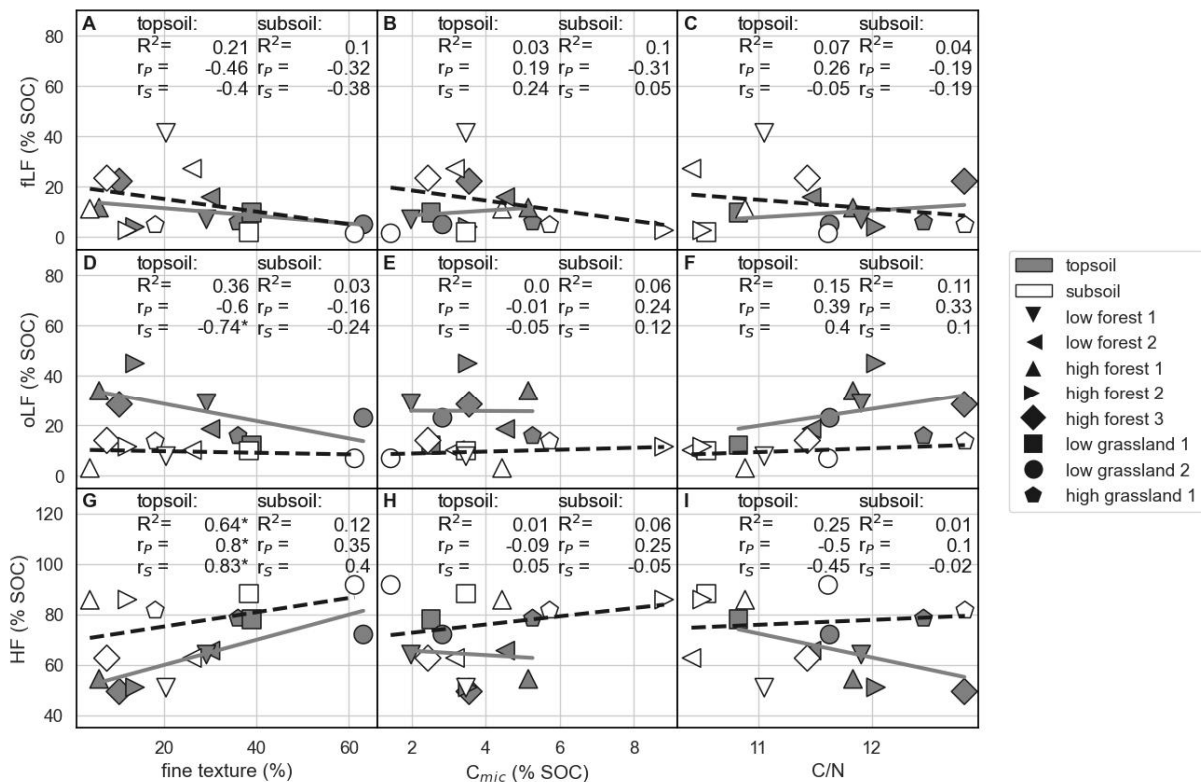
Fig. 10. Contributions the free light fraction (fLF), occluded light fraction (oLF), heavy fraction (HF) to total SOC (in % SOC) vs. fine texture (< 6.3 μm), microbial biomass per SOC (C_{mic}), and C/N ratio. The line indicates linear regression between variables in x and y (solid: topsoil (0–10 cm); dashed: subsoil (10–30 cm)).

3.3.4 Effects of fine texture and density fractions on SOC mineralization

Fine texture had a negative effect on C0 at both depth intervals, indicating that soils with a high fine texture content contain less mineralizable carbon (Fig. 11, A). C0 was unaffected by the oLF pool (Fig. 11, C). In the topsoil, the relative fLF pool increased (Fig. 11, B) and HF pool decreased (Fig. 11, D) with increasing C0. Thus, high contents of C0 in the

topsoil were mainly related to fLF pools, whereas SOC might be protected in the HF here. In the subsoil, relations between C0 and the contributions of the density fractions to SOC were mostly negligible. C0 (in % SOC) was unaffected ($p > 0.1$) by pH, C/N ratio, and qCO_2 (Fig. B 3 and Fig. B 4).
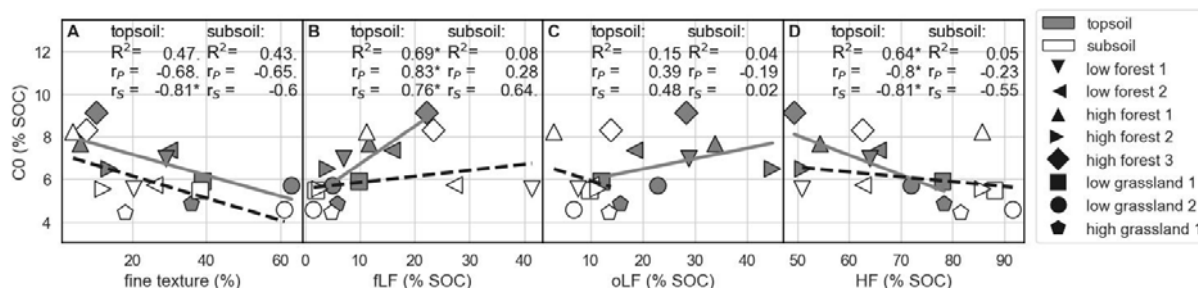
Fig. 11. C0 (mineralizable carbon) vs. contributions the free light fraction (fLF), occluded light fraction (oLF), heavy fraction (HF) to total SOC (in % SOC). The line indicates linear regression between variables in x and y (solid: topsoil (0–10 cm); dashed: subsoil (10–30 cm)).

The mineralization rate constant (k) was positively related to C/N in the fLF and oLF at both depth intervals (Fig. 12), though in the subsoil, the relation to fLF was weak ($p < 0.1$). Thus, high C/N ratios of the light fractions of SOC have positive effects on mineralization rate.
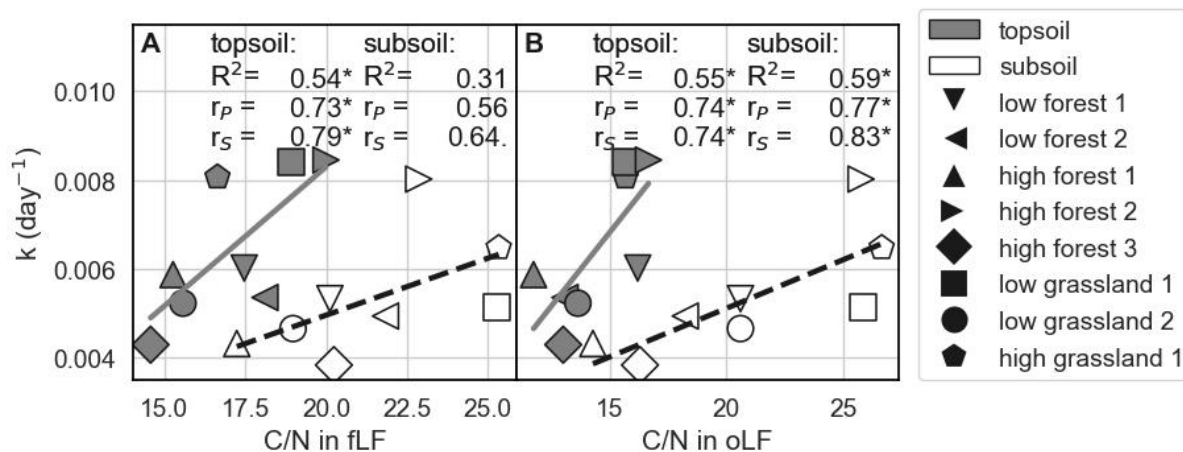
Fig. 12. The k (mineralization rate constant) vs. C/N in the free light fraction (fLF) and in the occluded light fraction (oLF). The line indicates linear regression between variables in x and y (solid: topsoil (0–10 cm); dashed: subsoil (10–30 cm)).

3.3.5 Effects of available SOC on qCO₂

The metabolic quotient (qCO_2) was negatively related to the relative contribution of C_{mic} to SOC in the topsoil, and an exponential fit explained 66% of variance in qCO_2 (Fig. 13). This indicates that metabolic respiration efficiency is related to SOC availability at this depth.
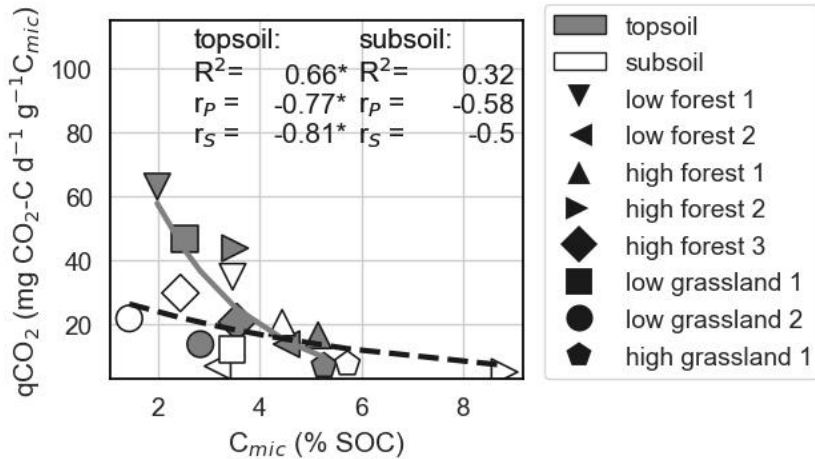
Fig. 13. Metabolic quotient (qCO_2) vs. the contribution of microbial biomass (C_{mic}) to SOC. The lines indicate exponential fit between the variables in x and y (solid: topsoil (0–10 cm); dashed: subsoil (10–30 cm)).

3.4 Discussion

3.4.1 Components of SOC in floodplains of the lower middle Elbe River

With 64%, HF was the largest SOC pool in the Elbe floodplain topsoils, and further increased with depth (76%) (Fig. 9 and Table 2). The oLF pool decreased from 26 to 10% with depth. The fLF pool did not change with depth, with 10% in top and 14% in the subsoil. Recoveries were similar to other studies (Cerli et al., 2012; Kreyling et al., 2013; Mayer et al., 2019).

The relative contribution of the HF to SOC (Table 2) was in the same magnitude as in subsoils of floodplain grasslands (of 55 to 91%) and top and subsoils hardwood floodplain forests (of 84 to 97%) in Germany and Austria (Graf-Rosenfellner et al., 2016; Mayer et al., 2019). Similar topsoil contributions of the LFs (fLF and oLF) to SOC (of up to 50%) have also been found in mollic fluvisols of the Elbe River (Rennert et al., 2018) and also in hardwood floodplain forests at the Danube River (Graf-Rosenfellner et al., 2016). The contributions of the LFs in the topsoil of the current study was also similar to topsoils of different land use types in Europe of 30 ± 16% (Schrumpf et al., 2013). The absolute SOC pool size of the HF (g kg⁻¹ soil)

of the current study was similar to topsoils of Danube hardwood floodplain forests and floodplain grasslands in southern Germany and Austria (Graf-Rosenfellner et al., 2016; Mayer et al., 2019). In the subsoil, the absolute LF pools were larger compared to those in subsoils of the Danube hardwood floodplain forest in floodplain grasslands of southern Germany. This could be because their total SOC content (up to 22.30 g kg^{-1}) was smaller than ours (up to 40.56 g kg^{-1}) at this depth interval. However, in general, the contributions of the SOC density fractions were similar to other German and Austrian floodplains but also to other ecosystems.

In the current study, the relative and the absolute C_{mic} content (Table 3) were above topsoils of eutric and mollic floodplains soils of the Elbe River (Rinklebe & Langer, 2006). C_{mic} contents were similar to Fluvisols of a pasture floodplain in Western Mongolia of 0.82 g kg^{-1} and 4% SOC (Goenster et al., 2017). They were also similar to lowland flooding-affected paddy soils, which contain C_{mic} twice as high as in upland soils (Wei et al., 2022). This high C_{mic} content can occur from a larger availability of SOC, slower microbial turnover due to oxygen scarcity, a high C assimilation efficiency (Wei et al., 2022). These processes may have caused the C_{mic} contents of the current study to be higher than of eutric and mollic Elbe River floodplain soils.

3.4.2 Factors affecting mineralization and stabilization of SOC in top- and subsoil

Progressed soil development with depth is indicated by narrower C/N ratios due to a higher contribution of more processed C and depletion in energy-rich plant material (Krishna & Mohan, 2017; Rumpel & Kögel-Knabner, 2011). The narrower soil C/N ratio with depth was also found in our study (Table 1). Depth differences in absolute SOC pool sizes (in g kg^{-1} soil) can be related to direct input of fresh plant detritus (e.g., leaves, roots) into the topsoil. The relative contribution of fLF to SOC did not differ between the depths (Table B 1). However, the contribution of HF increased weakly ($p < 0.1$) and that of oLF to SOC decreased ($p < 0.01$) with depth, suggesting that physical protection in aggregates is less important in the subsoil compared to SOC stabilization in organomineral associations. Thus, top- and subsoil differences of SOC pools are mostly reflected in oLF and HF contributions.

The abundance of roots, coal and lignite affect OC contents of the LFs. The OC content in the HF is often affected by dissolved C translocation processes (Schrumpf et al., 2013). This translocation process could have affected the decrease in OC of the HF with depth (Table 2) as floodplain soils are generally characterized by a strong soil moisture dynamic (Yin et al., 2019). The OC contents of the fractions were within the magnitude of topsoils and subsoils of floodplain grasslands in Germany (Mayer et al., 2019). The fLF and oLF—consisting of particulate organic matter—often have similar OC contents (Cerli et al., 2012). However, in the topsoil of the current study, the OC content in the oLF was larger compared to the fLF (Table 2). Also, the C/N ratio was smaller in the oLF compared to the fLF (Table 2). This has also been found in other forest ecosystems and could indicate an increased occlusion of already processed SOC (Griepentrog et al., 2014; Wagai et al., 2009). This occluded processed SOC could have been created by earthworms (Bossuyt et al., 2005), is of allochthonic origin (e.g., riverborne organomineral flocs or eroded material) (Graf-Rosenfellner et al., 2016; Marttila & Kløve, 2015), or contains a large amount of microbial biomass (Wagai et al., 2009). Our finding contradicts with previous results of mollic Elbe River floodplain soils, where oLF mostly consisted of recalcitrant charcoal with a wider C/N ratio (Rennert et al., 2018). However, C/N ratios in LFs of our study increased from top- to subsoil, which indicates a stronger abundance of recalcitrant organic matter in the subsoil. This finding would be again in agreement with other German floodplains (Mayer et al., 2019; Rennert et al., 2018) and is supported by the finding that C0 is significantly smaller in the subsoil (Table 3 and Table B 1). Thus, low density recalcitrant SOC seems to play a more important role in the subsoil, than in the topsoil.

C storage in floodplain soils is often associated with stabilization through adsorption to fine soil particles (Deiss et al., 2017) or preservations by oxygen scarcity (Hennings et al., 2021). In the current study, a positive relation between the contribution of the HF to SOC to fine texture was found in the topsoil (Fig. 10, G), which indicates stabilization of SOC to fine soil particles, such as clay and fine silt. The positive correlation of absolute contribution of the HF to SOC and fine texture (Fig. B 3 and Fig. B 4) supports this finding. An increase of the HF to SOC with fine texture was also found in topsoils of ecosystems differing in land use types

(Schrumpf et al., 2013). In the topsoil, fine texture also seems to decrease the contribution of the oLF to SOC (Fig. 10, D). This could be due to aggregate degradation, followed by incorporation of the C into organomineral complexes (Wagai et al., 2009). We could not indicate any significant factors stabilizing SOC into density fractions in the subsoil (Fig. B 4). In the subsoil, other factors, such as oxygen scarcity, could have preserved SOC pools (Hennings et al., 2021). Nevertheless, at both depth intervals, a negative relation of C0 to fine texture was found in the current study (Fig. 11), which supports the argument fine texture is the main driver SOC stabilization at both depth intervals.

Microbial mineralization of SOC is largely controlled by the microbial community composition, the availability of nutrients (e.g., N, P, S, C), physical and chemical soil conditions (e.g., temperature, moisture, pH) and their interaction with the soil matrix (Basile-Doelsch et al., 2020). In the current study, mineralization rate constant (k) was not directly related to most physical and chemical soil properties (Fig. B 3 and Fig. B 4). However, k was positively related to C/N ratios in the fLF and oLF (Fig. 12), which suggests that microbial mineralization is mainly related to the quality of the light fractions of SOC. This relation was also found in other ecosystems (Schrumpf et al., 2013). Our finding shows that the light fractions are important energy sources for microbial mineralization.

The amount of total available C is an important energy source for microbial metabolic efficiency (Basile-Doelsch et al., 2020). A similar negative relation of qCO_2 to C_{mic} (% SOC)—as in the current study (Fig. 13)—has also been found in floodplains in Mongolia and pasture floodplains in England, UK (Cressey et al., 2018; Goenster et al., 2017). This relation was also found in saline coastal soils of Bangladesh (Iqbal et al., 2016). It shows that mineralization efficiency is positively related to the amount of available SOC for C_{mic}. No relation between qCO_2 to the density fractions of SOC was found (Fig. B 3 and Fig. B 4), which could indicate that the contributions of the fractions to SOC do not affect mineralization efficiency. This could be because, in floodplains, the activity of microorganisms is strongly affected by soil moisture (Yin et al., 2019). This effect may have also caused qCO_2 to be unaffected by available SOC

in the subsoil (Fig. 13). Nevertheless, in the topsoil, available SOC (regardless of density fractions) for C_{mic} explained around 66% of variance in qCO_2.

In floodplains, SOC can relate strongly to relief position and vegetation composition due to dynamics in allochthonic and autochthonic C input (Giese et al., 2003; Swinnen et al., 2020). We did not study the effect of leaf litter input on SOC stabilization directly. However, compared to the C/N ratio of oak leaf litter in a floodplain forests of 42.7 (Lorencová, 2007), our top- and subsoil C/N ratios (11.9 ± 0.6 and 11.2 ± 0.8) are very low. This could indicate that most fresh plant litter in the soil is already processed or mineralized and that autochthonic C input only plays a minor role for SOC stabilization. The finding that low quality of plant litter is the most important energy source for microbial mineralization (Fig. 12) supports this finding. Our results showed that SOC stabilization relates strongly to fine texture, explaining about 64% of variance in the contribution of the HF to SOC (Fig. 10). Fine soil texture can be a proxy for flooding and sedimentation dynamics in floodplains (Cierjacks et al., 2011; Drouin et al., 2011). This implies that relief might be a major factor for SOC stabilization on floodplains of the lower middle Elbe River.

3.4.3   Implications of human impacts on SOC stabilization in floodplains

Anthropogenic landscape modifications—such as clearing, dike building and channelization—have affected the natural flooding regime of floodplains. Thus, today, two thirds of the floodplain area in Germany is unaffected from flooding and sedimentation because it is located behind a dike, i.e. in the former flooding zone (Brunotte et al., 2009). Additionally, effects of climate change on precipitation, evapotranspiration, and snow-melt may lead to more river water discharge in the winter and less river water discharge in the summer, which would cause increased soil erosion and decreased sedimentation (Middelkoop et al., 2001). This may result in a decreased SOC stabilization potential in floodplains.

3.5   Conclusion

SOC stabilization in Elbe River hardwood floodplain forests and floodplain grasslands was mainly controlled by fine texture. The contributions of the density fractions to SOC were similar to those reported for other temperate floodplain soils in Germany and Austria, where SOC was also dominated by the HF. In the topsoil, mineralizable C increased with the contribution of the fLF and decreased with the contribution of the HF to SOC. In the topsoil the contribution of the HF to SOC was related to fine texture (< 6.3 µm) and, at both depth intervals, the amount of mineralizable C was related negatively to fine texture. Both results indicated progressed stabilization due to fine texture content. qCO_2 was related to the amount of available SOC in the topsoil, but no relation was found in the subsoil. As water table depth fluctuations in floodplain soils are dynamic and controlled by the river, SOC protection by oxygen scarcity might play a more important role in the subsoil compared to the topsoil. However, in top- and subsoil, mineralization rate was positively related to C/N ratios of both light fractions (fLF and oLF), which indicated that high contents of energy rich fresh plant litter is important for microbial mineralization. Our results highlight the importance of fine texture and litter quality for SOC stabilization and mineralization estimates and floodplain forest management. Fine texture, as proxy for flooding and sedimentation, indicated that relief position might be a major factor controlling SOC stabilization on floodplains. Thus, anthrophonic changes to the natural flooding regime as well as climate change affected erosion and sedimentation properties could have severe impacts on SOC stabilization potential of floodplains.

4 Article III: Soil texture and pH affect soil CO_2 efflux in hardwood floodplain forests of the lower middle Elbe River

4.1 Introduction

Floodplain ecosystems play a significant role in the global carbon (C) cycle (Battin et al., 2009; Cole et al., 2007). In these ecosystems, soil organic carbon (SOC) has been acknowledged to be the largest organic C pool (Sutfin et al., 2016). Natural hardwood floodplain forests have particularly strong SOC sequestration potential due to autochthonic and allochthonic inputs from vegetation and flood induced sedimentation (Dybala et al., 2019; Lininger et al., 2018). C inputs are usually in an approximate balance with losses due to erosion and soil CO_2 efflux—through autotrophic root respiration and heterotrophic soil organic matter decomposition in the litter layer and soil (Melack & Engle, 2009). However, today, this balance is often disrupted because forests are cleared, managed or situated behind a dike, i.e. in the former flooding zone (Brunotte et al., 2009). Many hardwood floodplain forests have thereby lost their natural ecosystem functions, such as C retention, biodiversity and flood risk regulation (Hornung et al., 2019). Additionally, a heterogenic relief and periodic flooding affect metabolic and biogeochemical processes dynamically (Wilson et al., 2011). Therefore, it is difficult to understand how C loss through soil CO_2 efflux affects the C balance in hardwood floodplain forests (Valett et al., 2005). Understanding the effect of spatial and temporal dynamics on soil CO_2 effluxes in hardwood floodplain forests, would improve Earth System Models for climate change scenarios (Pfeiffer et al., 2017; Sutfin et al., 2016).

The most important drivers of temporal changes in soil CO_2 efflux are soil temperature and moisture (Davidson et al., 1998). Soil CO_2 efflux from soil and litter is usually positively related to soil temperature and mainly caused by heterotrophic respiration, where its magnitude depends on characteristics of the microbial community composition, and availability of SOC and nutrients (Fang & Moncrieff, 2001). Seasonal changes in temperature affects

autotrophic respiration due to C allocation patterns of trees, where C is directed downwards during late phases of summer and directed upwards in shoot extension phases (Fan & Han, 2018). Because the soil is usually under drought stress during summer and moist and cold during winter, the effects of soil moisture and temperature on soil CO_2 efflux co-vary during the season (Davidson et al., 1998). Soil CO_2 efflux is limited at high and low soil moisture (Tang & Baldocchi, 2005). Low soil moisture restricts the metabolic activity of roots and microbes due to a lack of soil water and dissolved organic matter. High soil moisture inhibits oxygen accumulation, caused by the water-filled pore space, which is needed for aerobic soil organic matter decomposition (Luo & Zhou, 2006). Due to inundation on floodplains, abrupt changes in soil moisture can cause shifts in microbial community structure and thereby affect soil respiration and enzymatic degradation rates (Wilson et al., 2011). Additionally, natural seasonal changes in soil moisture and temperature can have significant effects on soil CO_2 efflux (Janssens & Pilegaard, 2003).

On floodplains, microbial communities are adapted to relief-affected local moisture regimes, and the related variabilities of oxygen availability, soil pH, SOC and nutrient pool, and soil texture (Chen et al., 2014; Yin et al., 2019). Fine soil particles can physically protect SOC from decomposition by stabilization within aggregates and organomineral associations (Deiss et al., 2017). These particles can also retain water and nutrients better than sandy soils, which are important for SOC decomposition (Hamarashid et al., 2010). Also, root respiration can be smaller in clay-rich compared to sandy soils because low bulk densities lead to a smaller fine root density and autotrophic respiration decreases with root diameter (Tang et al., 2020). On floodplains, a micro-relief-driven heterogeneous soil texture distribution is very common (Drouin et al., 2011), which could have strong effects on the variability of soil CO_2 efflux. Due to flooding and relief-affected soil properties, soil CO_2 effluxes comparable to deserts (160 gC m^{-2} y^{-1}) up to rates comparable to tropical forest (> 1205 gC m^{-2} y^{-1}) can occur in a single floodplain ecosystem (Doering et al., 2011).

In hardwood floodplain forests, metabolic and biogeochemical processes that contribute to soil CO_2 efflux are controlled by dynamic changes in temperature and soil

moisture as well as relief-affected vegetation composition and availability of SOC and nutrients (Acosta et al., 2017; Chen et al., 2014; Cierjacks et al., 2010). At the Elbe River, SOC stocks are largely affected by natural and anthropogenic modified relief and related proxies, such as pH, hydromorphic features, soil texture, and the carbon to nitrogen ratio (Heger et al., 2021). To understand if soil CO_2 efflux is similarly affected by relief position, we measured soil CO_2 efflux and its driving factors during one year in 6 hardwood floodplain forests along the lower middle Elbe River, differing in relief (high and low) and flooding zone (active and former). We aim to (1) quantify the total annual soil CO_2 efflux, (2) characterize the effects of seasonal changes in soil temperature and moisture, (3) and determine the effects of soil properties, such as pH, N and SOC content and texture, on soil CO_2 efflux.

4.2 Material and methods

4.2.1 Study sites and categorization

The study area is located at the lower middle Elbe River in northern Germany (Fig. 14).

We selected 6 hardwood floodplain forests dominated by *Quercus robur*. The forests were

between 18 and 186 years old (Shupe et al., 2021). Each study site within the forests covered

an area of 625 m^2. The study sites were selected avoiding border effects (e.g., anthropogenic

disturbance, drainage) and had homogenous relief, vegetation cover, and soil characteristics,

respectively. To cover different hydrologic situations, the study sites were categorized into high

and low relief position in the active and former (situated behind a dike) flooding zone of the

Elbe River. The former low I (seepage) forest is hydrologically connected to the Elbe River

through seepage water inflow, whereas the former low II (disconnected) forest is located

adjacent to tributaries of the Elbe River (Sume-Konauer Graben and Sumter See), and is

unaffected from Elbe River water table fluctuations.
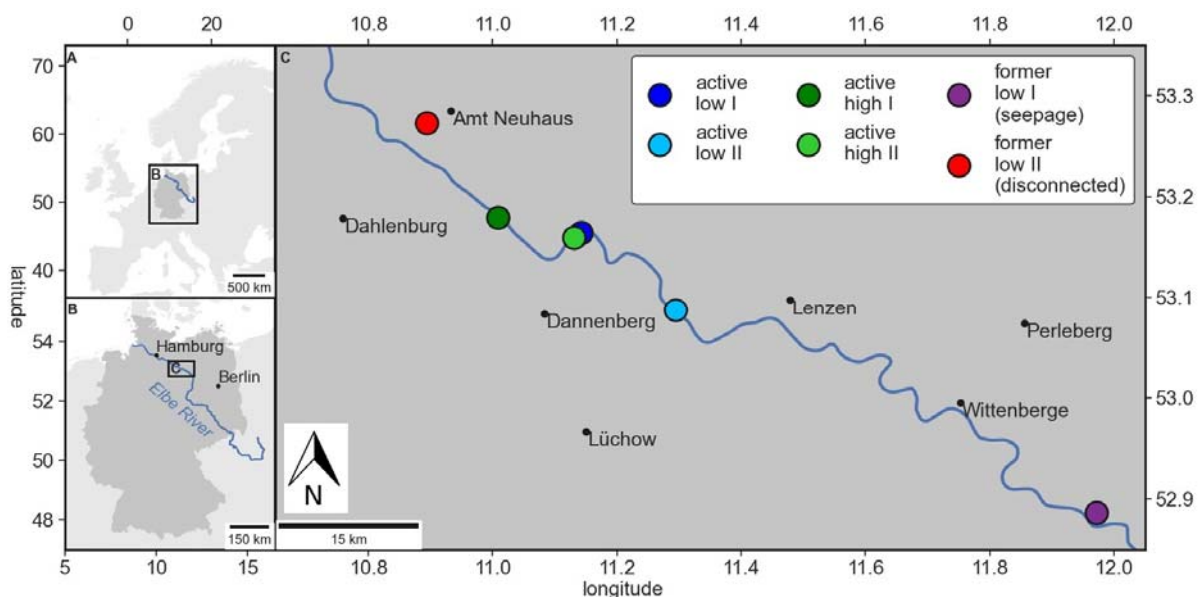
Fig. 14: Location of hardwood floodplain forest study sites. Low and high are height indications of the study sites. The forests are between 18 and 186 years old. The forests are either located in the active or former flooding zone of the Elbe River. The former low forest I is located behind a dike and affected from Elbe River water table fluctuations through seepage water inflow, from which former low II (disconnected) is unaffected.

4.2.2   Assessment of soil properties

At each study site, three soil profiles—evenly distributed over the site—were characterized and sampled between September 2018 and May 2019. The reference soil groups were characterized after IUSS Working Group WRB (2015) (Table C 1). Soil properties, such as SOC, nitrogen (N) content, their ratio (C/N ratio), pH (in 0.01 M $CaCl_2$), and contents of each texture fraction, were determined according the methods described in Heger et al. (2021). Horizon-wise weighted mean values of the texture fractions, SOC, N, C/N ratio, and pH, and the sum of SOC stocks (t ha^{-1}) were evaluated until 1 meter below soil surface (Table 4). The former low forest II is distinct from the other sites in texture class, with a fine texture content (sum of clay and fine silt, < 6.3 µm, in %) of > 50%, whereas active high forest I, is a rather sandy site with fine texture contents of < 5%. All other sites have intermediate fine texture contents and are loamy soils. Electric conductivity (EC) was measured in a solid to solution ratio of 1:2.5. To study the effects of hydromorphic features, we recorded the depth up to 2 m below the soil surface of each soil profile with the first appearance of hydromorphic mottling, i.e., where redoximorphic features covered an area of > 5% of the soil horizon according to Ad-hoc-AG Boden (2005), referred to as "hydromorphy" (m). In soil profiles where we did not find hydromorphic features until 2 m, we set the depth to 2 m, assuming that processes that contribute to hydromorphic mottling starts close to this depth.

Table 4: Displayed are means and the sum (for SOC stocks) for 1 m soil below the soil surface. Significant differences according to ANOVA with Tukey post-hoc comparison are annotated with letters.

Site	Soil Profile	Clay (%)	Silt (%)	Sand (%)	Fine texture[a] (%)	SOC stocks (t ha^{-1})	SOC (g kg^{-1})	N (g kg^{-1})	C/N ratio	pH[b]	Hydro-morphy[c] (m)
JB1	P1	13.05	21.04	65.91	16.89abc	93.85	7.6	0.8	9.5	5.9	0.15
	P2	10.22	15.66	74.12	12.98abc	93.05	7.9	0.7	11.5	5.4	0.09
	P3	14.24	27.51	58.25	18.43abc	104.73	9.3	0.8	10.5	5.1	0.20
LS1	P1	18.61	33.37	48.02	25.07b	168.56	15.3	1.4	10.0	5.4	0.18
	P2	13.63	21.03	65.34	17.53b	127.29	11.7	1.2	8.4	5.1	1.08
	P3	15.09	25.78	59.13	19.80b	193.44	17.5	1.6	8.6	5.7	0.50
JW1	P1	3.67	6.16	90.18	4.95c	43.75	3.2	0.3	10.6	5.9	2.00[d]
	P2	1.32	2.02	96.66	2.12c	40.39	3.3	0.3	7.9	5.6	2.00[d]
	P3	1.93	2.43	95.65	2.89c	71.27	6.2	0.6	8.0	5.6	1.20
JB3	P1	14.45	18.60	66.95	18.38ab	76.46	5.7	0.7	7.3	5.3	0.45
	P2	30.13	35.06	34.81	37.86ab	88.89	6.2	0.8	7.1	5.5	0.60
	P3	19.95	27.97	52.08	25.43ab	101.90	7.9	0.8	9.1	5.0	0.39
LE1	P1	17.74	15.78	66.48	21.50b	107.96	9.0	0.8	10.0	4.5	0.50
	P2	20.98	19.84	59.19	25.80b	134.72	11.3	1.0	10.3	4.6	0.48
	P3	17.97	11.78	70.25	21.32b	86.66	6.8	0.7	9.0	5.6	0.42
SU1	P1	44.45	48.08	7.48	56.46d	136.73	11.2	1.3	7.8	4.3	0.38
	P2	48.41	44.82	6.76	60.26d	138.65	11.3	1.5	6.9	4.4	0.50
	P3	41.38	53.35	5.27	55.09d	151.34	11.8	1.2	8.5	4.6	0.30

[a] sum of clay and fine silt fraction (< 6.3 μm) [b] measured in 0.01 M CaCl$_2$; mean was calculated using the pH.
[c] defined as the first appearance of hydromorphic mottling—where redoximorphic features covered an area of > 5% of soil horizon according to Ad-hoc-AG Boden (2005)—below mineral surface.
[d] assumed 2 m

4.2.3   Site instrumentation

All soil profiles were equipped with volumetric water content and temperature sensors (CS650, Campbell Scientific, UK) in 10 cm depth. Hourly measurements were logged onto a data logger (CR300, Campbell Scientific, UK). At the active low II, active high I, active high II, and former low I forests, climate stations—consisting of air temperature and humidity sensors (CS215, Campbell Scientific, UK) and a rain gauge (Kalyx-RG, Campbell Scientific, UK)—were installed directly outside of the forest at each study site. At the former low I forest, the climate station was placed inside a glade. Climate data from the active high II forest was regarded as representative for active low I and from active high I for former low II due to their close proximity (Fig. 14). A data logger (CR1000, Campbell Scientific, UK) recorded the data hourly. At the active high I forest, a barometer (Baro-Diver DI500, van Essen Instruments, The Netherlands) measured air pressure hourly. Groundwater fluctuations were measured hourly at every study site using a submersible transducer (TD-Diver, DI801, van Essen Instruments, The Netherlands).

Mean air temperature ranged between 9.6 ± 7.8 °C and 10.6 ± 8 °C inside the forests
(Table 5). The mean annual precipitation (MAP) ranged between 443.8 and 552 mm and was
below the annual mean from 1991 to 2020 of Lüchow (Fig. 14) of 563 mm (Deutscher
Wetterdienst, 2022).

Table 5: General study site characteristics: Low and high are height indications of the study sites. The forests are
between 18 and 186 years old. The forests are either located in the active or former flooding zone of the Elbe River.
The former low forest I is located behind a dike and affected from Elbe River water table fluctuations through
seepage water inflow, from which former low II (disconnected) is unaffected.

Study site	ID	Relief	Flooding zone	Forest age[a] (years)	Litter layer[a] (tC ha^{-1})	Basal area[a] (m^2 ha^{-1})	MAP[b] (mm)	GW[c] (cm)	GW SD (cm)
active low I	JB1	low	active	104	4.03	34.03	443.8	221	45
active low II	LS1	low	active	144	2.87	28.78	552.0	363	83
active high I	JW1	high	active	186	2.44	41.00	459.5	397	74
active high II	JB3	high	active	18	3.17	12.07	443.8	287	37
former low I	LE1	low	former (seepage)	121	4.82	28.93	447.9	178	38
former low II	SU1	low	former (disconnected)	170	6.03	39.77	459.5	181	24

[a] mean forest age, litter layer C stock and basal area (Shupe et al., 2021)
[b] mean annual precipitation
[c] mean depth to water table from the soil surface with annual fluctuation, given as standard deviation (SD).

4.2.4 Soil CO$_2$ measurements and efflux calculation

To estimate the CO$_2$ efflux from the soil surface, we used the closed-chamber method,
where the rate of CO$_2$ concentration increase inside the chamber is used for CO$_2$ efflux
evaluation (Madsen et al., 2010). To conduct repeated chamber measurements at the same
location, we inserted cylindrical collars (PE-100, ThyssenKrupp Plastics GmbH, Germany)—
with 15 cm height and 50 cm diameter—3 cm into the ground during January 2020. Three
collars were inserted in a radius of 1 to 3 m from each of the 3 instrumented profiles at random
locations, so that each study site comprised 9 chamber measurement locations in total. During
measurement, a rubber ring was placed between chamber and collar as a gas-tight seal.

The cylindrical chamber is made up of transparent acrylic glass (XT, 5 mm, Röhm
GmbH, Evonik Industries, Germany) and has a dome-shaped top cover (Halbkugel aus
Acrylglas 500mm, HB Präsentationssysteme oHG, Germany). It has a diameter of 0.5 m and
a volume of 0.12 m^3. To conduct dark measurements, the chamber was wrapped in aluminum

foil, which was covered with white duct tape to minimize radiative heating. A fan (120 mm, be quiet! – Pure Wings 2, Listan GmbH, Germany) mixed the air inside the chamber. A non-dispersive infrared (NDIR) CO_2 sensor module K30 (Senseair, Sweden) measured the CO_2 concentration inside the chamber. Air temperature and relative humidity was measured by a temperature and humidity sensor (Adafruit Sensiron SHT31-D, Adafruit Industries, USA) and air pressure by a barometric pressure and altitude sensor (Adafruit BMP280, Adafruit Industries, USA) inside the chamber. All data was logged using a microcontroller (MEGA 2560 Rev3, Arduino.cc, Italy) equipped with a data logging shield (Adalogger FeatherWing, Adafruit, USA). This logging device together with a 12 Volt battery was placed on the outside of the chamber. During measurements, the data was additionally displayed on a 4.5 inch display module (Joy-IT SBC-LCD20x4, SIMAC Electronics GmbH, Germany), which was connected to and placed on top of the logging device.

The measuring period encompassed one full year of 366 days, from February 27, 2020 18:00 to February 27, 2021 17:00 (UTC). Soil chamber measurements were conducted monthly. Field trips were partially restricted due to the CoVid-19-pandemic. Consequently, measurements during March and April 2020 as well as in December and January 2021 were not possible at some sites. Before the measuring campaign started, we clipped herbaceous vegetation and tree seedlings inside the collars to measure exclusively CO_2 effluxes from bare soil and litter. Any vegetation that grew inside the collars afterwards, was carefully clipped back prior measurement. Chamber-placement-duration was 4 minutes per measurement.

According to the ideal gas law, temperature and pressure affect the CO_2 readings of NDIR gas analyzers in a stable volume. Furthermore, water vapor dilution affects the measurements; therefore, a correction was included in the calculations. The CO_2 sensor module K30 performs a temperature compensation using a built-in temperature sensor. Soil air pressure correction and corrections due to the water vapor dilution effect on the measured CO_2 concentrations were applied according to the methods described in Heger et al. (2020). Soil CO_2 efflux ($\mu mol\ m^{-2}\ s^{-1}$) was evaluated using the ideal gas law (Pérez-Priego et al., 2015):

$$soil\ CO_2\ efflux = \frac{(p - e_a) \times V_C}{R \times T_a \times A_C} \times \frac{\Delta\chi c}{\Delta t} \tag{6}$$

Where ($p-e_a$) represents the partial pressure of dry air, e_a is the partial pressure of water vapor, V_C is the chamber volume plus the respective air volume for each collar above the soil surface, R is the ideal gas constant (8.314 J mol^{-1} K^{-1}), T_a is the air temperature, and A_C is the soil area inside the collar. $\frac{\Delta\chi c}{\Delta t}$ is the CO_2 concentration gradient from 30 to 210 seconds after the chamber was placed onto the collar. We used linear regression (mean R^2 was 0.96 ± 0.06; median R^2 was 0.98) to evaluate the concentration gradient.

4.2.5 Analyses of soil temperature and moisture response of CO₂ effluxes

To evaluate the soil temperature (T, in °C) response of soil CO_2 effluxes, we used an exponential temperature model, with which we were also able to calculate Q_{10}. Q_{10} is a measure for the temperature sensitivity of soil CO_2 efflux per 10 °C temperature increase (Lloyd & Taylor, 1994):

$$T\ model = \beta_0 \times e^{\beta_1 \times T} \tag{7}$$

Q_{10} was calculated according to:

$$Q_{10} = e^{10 \times \beta_1} \tag{8}$$

Where β_1 was derived from Eq. (7). Equations with exponential expressions were log-transformed to estimate the coefficients by linear regression (cf. Tang and Baldocchi (2005)). To eliminate the effect of temperature on soil moisture (M, volumetric water content, in m^3 m^{-3}), soil CO_2 efflux was normalized (Hirano et al., 2003).

$$normalized\ soil\ CO_2\ efflux = soil\ CO_2\ efflux \times e^{\beta_1 \times (T_b - T)} \tag{9}$$

Where T_b is the base temperature, which was set to 10°C. We then fitted a quadratic soil moisture function (Mielnick & Dugas, 2000):

$$M\ model = \beta_0 \times e^{\beta_2 \times M + \beta_3 \times M^2} \tag{10}$$

Based on the significance ($p < 0.05$) of linear regressions of Eq. (7) and Eq. (10), either the temperature model (T model) or a combined temperature and moisture model (TM model)

was fitted. The latter model has been proven to perform best among forest ecosystems (Tang & Baldocchi, 2005; Webster et al., 2009; Yoon et al., 2014):

$$TM\ model = \beta_0 \times e^{\beta_1 \times T} e^{\beta_2 \times M + \beta_3 \times M^2} \tag{11}$$

The linear regression R^2, adjusted R^2, akaike information criterion (AIC), and the mean square error (mse) of a 10-fold cross validation (Kohavi, 1995) were evaluated to compare the applicability for Eq. (7) or (11) for upscaling soil CO_2 efflux to one year. Data gaps in hourly measured T or M (comprised in total < 1% and occurred due to low battery capacity during winter) were filled using linear interpolation.

4.2.6 Statistical analyses

We used Python v3.7.10 (Van Rossum & Drake, 2009) for one-way analysis of variance (ANOVA) (with post-hoc tests) and univariate linear regression analysis (with Pearson (r_p) correlation). For ANOVA, Tukey HSD post-hoc comparison was used to identify significant differences between floodplain forest categories. Variance homogeneity was tested using Levene's test ($p < 0.05$), and residuals were checked for normality using the Shapiro-Wilk test ($p < 0.05$). In case of variance inhomogeneity, a Welch-ANOVA was performed instead, and category comparisons were conducted using pairwise t-tests with Bonferroni-Holm p-adjustment. Differences were considered significant for $p < 0.05$.

We used R v4.1.2 (R Core Team, 2021) for multiple linear regression analysis (MLR) and Monte Carlo simulations (MC). MLR was performed with a stepwise selection of predictors, based on the Akaike Information Criterion (AIC). The model with smallest AIC was selected. Residuals were checked for normality using the Shapiro-Wilk test ($p < 0.05$). Spearman correlation was used to identify correlations between the variables. Variance of inflation factor (VIF, with factors < 2.3) was used to estimate collinearity between the predicting variables. To upscale annual soil CO_2 effluxes, we performed 10000 simulations (with the MonteCarlo package) for each selected T (Eq. (7)) or TM model (Eq. (11)) (Huang et al., 2020; McMurray et al., 2017). Out of these annual soil CO_2 efflux simulations, a mean and a 95% confidence interval (CI) per study site was evaluated.

4.3 Results

4.3.1 Seasonal course of soil CO_2 effluxes

Annual mean soil CO_2 effluxes ranged between 3.19 and 6.52 µmol m^{-2} s^{-1} among the study sites (Fig. 15). Annual mean CO_2 effluxes were greatest in the former low II (disconnected) and smallest in the active low I forest. Mean soil CO_2 efflux among all study sites was larger during autumn (of 4.56 µmolm^{-2} s^{-1}) compared to late spring (of 3.83 µmol m^{-2} s^{-1}). Soil CO_2 effluxes were greatest during the summer months (June, July, and August) and smallest in winter (December, January, and February). During winter, monthly mean soil CO_2 effluxes ranged between 0.83 µmolm^{-2} s^{-1} (in active low I) and 3.79 µmolm^{-2} s^{-1} (in former low II). Monthly mean soil CO_2 effluxes during summer ranged between 2.54 (in active high I) and 12.06 µmolm^{-2} s^{-1} in (in former low II).
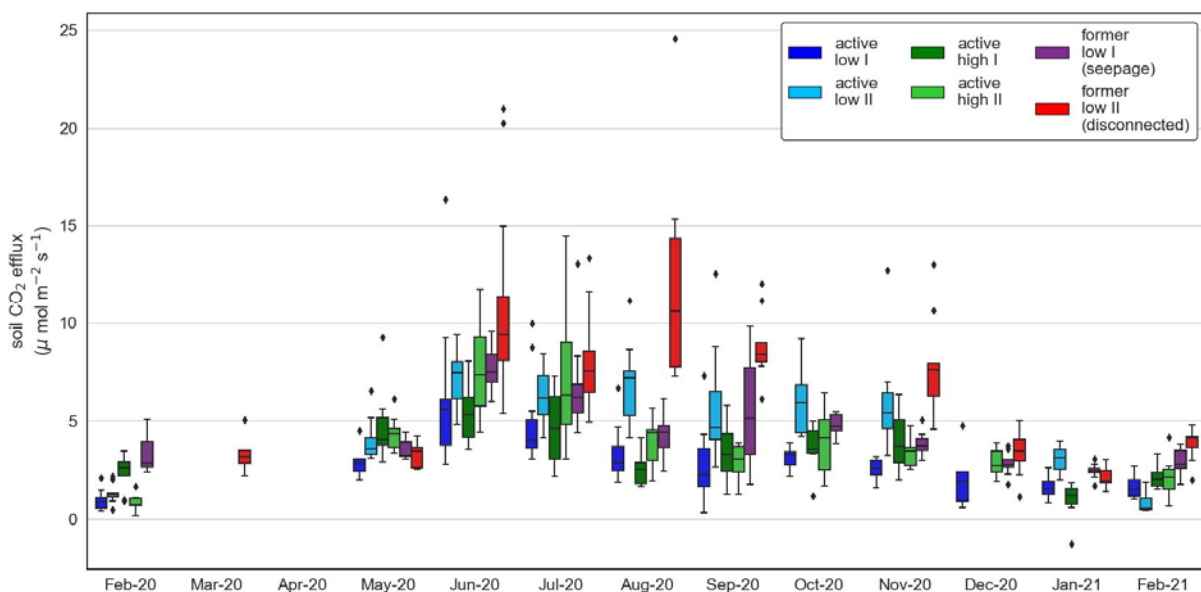
Fig. 15: Seasonal course of measured soil CO_2 effluxes during the study period in the 6 hardwood floodplain forests. Nine measurements per box. Due to the CoVid-19-measures, some sites during March and April 2020 as well as in December and January 2021 could not be monitored.

4.3.2 Effects of soil temperature and moisture on soil CO_2 efflux

The exponential T model (Eq. (7)) fitted the soil CO_2 efflux at every measured location significantly (Fig. 16). Standard deviations of the measurements increased with soil temperature. The Q_{10} ranged between 1.81 and 2.44 and was smallest in the former low I and

greatest in the former low II forest. The Q_{10} was not different among the study sites according

to ANOVA.
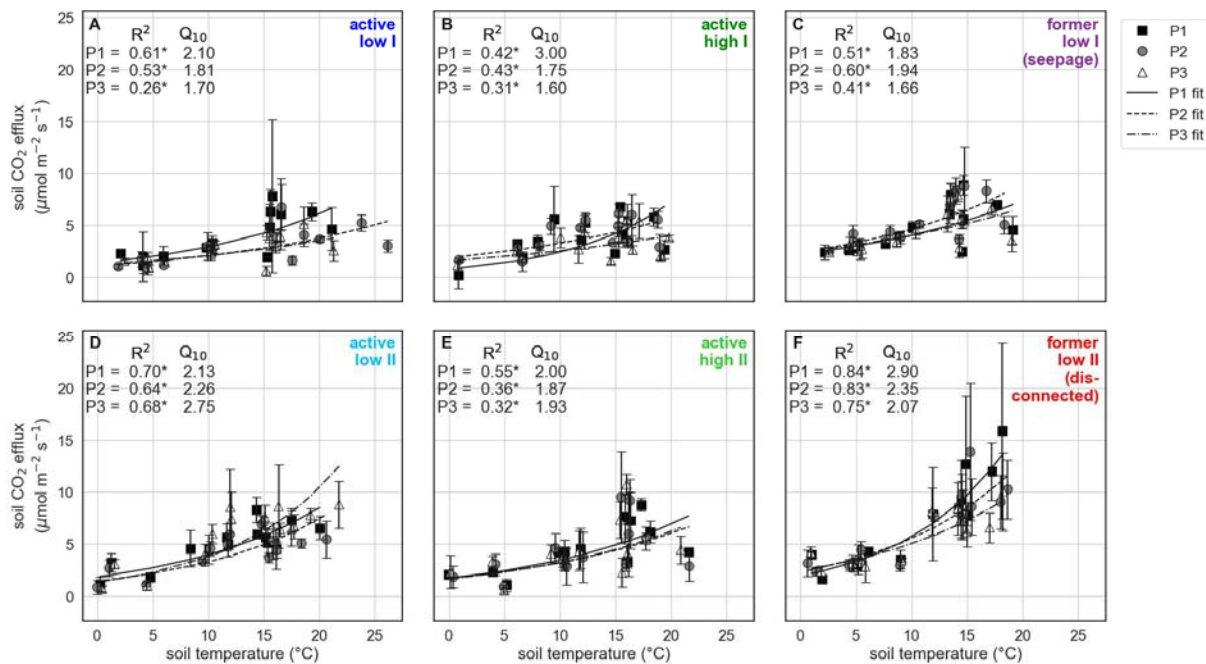
Fig. 16: Soil CO_2 effluxes vs. soil temperature at 10 cm for all study sites and soil profiles (P1, P2, P3). Error bars
are standard deviations of the soil profiles (3 spatial divided measurements per profile P1, P2, and P3). The R^2
and Q_{10} were evaluated from the exponential fit of Eq. (7).
*Significant fit of Eq. (7) between x and y at $p < 0.05$.

The quadratic M model—which describes an optimum at intermediate soil moisture—

fitted at all measured locations in the active low I and active high II forest (Fig. 17, A and E).

Optimum soil moisture for soil CO_2 efflux ranged between 0.17 and 0.26 m^3 m^{-3} in active low I,

0.22 and 0.28 m^3 m^{-3} in active low II, 0.09 and 0,11 m^3 m^{-3} in active high I, 0.10 and 0.16 m^3 m^{-3}

in active high II, and between 0.05 and 0.11 m^3 m^{-3} in former low I. In the former low II forest,

optimum moisture was 0.35 m^3 m^{-3} at P3, but no optimum moisture could be estimated for the

other two soil profiles (Fig. 17, F). The measured soil moisture range was smallest at active

high I and greatest in former low II with 0.01 to 0.17 m^3 m^{-3} and 0.22 to 0.48 m^3 m^{-3},

respectively. Soil moisture ranged between 0.06 and 0.41 m^3 m^{-3} in active low I, between 0.10

and 0.40 m^3 m^{-3} in active low II, between 0.04 and 0.29 m^3 m^{-3} in active high II, and between

0.02 and 0.31 m^3 m^{-3} in former low I.
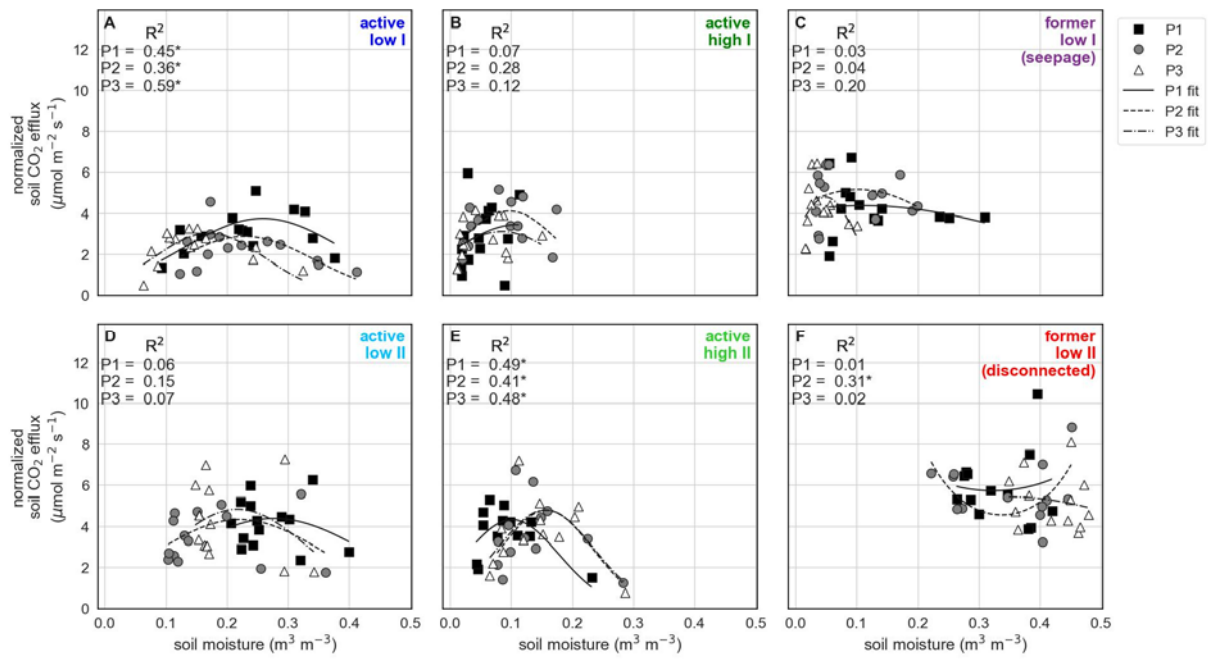
Fig. 17: Temperature-normalized soil CO_2 effluxes vs. soil moisture at 10 cm for all study sites and soil profiles (P1, P2, P3).
*Significant fit of Eq. (10) between x and y at $p < 0.05$.

4.3.3   Differences between hydrologic forest categories

Because the M model fitted soil CO_2 efflux from the active low I and active high II forest, the combined TM model was used for evaluation of the annual soil CO_2 efflux. For the other 4 forests, the T model was used (Table 6). The total soil CO_2 efflux differed between both low-lying forests (Fig. 18). However, all forests in the active zone as well as the former low I (seepage) forests had similar soil CO_2 efflux with a combined mean of 1355 gC m^{-2} y^{-1}. The maximum total soil CO_2 efflux, which occurred in the former low II (disconnected) forest, was 63% larger than this combined efflux of the others. Total soil CO_2 efflux from the 4 forests in the active flooding zone combined was 1275 gC m^{-2} y^{-1}. Total soil CO_2 efflux of both active low forests was 1301 gC m^{-2} y^{-1} and that of the active high forests 1250 gC m^{-2} y^{-1}.
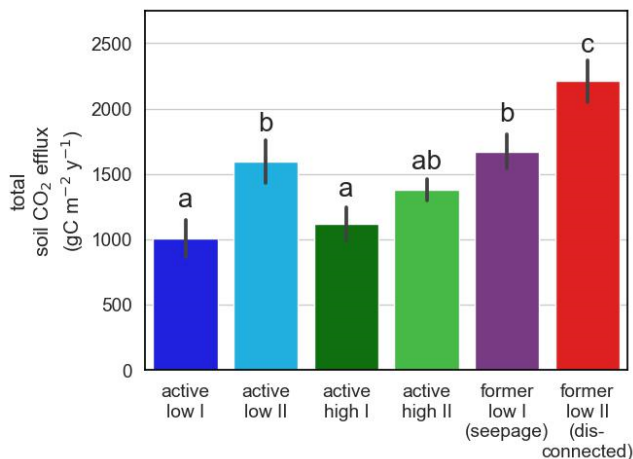
Fig. 18: Mean annual soil CO_2 efflux for all 6 study sites. Low and high are height indications of the study sites. The forests are between 18 and 186 years old. The forests are either located in the active or former flooding zone of the Elbe River. The former low forest I is located behind a dike and affected from Elbe River water table fluctuations through seepage water inflow, from which former low II (disconnected) is unaffected. Error bars indicate standard deviation of individual soil profiles (n = 3); significant differences according to ANOVA with Tukey post-hoc comparison are annotated with letters.

74

Table 6: Goodness of fit measures (Cross-validated mean standard error (CV MSE), akaike information criterion (AIC), R^2, adjusted R^2, p) of the selected model (T: temperature or TM: temperature and moisture) as well as the Monte Carlo (MC) mean and confidence interval (CI) of 10000 annual soil CO_2 efflux simulations per soil profile.

Site	Profile	model	CV MSE	AIC	R^2	adj. R^2	p	MC mean (gC m^{-2} y^{-1})	MC 95% CI (±) (gC m^{-2} y^{-1})	Study site mean (gC m^{-2} y^{-1})	Study site SD[*] (gC m^{-2} y^{-1})
JB1	P1	TM	0.10	8.0	0.84	0.79	0.000	1202	16	1006	171
	P2	TM	0.22	14.6	0.78	0.71	0.001	927	21		
	P3	TM	0.36	19.8	0.66	0.56	0.010	889	24		
JB3	P1	TM	2.15	9.8	0.82	0.76	0.001	1493	22	1381	99
	P2	TM	0.19	17.9	0.71	0.62	0.008	1346	33		
	P3	TM	0.12	11.7	0.86	0.81	0.000	1304	27		
JW1	P1	T	0.89	34.2	0.42	0.38	0.012	1085	41	1118	153
	P2	T	0.15	14.7	0.43	0.39	0.011	1284	21		
	P3	T	0.20	18.1	0.31	0.25	0.039	984	24		
LS1	P1	T	0.14	10.5	0.70	0.68	0.000	1625	18	1597	202
	P2	T	0.21	18.0	0.64	0.61	0.001	1382	24		
	P3	T	0.30	22.6	0.68	0.66	0.000	1783	29		
LE1	P1	T	0.13	13.0	0.51	0.46	0.004	1594	18	1672	159
	P2	T	0.10	8.0	0.60	0.57	0.001	1855	15		
	P3	T	0.13	12.1	0.41	0.36	0.014	1567	18		
SU1	P1	T	0.11	7.9	0.84	0.83	0.000	2387	18	2209	200
	P2	T	0.08	5.5	0.83	0.81	0.000	2248	16		
	P3	T	0.09	5.5	0.75	0.73	0.000	1993	16		

* standard deviation

4.3.4 Soil properties controlling total soil CO_2 efflux

The strongest univariate predictors for annual total soil CO_2 effluxes were fine texture (positive relation; Fig. 19, A), and pH (negative relation; Fig. 19, F) (both R^2 = 0.67). Further positive relations of total soil CO_2 efflux were found to SOC, SOC stock and N (Fig. 19, B, C, D) as well as a negative relation to EC (Fig. 19, G). The C/N ratio was negatively correlated (r_P = -0.45) but seemed to have no effect on total soil CO_2 efflux (Fig. 19, E).
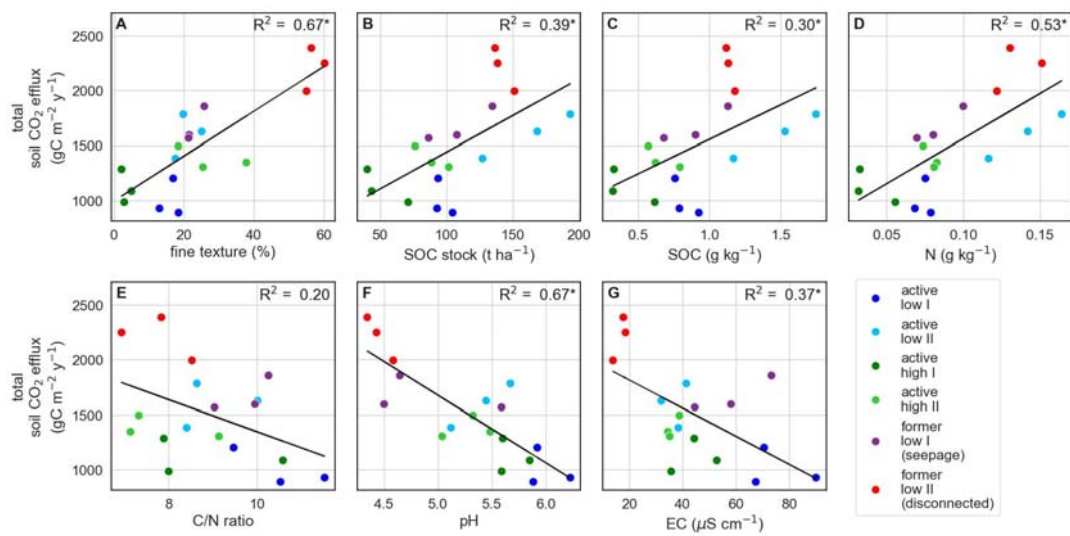
Fig. 19. Annual total soil CO_2 efflux vs. fine texture (< 6.3 µm) (A), SOC stocks (B), SOC content (C), N content (D), C/N ratio (E), soil pH (0.01 M $CaCl_2$) (F), and electric conductivity (EC) (G). The black line indicates linear regression between variables in x and y.
*Significant linear regression between x and y at $p < 0.05$.

In a stepwise MLR analysis, we used the same variables to explain variance in annual soil CO_2 effluxes, which have been used in these forests to predict SOC stocks (Heger et al., 2021): fine texture, soil pH, and C/N ratio. After the stepwise exclusion of confounding variables, the best performing model included fine texture and pH as predictors (Eq. (12)). They explained 75% ($p < 0.0001$, AIC = 196.45) of the variance in annual soil CO_2 effluxes. This shows that hardwood floodplain forests' soil CO_2 effluxes strongly relate positively to soil fine texture and negatively to pH.

$$total\ soil\ CO_2\ efflux = -359.41 \times pH + 11.55 \times clay \qquad (12)$$

4.3.5 Hydrologic control on relative soil CO_2 efflux

To evaluate the relative soil CO_2 efflux we divided the total efflux by the SOC stocks (Table 4). The relative soil CO_2 efflux of the active high I forest was more than twice as large as in its low-lying counterparts (Fig. 20). The relative efflux in active high I was 50% higher but not significantly different from its categorical partner forest (active high II) and from both forests in the former flooding zone. The relative soil CO_2 efflux seemed to be positively affected by hydromorphy (Fig. 21). Thus, a smaller proportion of C emitted in low forests where redoximorphic properties occur closer to the surface.
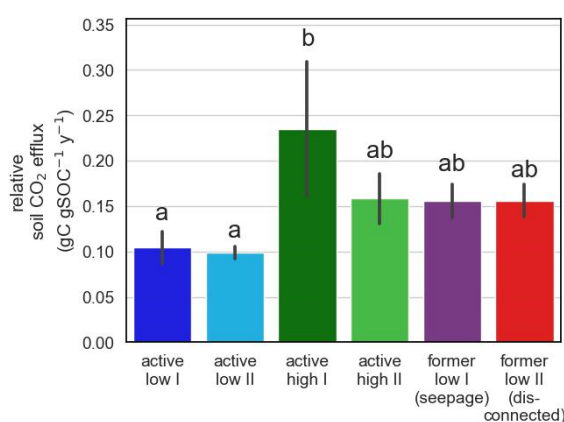
Fig. 20. Mean relative annual soil CO_2 efflux for all 6 study sites. Low and high are height indications of the study sites. The forests are between 18 and 186 years old. The forests are either located in the active or former flooding zone of the Elbe River. The former low forest I is located behind a dike and affected from Elbe River water table fluctuations through seepage water inflow, from which former low II (disconnected) is unaffected. Error bars indicate standard deviation of individual soil profiles (n = 3); significant differences according to ANOVA with Tukey post-hoc comparison are annotated with letters.
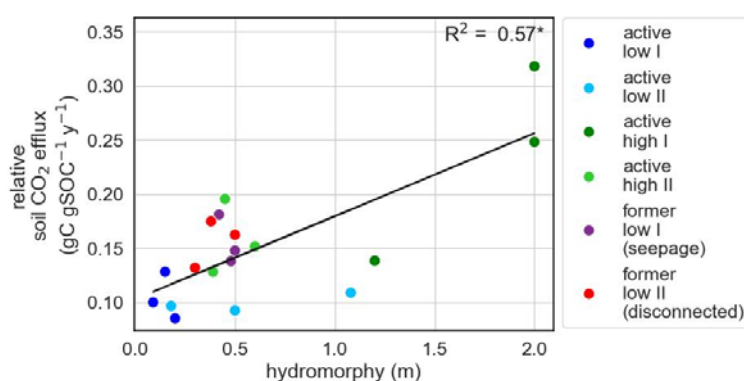
Fig. 21. Depth of hydromorphic features (hydromorphy) vs. the relative annual soil CO_2 efflux. The black line indicates linear regression between variables in x and y.
*Significant linear regression between x and y at $p < 0.05$.

4.4 Discussion

4.4.1 Annual carbon budget of hardwood floodplain forests of the lower middle Elbe River

Total soil CO_2 efflux ranged between 1006 and 1597 gC m^{-2} y^{-1} in active floodplain forests and between 1672 gC m^{-2} y^{-1} and 2209 gC m^{-2} y^{-1} in former floodplain forests.

Compared to similar ecosystems, total soil CO_2 effluxes of the current study of 897.94 to 2401.90 gC m^{-2} year^{-1} are above the mean soil CO_2 efflux for temperate biomes of 745 ± 421 gC m^{-2} y^{-1} (Bond-Lamberty & Thomson, 2010) and for deciduous broad leaf forests of 907 gC m^{-2} y^{-1} (Chen et al., 2014). Soil CO_2 effluxes are rather within the range of Amazonian evergreen forests with 1800 to 2000 gC m^{-2} y^{-1} (Davidson et al., 2000). However, mean soil CO_2 effluxes ranging from 3.19 to 6.52 µmol m^{-2} s^{-1} in this study, were in the same magnitude as in a temperate hardwood floodplain forests in Czech Republic, where mean and total effluxes of 4.07 µmol m^{-2} s^{-1} and 740 gC m^{-2} have been estimated from May to November (Acosta et al., 2017). They were also similar to an oak dominated northern Italian forest, where effluxes of about 1100 g C m^{-2} y^{-1} have been measured (Ferréa et al., 2012). Thus, most of the annual soil CO_2 effluxes of Elbe River hardwood floodplain forests were within measurements of similar ecosystems but can be as large as in tropical forests.

The quantity of mineralizable SOC in floodplain forests is controlled by autochthonic and allochthonic C inputs. Allochthonic inputs are controlled by relief and flood events (sedimentation and erosion) and authochthonic by photosynthetic C assimilation of the vegetation (gross primary productivity, GPP) (Lininger et al., 2018; Luo & Zhou, 2006). Assuming the annual GPP of a boreal forest of 1154 g C m^{-2} y^{-1} (Pumpanen et al., 2015) and of a mixed hardwood forest of 1585 g C m^{-2} y^{-1} (Curtis et al., 2005), most of the floodplain forests in the current study would be a C source. Also in the Archer Creek Watershed (New York State, USA), floodplain forests have been found to be C sources (Gomez et al., 2016). However, productivity rates in floodplain forests are highly diverse due to highly dynamic water-level control of it, resulting in a high variability of annual net primary productivity, which can

range from 200 to 2000 gC m^{-2} y^{-1} (Blosser, 2018). Also, allochthonous SOC inputs (by flood induced sedimentation) can be 6 times more abundant than the long-term (> 50 years) accumulation of autochthonous SOC in floodplain forest soils (González et al., 2014), which might compensate for C losses into atmosphere during years without flooding. Additionally, a larger amount of stabilized SOC is assumed to accumulate in hardwood floodplain forest due to larger flooding frequencies and less burial of particulate organic matter compared to softwood sites, which would contribute to the preservation of the SOC stocks in hardwood floodplain forests (Graf-Rosenfellner et al., 2016). Thus, the ability of our forests to act as an organic C sink seem to depend on flooding frequency.

4.4.2   Seasonal effects of soil temperature and moisture on soil CO_2 efflux

The most important drivers for soil CO_2 efflux are soil temperature and moisture. They control microbial and plant physiologic metabolism and diffusive flux in the air filled pore space (Fan & Han, 2018). In our study, soil temperature and moisture both had significant effects on soil CO_2 efflux.

Soil temperature described 26 to 85% of variance in soil CO_2 efflux at all measured locations. (Fig. 16). The temporal course of soil CO_2 effluxes reached maximum efflux during summer and minimum during winter (Fig. 15). This can be explained by the temperature sensitivity of root respiration, carbon oxidation by rhizosphere microbiota, as well as microbial soil organic matter decomposition (Boone et al., 1998). Greater effluxes in autumn compared to late spring (Fig. 15) can also be affected by autotrophic respiration, which follows C allocation patterns of trees, where C is directed downwards during late phases of summer and directed upwards in shoot extension phases (Fan & Han, 2018). Spatial heterogeneity from root and rhizosphere respiration and fine root production could also be responsible for the high standard deviation with increasing soil temperature (Stoyan et al., 2000), because their sensitivity is larger during warmer periods (Boone et al., 1998). The Q_{10}—that describes the temperature sensitivity—ranged from 1.81 to 2.44 but was not significantly different between our forests. A similar Q_{10} of 2.23 was also found in hardwood floodplain forests in Czech Republic (Acosta et al., 2017). However, Q_{10} values from the northern hemisphere are usually

greater (Davidson et al., 1998) and our Q_{10} is also comparable to subtropical forests of 1.95 (Liu et al., 2019). Our Q_{10} values are also below the Q_{10} of an Belgian oak forest of 3.25 (Yuste et al., 2004) and below the global mean of 3 at a temperature range of 0 to 20 °C (Bond-Lamberty & Thomson, 2010), which is the temperature range of our study. A reason for small Q_{10} could be that the microbial community structure is adapted to higher moisture contents (Meyer et al., 2018), as the soils were not flooded during the measurement period. Also, after a week of inundation, shifts in microbial community structure can enhance microbial respiration and enzymatic degradation rates in floodplain forests (Wilson et al., 2011). Both effects could be responsible for small Q_{10} values. Thus, in all forests of the current study, the temperature sensitivity of soil CO_2 efflux was significant but small compared to other temperate forest ecosystems.

Soil moisture affects soil CO_2 efflux directly by its effects on metabolic activity of roots and microorganisms and indirectly by providing available dissolved organic matter and oxygen for heterotrophic respiration. Usually small or large soil moisture levels limits soil CO_2 efflux (Tang & Baldocchi, 2005). The quadratic function (Eq. (10)) only described the data from 2 out of 6 forests of the current study (Fig. 17) sufficiently, which could be due to small variability in soil moisture conditions during the measurement period. For example, constant moistening (between 0.22 to 0.48 m^3 m^{-3}) might be the reason for moisture changes having no effects on soil CO_2 efflux in the former low II (disconnected) forest. Similarly, constant dry conditions (especially in active high I), could have had the same effect. However, soil moisture on floodplains is directly affected by periodic flooding (Yoon et al., 2014), which did not occur in the measurement period. Thus, a lack of flooding periods could be responsible for the little effect strength of soil moisture on CO_2 effluxes in our forests.

4.4.3 Effects of soil properties on soil CO_2 efflux

Spatial heterogeneity in soil CO_2 effluxes is strongly affected by the response of roots and microorganisms to soil texture, nutrient availability and pH (Yin et al., 2019). Annual soil CO_2 efflux was positively related to N, SOC, SOC stocks, and fine texture. Soil CO_2 efflux was negatively related to pH and EC. A MLR yielded a model that describes annual soil CO_2 efflux

using the variables fine texture and pH. We interpret these variables in a process-based way and argue that they reflect the positive effect of fine texture on water supply and available SOC as well as a microbial community, which is adapted to rather acidic conditions.

Soil microbial communities are often adapted to specific pH and salinity levels (Chen et al., 2014; Sardinha et al., 2003). High soil salinity can stress plants and microorganisms and diminish metabolic efficiency (Lai et al., 2012). The negative relation of soil CO_2 efflux to EC (Fig. 19 G) could reflect this stress effect, which often occurs in coastal wetlands (Song et al., 2021). In low saline floodplain soils, also the contribution of fungi to the microbial community can be large (Sardinha et al., 2003). The soil pH of our study sites ranged between 4.3 and 6.3 (Fig. 19 F). This pH range is often preferred by acidophilic bacterial and fungi species, which could explain the negative relation of soil pH to CO_2 efflux (Luo & Zhou, 2006). A negative correlation of soil CO_2 efflux to pH has also been found in Californian pine plantations (Xu & Qi, 2001), and in global annual soil CO_2 efflux models (Chen et al., 2014). In floodplain soils, a negative relation of pH with mineralization rate has been found when soil moisture was low but at an optimum level for microbial decomposition (~30% water holding capacity) (Yin et al., 2019). Considering that the experimental period of the current study comprised a year with MAP below the annual average (Deutscher Wetterdienst, 2022)—which was already followed by summer droughts in 2018 and 2019 (Boeing et al., 2021)—could indicate that the microbial community in our floodplain forests is adapted to these low pH and soil moisture conditions. Additionally, large EC can stress the microbial communities and plants and thus decline soil CO_2 efflux.

Soil microorganisms use organic matter—with its main components, SOC and N— as energy source for mineralization (Basile-Doelsch et al., 2020). This process could explain the positive relation of N, SOC and SOC stocks to soil CO_2 effluxes (Fig. 19). This relation could also explain the difference in annual soil CO_2 effluxes between forests of the same hydrologic situation (Fig. 18 and Fig. 20). In the former low II (disconnected) forest, the large litter layer C stock (Table 5) could have served as an additional source for organic matter, contributing to maximum annual effluxes (Fig. 18). The C/N ratio indicates if the SOC pool is composed of

plant detritus or more processed organic matter with a higher contribution of microbial residues (Schrumpf et al., 2013). In our study, this SOC quality parameter seemed to have no effect on soil CO_2 efflux (Fig. 19, E) but rather the total content of SOC and N.

Periodic flooding partly controls soil CO_2 efflux in wetland forests (Yoon et al., 2014), and oxygen scarcity in low-lying wetlands can reduce aerobic SOC mineralization (Yin et al., 2019). At Elbe River floodplains, groundwater fluctuations are controlled by the river at both sites of the dike, i.e. floodplains in the seepage water zone are hydrologically connected to the Elbe River though seepage water inflow (Schwartz et al., 2003). This could explain why CO_2 effluxes in the floodplain forests of the seepage zone was similar to its active counterpart (Fig. 18). The positive correlation of hydromorphy with relative CO_2 efflux (Fig. 21) also indicates SOC protection from mineralization due to saturation conditions close to the soil surface (Hennings et al., 2021). This relation was also reflected in the category comparison of relative annual soil CO_2 effluxes (Fig. 20), where the low-lying forests in the active flooding zone experienced the smallest relative annual soil CO_2 efflux. Groundwater fluctuations can also control dissolution and precipitation of Fe and Mn, which can be involved in metal organic complexes and protect SOC even under aerobic conditions (Wang et al., 2017). Thus, our study showed that in low-lying hardwood floodplain forests of the active flooding zone, SOC might be protected from mineralization by oxygen scarcity, which was also reflected by the appearance of hydromorphic features close to the surface (Fig. 21).

In low-lying hardwood floodplain forests, also fine texture can protect SOC from microbial degradation by adsorption to clay minerals or incorporation within clay and silt aggregates (Deiss et al., 2017). Soils with small fine texture content are less effective at retaining water with easy available dissolved organic matter and nutrients, which are important for mineralization (Hamarashid et al., 2010). This could explain the large relative effluxes in the sand-dominated active high I forest (Table 4 and Fig. 20). However, in fine textured soils, also the labile fraction of SOC and N can be available in a large amount and contribute a large energy source for mineralization (Luo & Zhou, 2006). This could also have contributed to the greatest soil CO_2 efflux in the forest with maximum fine texture content (Table 4 and Fig. 18).

Soil texture can also affect the root system, since compared to loamy soils, in sandy soils, low fertility, unsaturated hydraulic conductivity and water holding capacity negatively affect root vitality and decomposition of root litter, and thus autotrophic and heterotrophic respiration in the rhizosphere (Luo & Zhou, 2006). This effect supports the finding that autotrophic and heterotrophic respiration benefits from indirect positive effects of fine texture on soil moisture and availability of nutrients and SOC.

In the current study, soil CO_2 efflux—autotrophic and heterotrophic—could be related to soil properties, such as fine texture, its association with optimum moisture conditions, SOC and N availability, as well as to soil pH, and EC. The positive relation to fine texture and the negative relation to pH resulted to be the most important drivers for soil CO_2 efflux. However, autotrophic respiration can also be positively related to soil sand content and pH. Large sand content is related to soils with higher bulk densities where a denser fine root system is favorable, while respiration decreases with root diameter (Tang et al., 2020). High soil pH could have a positive feedback on forest primary productivity due to higher nutrient availability as a consequence of high soil cation exchange capacity (Härdtle et al., 2004), which would contribute to enhanced autotrophic respiration. In deciduous temperate hardwood forests, root and rhizosphere respiration can contribute up to 90% to total soil CO_2 efflux (Boone et al., 1998). No information about the contribution of root and rhizosphere respiration is known for hardwood floodplain forests, further studies are needed. Our results suggest that fine texture provides positive feedback mechanisms on soil moisture, SOC and nutrient stock, which is important for autotrophic and heterotrophic respiration. Low soil pH and EC could also be related to a well-adapted microbial community.

4.4.4 Implications of climate change on floodplains

Floodplains are ecosystems where decomposition and mineralization of organic matter is largely controlled by periodic flooding and sedimentation. Usually flood induced oxygen scarcity reduces aerobic mineralization of SOC (Hennings et al., 2021). However, oak trees in floodplain ecosystems are able to transport oxygen from the leaves to the roots, during flooding periods, and are thereby able to activate respiration from the roots and create aerobic conditions for heterotrophic microorganisms in the rhizosphere (Good & Patrick, 1987). The role of this flood induced CO_2 efflux as well as of other greenhouse gases (e.g., CH_4, N_2O) during and after floods remains to be studied in hardwood floodplain forests (Gomez et al., 2016).

Furthermore, it is unclear how possible climate change scenarios (e.g., a changed frequency of the 100-year flooding events) affect sedimentation and erosion of SOC in floodplain ecosystems (Eccles et al., 2021). Several studies suggested that climate change might have negative effects on river water discharge during summer due to smaller meltwater resources (Gellens & Roulin, 1998; Middelkoop et al., 2001; Pfister et al., 2004). At the Elbe River, there has not been an extreme flooding since 2013 (Schindler et al., 2021). If there is no soil CO_2 efflux limitation due flood induced oxygen scarcity on floodplains, global warming could enhance soil CO_2 efflux due to its temperature sensitivity (Fig. 16) (Lloyd & Taylor, 1994).

4.5 Conclusion

Soil CO_2 efflux in Elbe River hardwood floodplain forests was mainly related to fine texture and soil pH. Seasonal temperature changes were related to effluxes in all studied forests and Q_{10} did not differ between them. Soil moisture, as limiting factor for soil CO_2 efflux, was significantly related only in 2 out of 6 forests, which could be due to a lack of flooding conditions in the studied period. Total soil CO_2 efflux ranged between 1006 and 2209 gC m^{-2} y^{-1}. Maximum efflux occurred in a former floodplain forests, which was disconnected from Elbe River water table fluctuations. Relief or flooding zone did not indicate differences in total soil CO_2 efflux between the other forests. However, relief effects on relative soil CO_2 efflux (gC $gSOC^{-1}$ y^{-1}) indicated, that SOC might be protected from mineralization in low-lying forests of the active flooding zone due to oxygen scarcity. This protective effect on SOC mineralization was also reflected by the appearance of hydromorphic features close to the soil surface. Large fine texture content and its indirect positive effects on soil moisture, SOC and nutrient pool contributed to larger total soil CO_2 effluxes. A highly active microbial community adapted to acidic soil conditions, low electric conductivity and constant oxygen supply, contributed thereby to annual soil CO_2 effluxes comparable to those in tropical forests. The effect of climate change on flooding frequency and temperature could cause an increase of soil CO_2 efflux as well affect erosion and sedimentation of SOC, so that hardwood floodplain forests could turn from C sinks to sources.

5 Article IV: Application of a low-cost NDIR sensor module for continuous measurements of *in situ* soil CO$_2$ concentration

5.1 Introduction

Conventional probes applicable for continuous soil CO$_2$ measurements (see overview in (Zhang et al., 2015)) are costly. Other in situ methods to determine the soil CO$_2$ concentration, e.g. by collecting soil gas samples using tubes of different length, are work-intensive and therefore limited regarding spatial and temporal coverage (Luther-Mosebach et al., 2018).

The non-dispersive infrared (NDIR) CO$_2$ sensor module K33 ICB (Senseair, Sweden) is commonly used in measurement systems for indoor air quality monitoring. It measures CO$_2$ concentrations from 0 to 30%, which is above the range of conventional CO$_2$ sensors (usually 0 - 2% CO$_2$). Probes with a higher measurement range than 2% are interesting, since soil CO$_2$ concentrations up to 9% are common, e.g. in urban soils (Schaaf-Titel, 2019). Senseair CO$_2$ sensor modules as the K33 are known in the scientific community (e.g., Bastviken et al. (2015); Harmon et al. (2015); Martin et al. (2017); Yasuda et al. (2012)) but have not been used for in situ soil measurements yet.

The manufacturer states a response time of the K33 sensor module of < 20 s. However, in a recent thesis, a value of 22 s was measured (Keimel, 2019). Harmon et al. (2015) tested the sensor module K33 for the suitability for closed-chamber measurements of soil surface CO$_2$ fluxes. They installed the sensor modules in a flow-through chamber and monitored the CO$_2$ concentration in ant nests. By comparing to other instruments (LI-COR LI-6400, Vaisala GMP343), Harmon et al. (2015) found that the sensor module K33 measures CO$_2$ concentration from > 1500 ppm in comparable temporal patterns.

We integrated the low-cost CO_2 sensor module K33 ICB in a newly developed probe for in situ soil measurements. We call this self-designed soil CO_2 probe "K33SOIL" throughout this article. First, we compared the measurements of K33SOIL with the conventionally used CO_2 probe GMP343 (Vaisala, Finland) under controlled temperature and humidity inside a calibration box. Then we tested its performance under in situ soil conditions and compared the readings with analyses of discrete soil gas samples by a portable infrared gas analyzer (IRGA).

5.2 Material and methods

5.2.1 Device construction

The sensor module K33 includes the actual CO_2-measuring cell placed on top of the circuit board (51 mm x 57 mm, Fig. 22). The CO_2 concentration is measured in an NDIR absorption cell. The data is calculated in units of µmol mol^{-1} and can be read via a digital (I^2C) or analog output. To adapt the sensor module to harsh soil conditions, we protected it with a surrounding layer of epoxy resin (LS 60/45, von Corvin, Germany) leaving open only the diffusive membrane, under which the NDIR cell is located.

Fig. 22. Photo of the K33SOIL. The circuit board of the sensor module K33 has an area of 51 mm x 57 mm. We covered it with epoxy resin. The measuring NDIR cell is located below the diffusive membrane, which is the only part not covered in epoxy resin.

For the laboratory experiments, we connected the K33SOIL to a microcontroller (MEGA 2560 Rev3, Arduino.cc, Italy), which was connected to a laptop. The data was logged every 5 seconds using the Microsoft Excel add-in PLX-DAQ (Parallax Inc., U.S.A). Data transfer was

conducted using the I^{2}C bus. We adjusted the addresses for the sensor modules using the development kit SADK (Senseair, Sweden) together with the UIP5 software.

For continuous in situ measurements, we connected the K33SOIL to the same microcontroller type we used in the laboratory experiment. We equipped this microcontroller with a data logging shield (Adalogger FeatherWing, Adafruit, USA). We measured a power consumption of the K33SOIL of < 3 W when the IR light flashed (optics heating) and below < 0.8 W without, while using a 12 V power source (for comparison: the GMP343 has a consumption of < 3.5 W with optics heating and < 1 W without). To save electricity consumption, a second microcontroller (NANO, Arduino.cc, Italy) with a programmed timer controlled the activation of a relay, which switched the power supply for the data logger module and our K33SOIL. In this set-up, the device was programmed to switch on the logger module every hour for two minutes and the K33SOIL performed eight measurements in 15 s intervals. With respect to the warm-up time of one minute, we only took the last four values to calculate a mean for the respective hour.

5.2.2   Calibration and laboratory experiments

To compare the signal of our K33SOIL to a conventional CO_2 probe, we placed three of the K33SOIL together with the GMP343 (diffusion filter mounted) into a 15 L air-filled calibration box. Prior to the measurement, we calibrated the sensor module K33 using the GMP343 as reference probe. We programmed the CO_2 concentration reading of the GMP343 onto the K33SOIL (using the SADK together with the UIP5 software) at 1.3% CO_2, as this is in the concentration range we want to study in situ. We applied this concentration inside the box by extracting the CO_2 enriched air of sparkling water bottles. Then we inserted this air into the box using a syringe. A fan (120 mm, be quiet! – Pure Wings 2, Listan GmbH, Germany) circulated the air inside the box.

We performed four experiments with varying humidity or temperature inside the calibration box while keeping the CO_2 concentration between 1 and 2%. We simulated the following four situations: a cold environment with rising humidity (CH), a warm environment

with rising humidity (WH), a cold environment with drying conditions (CD), and an environment with increasing temperature at moderate humidity (WD). During CH and WH, we raised the humidity up to 100% as it appears in soils. We applied maximum relative humidity using a dew point generator (LI-610, LI-COR Biosciences GmbH, Germany). To simulate a cold environment (CH and CD), we performed the experiment inside a refrigerator at 7.27 ± 0.54 °C. For a stable warm environment (WH), we placed the box inside an incubation room at 19.55 ± 0.22 °C. During CD, we applied drying conditions by drying the air inside the box with silica gel, which produced a decrease in relative humidity from 90 to 46%. During WD, we raised the temperature using a lamp from 10.84 to 28.76 °C and kept the humidity constant at 41 ± 3% by occasionally drying the air (due to the built up of water vapor). We measured air pressure, temperature and relative humidity using a BME280 (Bosch Sensortec, Germany). For the high humidity range (relative humidity of 95-100%), we used the relative humidity and temperature probe CS215 (Campbell Scientific, UK).

We describe the accuracy of the K33SOIL in this study as the difference between the CO_2 concentration of each of the three K33SOIL and the reference sensor GMP343 ($\Delta C_{K33SOIL\ (1\text{-}3)\text{-}GMP343}$). We calculated the precision as the mean deviation from a running mean of each K33SOIL with a time window of 400 s. For comparison between the sensors, we calculated the RMSE from each of the K33SOILs against the GMP343.

To examine the stability of the K33SOIL under water-saturated conditions, we placed it together with two soil moisture probes (CS616, Campbell Scientific, UK) inside the calibration box, which we filled with sand. Afterwards we filled the box with water and emptied it again. The measurement comprised waterlogging conditions for 21 days in total. We logged all data with a CR800 (Campbell Scientific, UK).

5.2.3 Field tests

To test the performance of the K33SOIL under in situ soil conditions, we installed them in two depths (20 cm and 50 cm) at a grassland site in the city of Hamburg. We placed the probes with the diffusive membrane facing down. The CO_2 concentration measurements were

supported by soil temperature and volumetric water content measurements (5TM 311/400, Decagon Devices, USA). To evaluate the measurements of the K33SOIL, we installed aluminum tubes (7 mm inner diameter) at each depth, which were closed with a septum plug for syringes at the top. We placed three tubes around each probe (with 20 cm distance) to cover the small-scale spatial variability. We extracted soil gas samples out of the tubes using a 60 ml syringe. Prior measuring the soil CO_2 concentration manually with a portable IRGA (Biogas, Geotechnical Instruments, UK), we flushed the volume specific amount of residual air inside the tube to clean it. We conducted these comparison measurements from the first to the fourth day as well as from the seventh to the eleventh day of monitoring.

To check the stability of measurements under the harsh conditions of waterlogging, we buried the K33SOIL at two depths below surface (20 cm and 40 cm) into a water retention pond in water-saturated soils. The measurement was supported by soil temperature (PT100/3, Campbell Scientific, UK) and volumetric water content measurements (CS616, Campbell Scientific, UK) at corresponding depths.

5.2.4 Corrections

According to the ideal gas law, temperature and pressure affect the CO_2 readings of IRGAs in a stable volume. Furthermore, humidity and oxygen concentrations affect the measurements. Therefore, the readings have to be corrected. The portable IRGA used in the field experiment has an internal air pressure and temperature compensation. The K33SOIL as well as the GMP343 perform a temperature compensation using a built-in temperature sensor. The K33SOIL is not capable of humidity, oxygen or air pressure compensation during the measurement. For the GMP343, the default option for relative humidity, oxygen and air pressure compensation was disabled. According to the GMP343 user's guide, the effect of humidity and oxygen is less significant compared to the effect of temperature and pressure. However, as we are measuring in high relative humidity range of up to 100%, we compensated for effects of water vapor dilution as well as for air pressure variations in a subsequent correction. For the K33SOIL, we used the application note "Pressure Dependence of Senseair´s NDIR sensors" (CO2Meter.com, Florida, USA) for air pressure compensation:

$$\chi_{cw} = \frac{\chi_{cw}'}{4.026 \times 10^{-6} \times p + 5.780 \times 10^{-11} \times p^2} \qquad (13)$$

where χ_{cw} is the pressure-corrected CO_2 concentration, χ_{cw}' is the measured K33SOIL

output concentration and p the pressure in Pa. For the GMP343, we used the equation given

by Vaisala's application note "How to Measure Carbon Dioxide" (Vaisala, Finland):

$$\chi_{cw} = \chi_{cw}' \times \frac{p_{ref}}{p} \qquad (14)$$

Where χ_{cw} and χ_{cw}' are the respective pressure-corrected and measured concentration

from the GMP343. p_{ref} is the reference value used by the GMP343 (101300 Pa). To remove

dilution effects of water vapor, we calculated the CO_2 concentration in dry air as described in

(Hupp, 2011) and Welles et al. (2001) using the following equation:

$$\chi_c = \frac{\chi_{cw}}{1 - \chi_w} \qquad (15)$$

where χ_c is the CO_2 concentration in dry air and χ_w is the molar fraction of water vapor

in air. As we do not have direct measurements of χ_w, we estimated this value by calculating

the water vapor pressure at saturation (e_s) according to Buck (1981) and by using direct

measurements of relative humidity (RH), temperature (T) and p:

$$\chi_w = \frac{e_s(T) \times RH}{p} \qquad (16)$$

In this manuscript, χ_c is converted to % CO_2. RH and T is measured in % and °C,

respectively. For the field experiment, RH was assumed to be 100% and p at 101300 Pa.

5.3 Results

5.3.1 Laboratory experiments

The time series of temperature and relative humidity is shown in Fig. 23 (top graphs).

Changes in air pressure were minor during all experiments (< ± 0.5 kPa). Also in WD, where

we applied rising temperature, air pressure increased only by ~0.2 kPa. Concentration

changes of the K33SOIL (1-3) and the GMP343 are displayed in the middle graphs. Due to

slight leakage of the calibration box, the initial CO_2 concentration decreased over the time

during the experiments CH, WH and CD. However, in WD the measured concentration rises.

This is probably caused by CO_2 outgassing during evaporation of water, which condensed

inside the calibration box during previous experiments. We additionally noted a strong increase

in the water vapor molar fraction χ_w (from 5 to 16 mmol mol^{-1}) during this experiment.
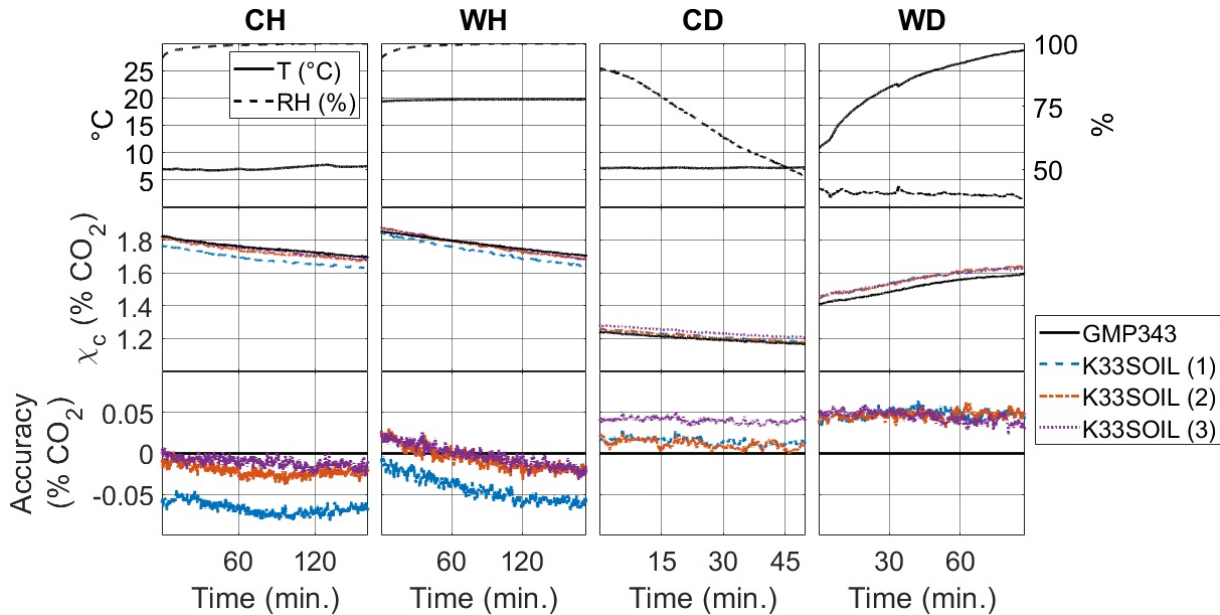
Fig. 23. Temporal courses of the four laboratory experiments: Rising humidity in a cold environment (CH), rising humidity in a warm environment (WH), drying conditions in a cold environment (CD), and rising temperature at moderate humidity (WD) inside the air-filled calibration box. Top: temperature (T) and relative humidity (RH), middle: CO_2 concentration of the reference probe GMP343 and three K33SOIL (1-3), bottom: the accuracy of the three K33SOIL (1-3) given as $\Delta C_{K33SOIL\ (1-3)-GMP343}$.

The differences in CO_2 concentration between the K33SOIL (1-3) and the GMP343

(shown as the accuracy of the K33SOIL) can be seen in the lower graphs of Fig. 23. In CH,

K33SOIL (1) showed the largest deviations from the GMP343 with a maximum at 0.085% CO_2

(RMSE = 0.067% CO_2), whereas the K33SOIL (2) and (3) showed measurements closer to

the reference and also similar to each other (RMSE = 0.022% and 0.012% CO_2). In WH,

accuracy changed from positive to negative deviation. The largest deviation was again found

in the measurements of K33SOIL (1) with -0.071% CO_2. The RMSE of K33SOIL (1-3) was

0.046%, 0.015% and 0.013% CO_2 during this experiment. The change in accuracy in

experiments CH and WH does not seem to be linear, as in both experiments, after

approximately 90 minutes, the accuracy moves slightly towards 0. Compared to that, in

experiment CD the accuracies of the K33SOILs stayed relatively stable. Here, K33SOIL (3)

showed the highest deviation with 0.05% and a RMSE of 0.04% CO_2. K33SOIL (1) and

K33SOIL (2) had RMSE values of 0.015 and 0.012% CO_2. During WD, the deviations of all

three K33SOILs stayed very close together and had RMSE values between 0.045% and

0.048% CO_2. In all four experiments, the maximum deviation between the K33SOILs and the

reference sensor was always lower than the accuracy specified by the manufacturer

($\pm$ 0.5% CO_2) but was slightly higher than the given relative accuracy ($\pm$ 3% of the measured

value). The RMSE off all three K33SOILs combined in all four experiments lies between

0.012% and 0.067% CO_2, whereas the maximum was calculated from K33SOIL (1) in

experiment CH. The average and the median RMSE is 0.032% and 0.031% CO_2, respectively,

which indicates a good agreement of the K33SOIL and the GMP343.

The changes in precision and accuracy of the K33SOILs' CO_2 reading against changing

T and RH are displayed in Fig. 24. Even though the precision data of the three K33SOILs is

overlapping in all four experiments, some patterns are still visible. The precision seems to

decrease (deviations from 0 grow higher) at RH close to 100% (CH and WH) and with rising T

(WD). However, the precision was always < $\pm$ 0.012% CO_2. The precision value was lower

than the given repeatability value by the manufacturer of $\pm$ 0.1% CO_2 (or $\pm$ 2% of measured

value).
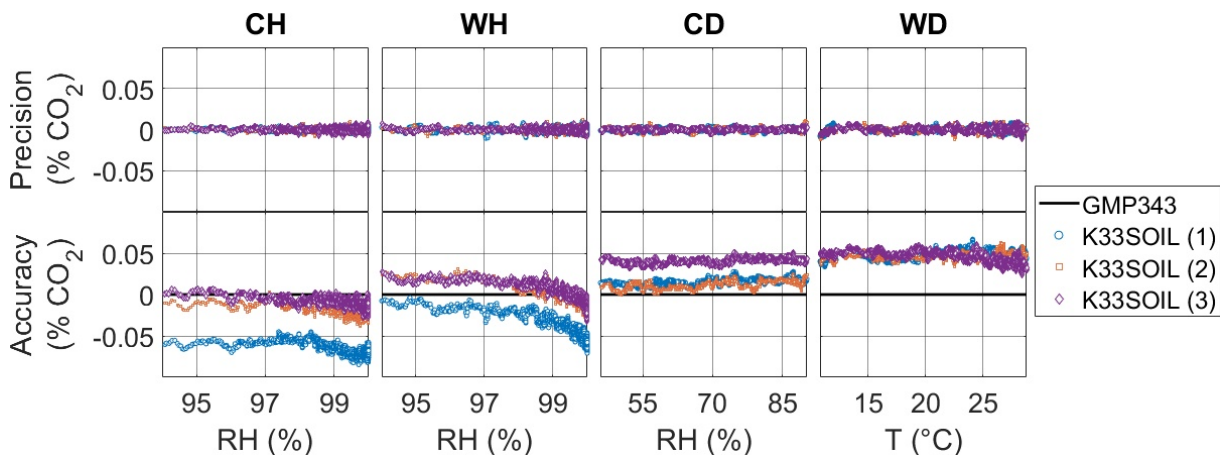
Fig. 24. Precision (top) and accuracy (bottom) of the K33SOIL (1-3) at changing relative humidity (RH) and
temperature (T) during our treatments: Rising humidity in a cold environment (CH), rising humidity in a warm
environment (WH), drying conditions in a cold environment (CD), and rising temperature at moderate humidity (WD)
inside the air-filled calibration box.

The accuracy under changing RH and T is displayed in the lower graphs of Fig. 24.

During CH, the largest deviation is visible coming from the reading of K33SOIL (1). Larger

variation in accuracy of all three K33SOILs appear from RH of > 98%. This larger variation can

also be noted in WH. In addition, all three K33SOILs show a drift of ~0.04% CO_2 from RH

> 97%. However, the deviations do not exceed $\pm$ 0.1% CO_2, while it is not clear if this drift is

caused by the K33SOILs or the GMP343. During CD, it seems that the concentration stays

relatively stable. Visible in the overlapping data of K33SOIL (1) and (2) is a slight change from

accuracy 0.01 to 0.02% CO_2 with higher growing RH. The accuracy of K33SOIL (3) stayed

relatively stable at approximately 0.04% CO_2 during this experiment. In WD, the accuracy

(mean accuracy for all K33SOIL: 0.05% CO_2) varies slightly stronger with rising temperature.

However, the deviations are still below $\pm$ 0.1% CO_2 and temperature changes simulated in this

experiment are typically much slower under in situ conditions. To conclude, changes in

accuracy measured here with the GMP343 as reference probe at changing RH or T occurred

in a range (< $\pm$ 0.1%CO_2), which is applicable for in situ soil measurements at high CO_2

concentration. Minor systematic changes were only visible during WD.

Influence of waterlogging

In the lab experiment during the 21 days of waterlogging, the K33SOIL CO_2

concentrations were higher than in the phase before and increased up to 3.7% CO_2. After

draining the calibration box, the CO_2 concentration went down to the atmospheric level

immediately. Ten days later, the K33SOIL still measured with the same accuracy as before

flooding (results are not shown).

5.3.2   In situ field test

Fig. 25 displays the in situ CO_2 concentration at 20 cm and 50 cm soil depth in an urban

soil measured by the K33SOIL and of discrete pore air samples analyzed by the portable IRGA.

On the first and on the second day, heavy precipitation (27.8 mm) caused a wetting of the soil

profile.
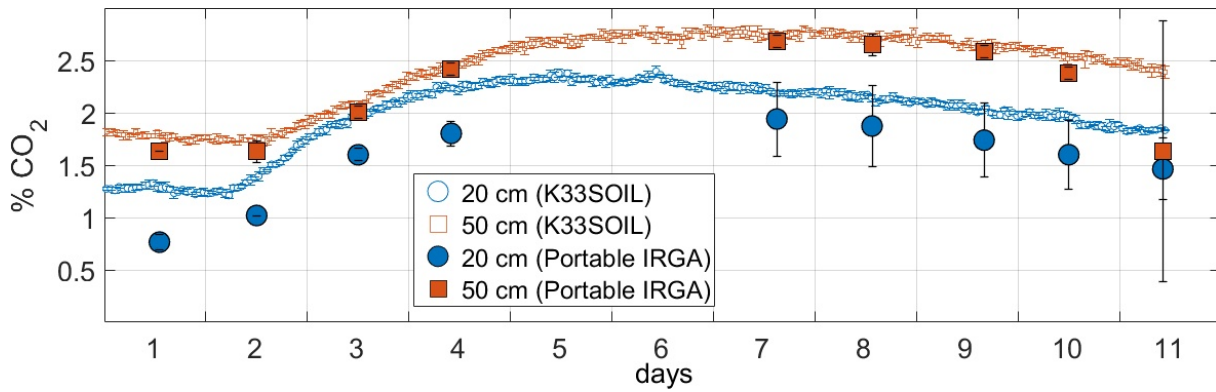
Fig. 25. Time series of CO_2 concentration in soil gas phase at two different depths (20 cm and 50 cm) measured by the K33SOIL (each data point represents the mean of four measurements each hour for one K33SOIL per depth) and by a portable IRGA in discrete soil air samples (mean of three measurements each hour at each of the three tubes surrounding a K33SOIL) at an urban grassland in the city of Hamburg.

The temporal course of the CO_2 concentration during the field experiment measured with the two methods was similar, though an attenuation of the CO_2 concentration measured by the portable IRGA at 20 cm is clearly visible in the first four days of monitoring. A possible explanation for this is an effect caused by the mixing of ambient air with soil gas when we drew the gas sample out of the tube. In addition, as these measurements are conducted in an urban soil, which contains technogenous material, lateral diffusion caused by e.g. bricks inside the substrate, could have been responsible for this variation Maier and Schack-Kirchner (2014). The standard deviation between the concentrations measured through three gas tubes with the portable IRGA are higher in 20 cm than in 50 cm and likely the result of small-scale variations in soil gas composition. However, the CO_2 concentration measured by our K33SOILs and the portable IRGA were in good agreement at 50 cm. The relative changes in the time series as measured by the portable IRGA are well represented at both depths by the K33SOIL.

In the second field test, we found that four weeks after we installed the K33SOILs into the ground of the waterlogged retention pond, they still measured with the same accuracy as before (results are not shown).

5.4 Conclusion

We present the construction and application of the low-cost soil CO_2 probe K33SOIL. During the comparison between the K33SOIL and the GMP343 in the laboratory experiments,

the most noticeable effect on the CO_2 measurements was visible at RH > 97% at room temperature when a drift of about ~0.04% CO_2 was visible. However, the absolute deviations measured here stayed below ± 0.1% CO_2 while it is not entirely clear if this drift occurs from the K33SOIL or the reference sensor GMP343. Also, these deviations are in a range that are not crucial for in situ CO_2 measurements in the soil at a high concentration, e.g. of up to 9% CO_2. A noticeable Temperature-dependence of the deviations was not detected during the laboratory experiments. The averaged RMSE throughout all experiments of 0.032% CO_2 is slightly below the value measured by Harmon et al. (2015) (here: 0.042% CO_2). For further applications of the K33SOIL, the accuracy of the K33SOIL could be improved, by performing a two- or multipoint calibration with calibration gases of different CO_2 concentrations prior the application in the soil. Furthermore, a compensation for background gas concentration, e.g. oxygen, could also help to improve accuracy.

The in situ experiment reveals that the K33SOIL is a valuable device for measurements of soil CO_2 concentration for the presented time of measurement (11 days). Although deviations from the K33SOIL to the reference sensor were stronger in the in situ experiment compared to the laboratory experiment, the accuracy of the K33SOIL is sufficient for our studies. Also the ability to measure CO_2 concentrations over 2% proved to be useful in this experiment. With regard to long term measurements in the soil, a weekly calibration of the sensor module, as recommended by the manufacturer, could be made possible by a modified housing with attached calibration tubes, similar to the soil adapter kit for the GMP343.

In our study, we used the sensor module K33 ICB for the first time to measure soil CO_2 concentrations by integrating it into a newly developed probe: K33SOIL. Our experiments showed that K33SOIL competes well with conventional soil CO_2 measuring devices (e.g. GMP343, IRGA Biogas) in accuracy. The precision was better than the repeatability value given by the manufacturer. The cost-efficient availability of the K33SOIL opens up the opportunity to carry out continuous soil CO_2 measurements over long time periods with simultaneously high spatial resolution.

6 Synthesis

6.1 Summary of key results

Soil organic carbon (SOC) stocks in lower middle Elbe River hardwood floodplain forests ranged between 99 and 149 t ha^{-1} (Fig. 4), and were mainly controlled by proxies for floodplain relief and sedimentation processes (e.g., hydromorphic features, flooding duration, fine texture (< 6.3 µm)). Forest age played only a minor role and SOC stocks were unaffected from the vegetation type (forest or grassland). Fine texture, pH, C/N ratio and forest age explained 86% of variance in SOC stocks according to a multiple linear regression (Eq. (4)). SOC stocks of forests in low relief position of the active flooding zone were 50% greater than in high elevated forests or in forests of the former flooding zone. These results showed that the hydrologic situation of the floodplain (high and low relief; active and former flooding zone) strongly controls SOC storage.

The heavy density fraction (HF)—where SOC is mostly occurs in organomineral complexes—was the most important SOC pool, dominating with > 64% in top- and subsoil (Fig. 9). The most important driver for mineralization was unprocessed fresh plant litter, explaining 31-59% of variance in mineralization rate (Fig. 12). The most important driver for SOC stabilization in floodplain topsoils was the fine texture content (R^2 = 0.64). Fine texture was also negatively related to mineralizable C, explaining 43-47% of variance in top- and subsoil (Fig. 10 and Fig. 11). These results indicated that sedimentation of fine textured material is a key driver for SOC stabilization processes in floodplains.

Total soil CO_2 effluxes in hardwood floodplain forests of the lower middle Elbe River ranged between 1006 and 2209 gC m^{-2} y^{-1} (corresponding to 10 and 22 t ha^{-1} y^{-1}) (Fig. 18). Soil CO_2 efflux was mainly related (negatively) to pH and (positively) to fine soil texture (Fig. 19). Soil pH and fine texture explained 75% of variance in soil CO_2 efflux according to a multiple linear regression (Eq. (12)). This result seems to contradict to the finding of Article I and II where fine texture content was related to SOC storage. However, relative soil CO_2 effluxes

(in gC gSOC^{-1} y^{-1}) were partly more than 50% smaller in low lying forests—where large fine texture contents and enhanced preservation through oxygen scarcity occurs—than in high elevated forests (Fig. 20). Thus, positive effects of fine texture on soil moisture and SOC content contributed to large soil CO_2 efflux, while SOC was protected in forests with low relief position.

The self-designed soil CO_2 probe, K33SOIL, competed well (RMSE = 0.032% CO_2) with the often used GMP343 (Vaisala, Finland) in precision and accuracy (Fig. 24). A field experiment (Fig. 25) showed that the K33SOIL is also suitable for *in situ* applications.

6.2 Effects of vegetation on the soil carbon balance

Usually, forest aging contributes to larger SOC stocks due to a higher litter input to the soil (Lal, 2005). SOC stocks did not differ between vegetation categories (grassland, forest, and forest age; Fig. 4) and forest age played only a role for SOC stocks once confounding variables were kept constant (Eq. (4)). The quality of litter was the most important energy source for SOC mineralization, i.e. fresh plant detritus containing wide C/N ratios contributed to fast turnover rates (Fig. 12). This could imply that in forests where the litter generally has wider C/N ratios, more SOC is directly mineralized. However, SOC stocks increased with soil C/N ratio according to a multiple linear regression (Eq. (4)), which was related to the amount of autochthonic C input and SOC preservation by oxygen scarcity. Consequently, fresh plant litter is predominantly preserved in low lying forests where oxygen scarcity occurs close to the soil surface. A weak ($p < 0.1$) negative relation between C/N ratio and soil CO_2 effluxes (Fig. 19) would support the finding that fresh plant litter is protected in low lying forests. The results show that forest age and litter input play a minor role for SOC storage because most effects are overprinted by the hydrologic situation.

6.3 Effects of hydrologic situation on the soil carbon balance

Periodic flooding partly controls soil respiration and oxygen scarcity can preserve SOC in floodplains (Hennings et al., 2021; Yoon et al., 2014). SOC stocks and relative soil CO_2 efflux was mainly controlled by proxies for floodplain relief and sedimentation processes (e.g.,

hydromorphic features, flooding duration, soil texture) and showed that the hydrologic situation plays a key role in the soil C balance of hardwood floodplain forests. In low lying forests, the SOC stocks were greatest and relative soil CO_2 effluxes were smaller compared to their high counterparts and to forests in the former flooding zone (Fig. 4 and Fig. 20). Flooding duration was closely positively related to SOC stocks (Fig. 7), indicating that preservation by oxygen scarcity and allochthonous C input play an important role for SOC storage. The strong relation of SOC stabilization in organomineral complexes to fine texture (Fig. 10) confirmed that also the sedimentation of fine-textured material plays a key role for SOC stabilization. Relief affects on soil properties were also reflected by the relation of soil pH on SOC stocks and soil CO_2 efflux (Eq. (4) and Fig. 19). Greatest SOC stocks and smallest total soil CO_2 effluxes were found on sites with high pH (i.e., close to neutral), which were mostly low lying forests of the active floodplain, and indicated that microbial SOC mineralization is increased on sites with more acidic soil conditions. These results showed that SOC protection is increased in forests with low relief position due to allochthonous C input, oxygen scarcity, and stabilization to fine soil particles.

Groundwater fluctuations—induced by river water table fluctuations in floodplains— also control dissolution and precipitation of Fe and Mn, which appear in oxidative or reductive form as hydromorphic features of the soil. Fe and Mn can also be involved in metal organic complexes, and in wetlands, Fe oxides and hydroxides are able to protect SOC from mineralization (Wang et al., 2017). In my studies, the occurrence of hydromorphic features close to the soil surface was related to large SOC stocks (Fig. A 2) and to a decrease in relative soil CO_2 efflux (Fig. 21). Both results indicated that the characterization of hydromorphic features could be used as a helpful indicator for SOC storage in hardwood floodplain forests.

In floodplains, relief controls the sedimentation and erosion of fine soil particles (González et al., 2014). Fine soil texture was the most important driver for SOC stocks, SOC stabilization and soil CO_2 efflux. The positive relation of fine texture to SOC stocks and SOC stabilization indicated that SOC is largely protected by organomineral complexes in floodplains. Fine texture was also the strongest (positive) univariate predictor for soil CO_2

efflux, which contradicted to the finding that fine texture protects SOC from mineralization. However, the strong positive effect of fine texture on soil CO_2 efflux was related to indirect positive effects on soil moisture and SOC content, which both strongly affect activity of microbial mineralization. Furthermore, the positive effect of soil moisture on root vitality in fine textured soils might have contributed to these large soil CO_2 effluxes. The finding that relative soil CO_2 effluxes were smallest in low lying forests (Fig. 20)—which are dominated by fine texture (Fig. 7)—agrees again with the strong SOC protection mechanisms by stabilization to fine soil particles and oxygen scarcity. Thus, floodplain relief and sedimentation processes are the most important drivers for C loss through soil CO_2 efflux, SOC stocks and SOC stabilization processes, which are key parameters of the soil C balance. Therefore, the hydrologic situation is the most important factor for the soil C balance in hardwood floodplain forests of the lower middle Elbe River.

My dissertation has shown that in hardwood floodplain forest of the lower middle Elbe River, floodplain relief and sedimentation processes and their related soil properties, such as oxygen supply, fine soil texture content, soil pH, hydromorphic features and C/N ratio, mainly control SOC preservation, and processes contributing to microbial SOC mineralization, stabilization and root respiration. The hydrologic situation was the most important factor for SOC storage, while vegetation type or age played only a minor role. Hardwood floodplain forests are better C sinks once located in the active flooding zone, storing up to 50% more SOC than their former counterparts. This dissertation reveals important knowledge about the controlling factors of the process-based soil C balance in hardwood floodplain forests. The studies improve methodological applications for *in situ* CO_2 measurements and provide important empirical data for estimations of climate change scenarios. My results imply that the C storage potential of hardwood floodplain forests is increased once they are located in the active flooding zone and naturally affected by flooding and sedimentation processes, which could have positive effects on global warming mitigation.

7 Outlook

I have shown that hardwood floodplain forests can only address their high C storage potential once they are located in the active flooding zone and the floodplain is left in its natural state, where flooding and sedimentation processes occur. However, today, there are anthropogenic negative effects on the SOC storage potential in hardwood floodplain forests. For example, anthropogenic landscape modifications, such as dike building, clearing, and channelization, have decreased allochthonous and autochthonous C inputs and affected the flooding regime (e.g., soil erosion, sedimentation and oxygen supply) (Brunotte et al., 2009). This has reduced the C storage potential of floodplains drastically (Hornung et al., 2019).

For future floodplain management, my results imply that the C storage potential of floodplains can be increased by establishing hardwood floodplain forests in the active flooding zone, allowing flooding and allochthonous C input. Forests in the active flooding zone can also affect flood risk regulation positively by providing natural buffer zones (Hornung et al., 2019). During flooding, also nutrients are deposited, which are important energy sources for flora and fauna. Since I found that soil pH was higher (i.e., closer to neutral) in the active flooding zone, compared to the former, a stronger nutrient availability—as a consequence of a strong soil cation exchange capacity at high pH (Härdtle et al., 2004)—could occur in the active flooding zone as well. Further studies would need to prove that. After flooding events, soil microorganisms break down fresh sedimented coarse organic matter and make even more nutrients available (Sutfin et al., 2016). SOC is the most important energy source for microorganisms; and micro- meso- and macro-fauna benefit from larger microorganism contents, particulate organic matter, and available nutrients (Basile-Doelsch et al., 2020). These could have positive effects for biodiversity. Thus, establishing hardwood floodplain forests in a natural active flooding zone could not only increase the C storage potential of floodplains but also biodiversity.

Since the hydrologic situation was the most important factor for SOC storage, further studies should give more insights about C stabilization, mobilization and degradation

processes induced by flooding and groundwater fluctuations in floodplains. For example, in other wetlands, such as peatlands, the co-precipitation of C with Fe plays an important role in C protection, but anoxic soil conditions can also reduce $Fe(III)$ to $Fe(II)$, causing a C release (Chen et al., 2020; Patzner et al., 2020). Groundwater fluctuations also control transfer processes of dissolved organic C, which is an easy available component for SOC mineralization (Basile-Doelsch et al., 2020). Knowledge about C transfer and stabilization processes of C during groundwater fluctuations and changing oxygen supply would give more certainty about the C storage potential of floodplains.

My studies showed that sedimentation of allochthonous C can be important for the forests to act as C sinks and that the relative soil CO_2 efflux is reduced at sites with a narrow water table depth due to oxygen scarcity. However, during my measurement period, no flooding occurred on the study sites. Due to this, effects of flooding, erosion and sedimentation on SOC were not measured directly. Also another important greenhouse gas, CH_4—which predominately releases during anaerobic soil conditions (Schindler et al., 2020)—could therefore not be measured. To measure gas fluxes during future flooding events, low-cost greenhouse gas sensors (Heger et al., 2020) could be installed permanently in floodplains. They could also help to identify the spatial and temporal coverage of *in situ* leaf C assimilation and respiration because conventional methods, e.g., the eddy covariance technic, are costly and work-intensive (Myklebust et al., 2008). However, for the soil C balance in hardwood floodplain forests, I found that flooding and sedimentation are the most important processes. I suggest that the prediction of future flooding events would therefore improve the understanding of the implications of flooding on the soil C balance in hardwood floodplain forests and infer important impacts on global warming.

To compare the total C storage (as mass value) of hardwood floodplain forests to other ecosystems globally, my data should be combined with biomass C stocks and interpolated with area coverage information of vegetation type and elevation. These results would further show the C storage potential of floodplains and improve the importance of hardwood floodplain forests for humans and climate change.

8 Appendices

8.1 Appendix A: Article I

Table A 1. Descriptive soil data.

Category	Dominating Reference Soil Group[a]	Hydromorphy[b] (m)	
		mean	SD
low grassland (active) (n = 5)	Gleyic Cambisol Fluvic Gleysol	0.44	0.20
low forest (active) (n = 10)	Gleyic Fluvic Cambisol Fluvic Gleysol	0.55	0.39
low/high young forest (active) (n = 5)	Gleyic Cambisol Fluvic Gleysol	0.72	0.38
high grassland (active) (n = 5)	Fluvic Cambisol	0.94	0.34
high forest (active) (n = 10)	(Lamelli-)Fluvic Arenosol	1.24	0.47
low forest (former) (n = 5)	Gleyic Fluvisol	0.39	0.32

[a] According to IUSS Working Group WRB (2015)
[b] Defined as the first appearance of hydromorphic mottling—where redoximorphic features covered an area of > 5% of the soil horizon according to Ad-hoc-AG Boden (2005)—below the mineral surface

Table A 2. Analytical composite topsoil (0–10 cm) data.

Category	SOC stock (t ha^{-1})		SOC (g kg^{-1})		C/N ratio		pH[a]		fine texture[b] (%)	
	mean	SD	mean	SD	mean	SD	mean	SD	mean	SD
low grassland (active) (n = 6)	40.99	7.03	42.64	10.44	11	0.7	5.2	0.4	41.87	21.47
low forest (active) (n = 11)	47.04	7.99	47.13	10.97	11.6	1.0	5.3	0.5	35.30	19.51
low/high young forest (active) (n = 7)	35.66	15.97	34.17	19.44	10.7	0.8	5.2	0.3	33.80	24.48
high grassland (active) (n = 5)	25.50	4.40	22.58	4.88	10.9	1.1	5.3	0.4	13.23	2.82
high forest (active) (n = 13)	30.74	4.64	27.05	5.02	11.8	1.2	5.0	0.3	14.17	6.60
low forest (former) (n = 7)	31.61	4.81	28.79	3.98	13.0	1.4	4.1	0.5	14.97	13.30

[a] measured in 0.01 M CaCl$_2$; mean and SD was calculated using the pH
[b] sum of clay and fine silt fraction (< 6.3 μm)

Table A 3. Analytical profile (0–100 m) data.

Category	Depth (cm)	SOC stock (t ha^{-1})		SOC (g kg^{-1})		C/N ratio		pH[a]	
		mean	SD	mean	SD	mean	SD	mean	SD
low grassland (active) (n = 5)	0–10	45.90	8.49	51.54	13.91	11.5	0.2	5.3	0.4
	10–30	56.19	11.21	25.73	6.38	11.8	1.5	5.4	0.2
	30–60	21.94	6.49	5.43	1.73	9.7	1.9	5.6	0.2
	60–100	20.02	14.48	3.75	2.93	8.5	1.7	5.7	0.6
	0–100	144.05	35.82	13.43	3.88	9.8	1.3	5.6	0.3
low forest (active) (n = 10)	0–10	43.43	9.40	44.02	12.55	11.2	0.8	5.3	0.4
	10–30	47.89	13.73	21.09	7.63	10.9	3.0	5.2	0.6
	30–60	32.18	11.72	8.27	3.43	8.8	1.3	5.7	0.5
	60–100	25.57	8.36	4.61	1.57	7.8	0.8	6.1	0.4
	0–100	149.07	33.45	12.94	3.35	9.1	1.3	5.7	0.4
low/high young forest (active) (n = 5)	0–10	34.51	16.91	36.88	26.47	11.3	0.7	5.2	0.3
	10–30	31.29	17.72	12.95	8.40	9.5	1.4	5.1	0.4
	30–60	22.94	11.08	5.60	2.92	7.6	0.8	5.5	0.7
	60–100	21.63	13.19	3.88	2.44	6.6	2.1	5.8	0.5
	0–100	110.37	50.00	9.51	5.18	8.0	1.1	5.5	0.5
high grassland (active) (n = 5)	0–10	28.51	3.88	26.19	4.31	11.0	0.6	5.2	0.5
	10–30	30.04	4.96	12.09	2.35	10.3	0.9	5.2	0.4
	30–60	20.17	6.31	4.93	1.69	8.9	0.9	5.3	0.4
	60–100	9.82	2.52	1.68	0.45	8.1	1.6	5.7	0.2
	0–100	88.54	12.55	7.19	1.12	9.1	1.1	5.4	0.3
high forest (active) (n = 10)	0–10	37.58	6.23	36.25	8.18	12.2	0.9	5.2	0.4
	10–30	30.64	8.73	12.21	3.94	10.8	1.3	4.7	0.4
	30–60	16.16	7.80	3.88	1.99	8.3	1.4	5.2	0.5
	60–100	14.69	6.41	2.59	1.19	6.9	1.2	5.5	0.3
	0–100	99.07	22.19	8.27	2.03	8.6	0.9	5.2	0.4
low forest (former) (n = 5)	0–10	35.59	6.34	35.21	8.18	12.5	1.1	4.1	0.4
	10–30	23.11	9.40	9.25	4.14	9.7	0.9	4.4	0.6
	30–60	17.15	10.53	4.33	2.77	6.7	1.8	5.2	0.8
	60–100	23.60	11.01	4.17	1.97	6.3	1.7	5.6	0.8
	0–100	99.45	32.01	8.34	2.73	7.7	1.4	5.1	0.7

[a] measured in 0.01 M CaCl$_2$; mean and SD was calculated using the pH
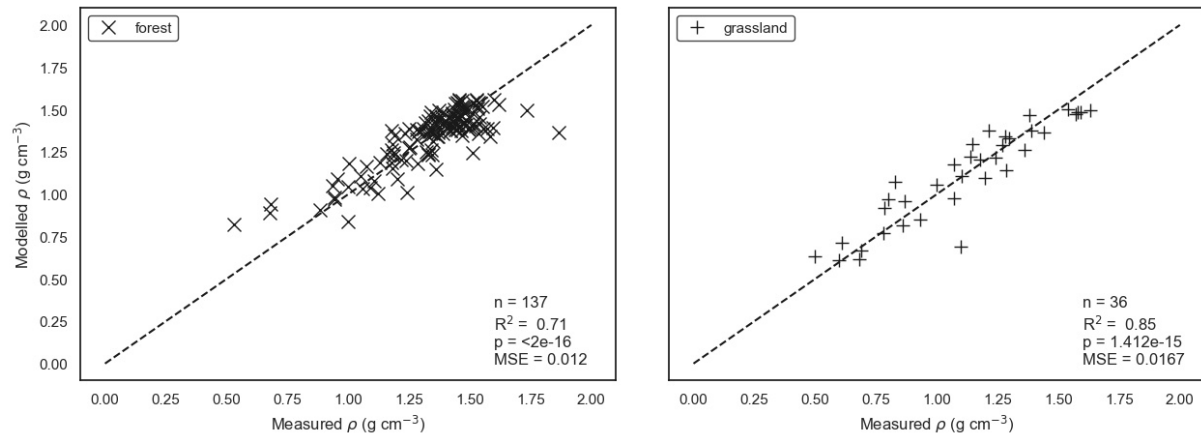
Fig. A 1. Measured vs. modelled ρ for forest (x) and grassland (+) study sites.

Table A 4. Table with scores of the NMDS1 and NMDS2.

	NMDS1	NMDS2
SOC stock	0.04	0.81
SOC	0.00	0.82
pH	-0.23	0.30
flooding	-0.16	0.83
hydromorphy	0.18	-0.35
C/N ratio	0.37	-0.25
age	0.95	0.06
basal area	0.93	0.06
litter-C	0.72	-0.06
fine texture	-0.13	0.82
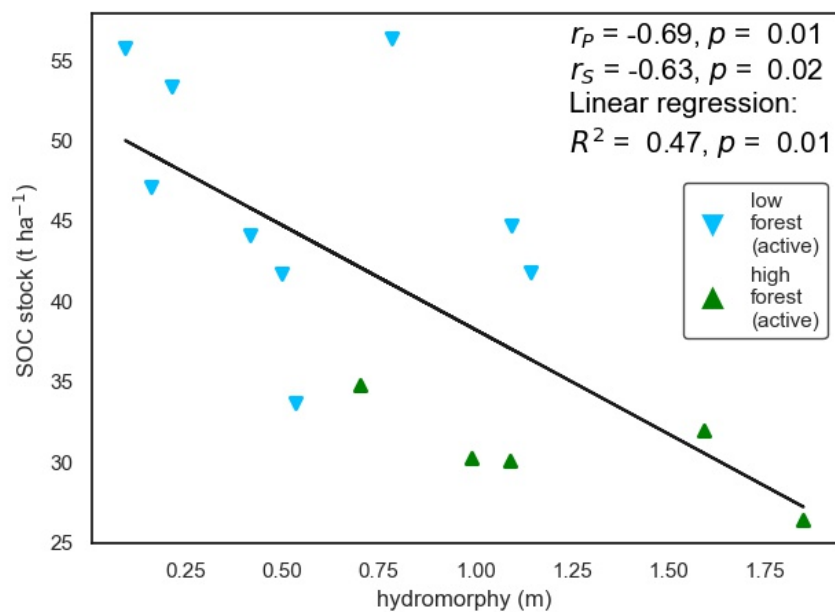
Fig. A 2. Depth of hydromorphic features (hydromorphy) vs. SOC stocks. Only old forests of the active floodplain are displayed.

Table A 5. Summary of the stepwise MLR of SOC stocks in dependence of pH, C/N ratio, age, and fine texture. Residual standard error = 4.1 on 33 degrees of freedom. Multiple R^2 = 0.87. Adjusted R^2 = 0.86. F-statistic = 57.19, p = < 0.001.

Predictor	Estimate	Std. error	t value	p[a]
pH	5.96	1.30	4.59	***
C/N	3.39	0.63	5.40	***
age	0.04	0.01	2.98	**
fine texture	0.56	0.04	13.99	***

[a] Significance codes for p: *** < 0.001, ** < 0.01

8.2 Appendix B: Article II

Table B 1. Results of the pairwise t-test between top- (0–10 cm) and subsoil (10–30). Variables are the total soil organic carbon (SOC) content, metabolic quotient (qCO_2), mineralization rate constant (k), as well as the absolute (g kg^{-1} soil) or relative (% SOC) contributions of the density fractions (fLF, oLF, HF), mineralizable carbon (C0), and microbial biomass (C_{mic}) to SOC.

T	dof	p	BF10	hedges	normality	p (wilcoxon)	variable
5.047	7	0.0015	29.926	1.264	TRUE		SOC
2.280	7	0.0567	1.730	0.776	TRUE		fLF (g kg^{-1})
5.170	7	0.0013	33.407	2.280	TRUE		oLF (g kg^{-1})
4.790	7	0.0020	23.619	0.972	TRUE		HF (g kg^{-1})
-0.862	7	0.4174	0.454	-0.339	FALSE	1	fLF (% SOC)
3.826	7	0.0065	9.177	1.911	TRUE		oLF (% SOC)
-2.072	7	0.0770	1.381	-0.844	TRUE		HF (% SOC)
1.518	7	0.1729	0.781	0.758	TRUE		OC of fLF
-0.040	7	0.9691	0.336	-0.016	FALSE	0.461	OC of oLF
4.679	7	0.0023	21.284	1.003	TRUE		OC of HF
6.354	7	0.0004	90.212	1.627	TRUE		N of fLF
2.856	7	0.0245	3.259	1.395	FALSE	0.016	N of oLF
4.590	7	0.0025	19.570	0.867	TRUE		N of HF
-5.461	7	0.0009	43.162	-1.704	TRUE		C/N of fLF
-5.768	7	0.0007	56.085	-1.753	TRUE		C/N of oLF
1.365	7	0.2145	0.677	0.347	TRUE		C/N of HF
3.427	7	0.0110	6.048	1.405	TRUE		C_{mic} (g kg^{-1})
-0.567	7	0.5885	0.384	-0.232	FALSE	0.945	C_{mic} (% SOC)
1.542	7	0.1671	0.800	0.626	TRUE		qCO_2
5.850	7	0.0006	60.033	1.752	TRUE		C0 (g kg^{-1})
3.179	7	0.0155	4.636	0.520	TRUE		C0 (% SOC)
3.190	7	0.0153	4.692	0.716	FALSE	0.008	k
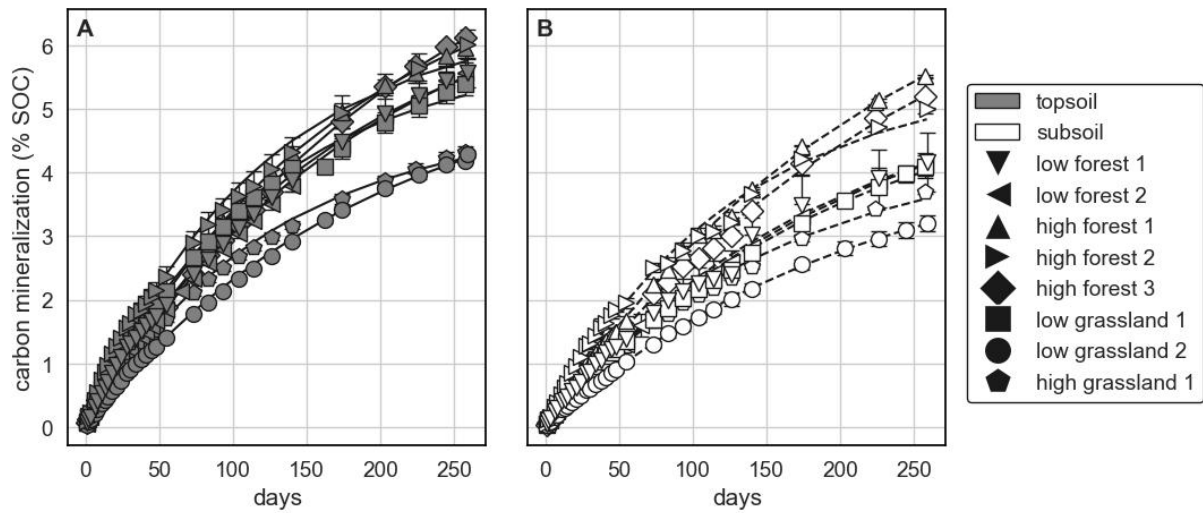
Fig. B 1. Cumulative relative mineralization of SOC. The lines (straight: topsoil (0–10 cm), dotted: subsoil (10–30 cm) show the fit of Eq. (5).
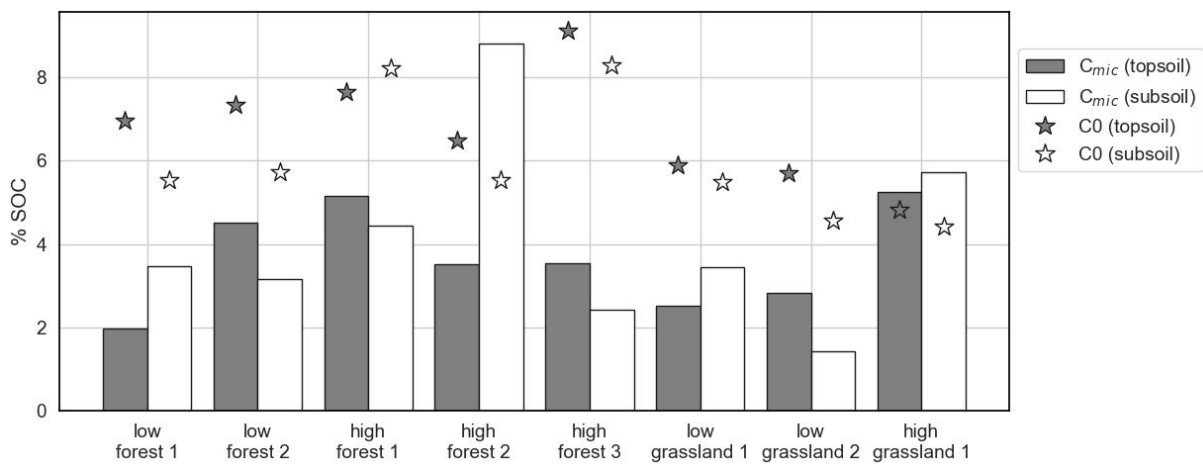
Fig. B 2. Microbial biomass (C_{mic}, in % SOC) and mineralizable carbon (C0, in % SOC) for the 8 study sites in top- (0–10 cm) and subsoil (10–30 cm). Depth differences were significant for C0 ($p < 0.05$) but not for C_{mic} according to pairwise t-test.

Fig. B 3. Correlation matrix with Pearson correlation coefficient in the topsoil (0–10 cm).

Fig. B 4. Correlation matrix with Pearson correlation coefficient in the subsoil (10–30 cm).

8.4 Appendix C: Article III

Table C 1. Reference soil groups (RSG, according to IUSS Working Group WRB (2015)) and coordinates of studied soil profiles.

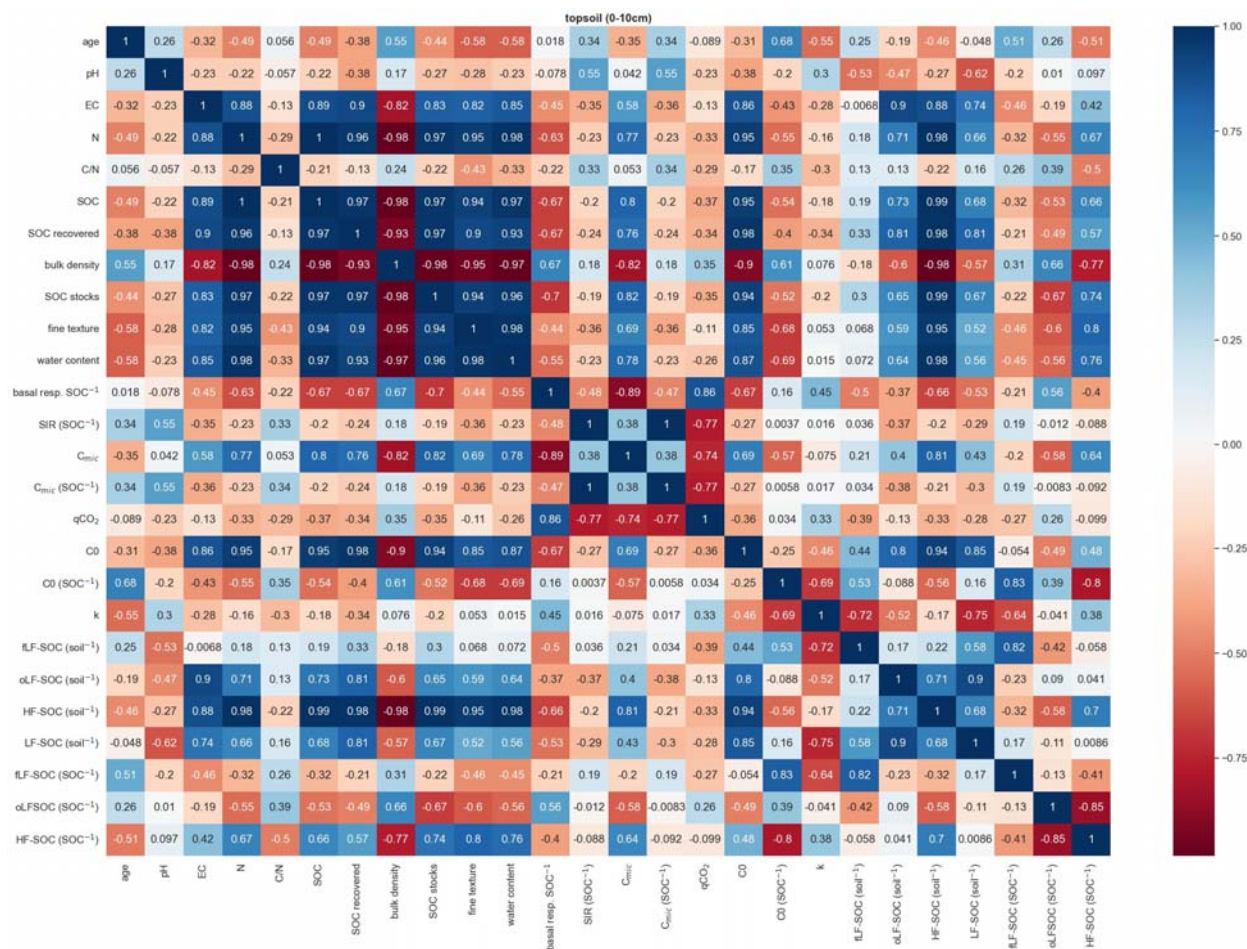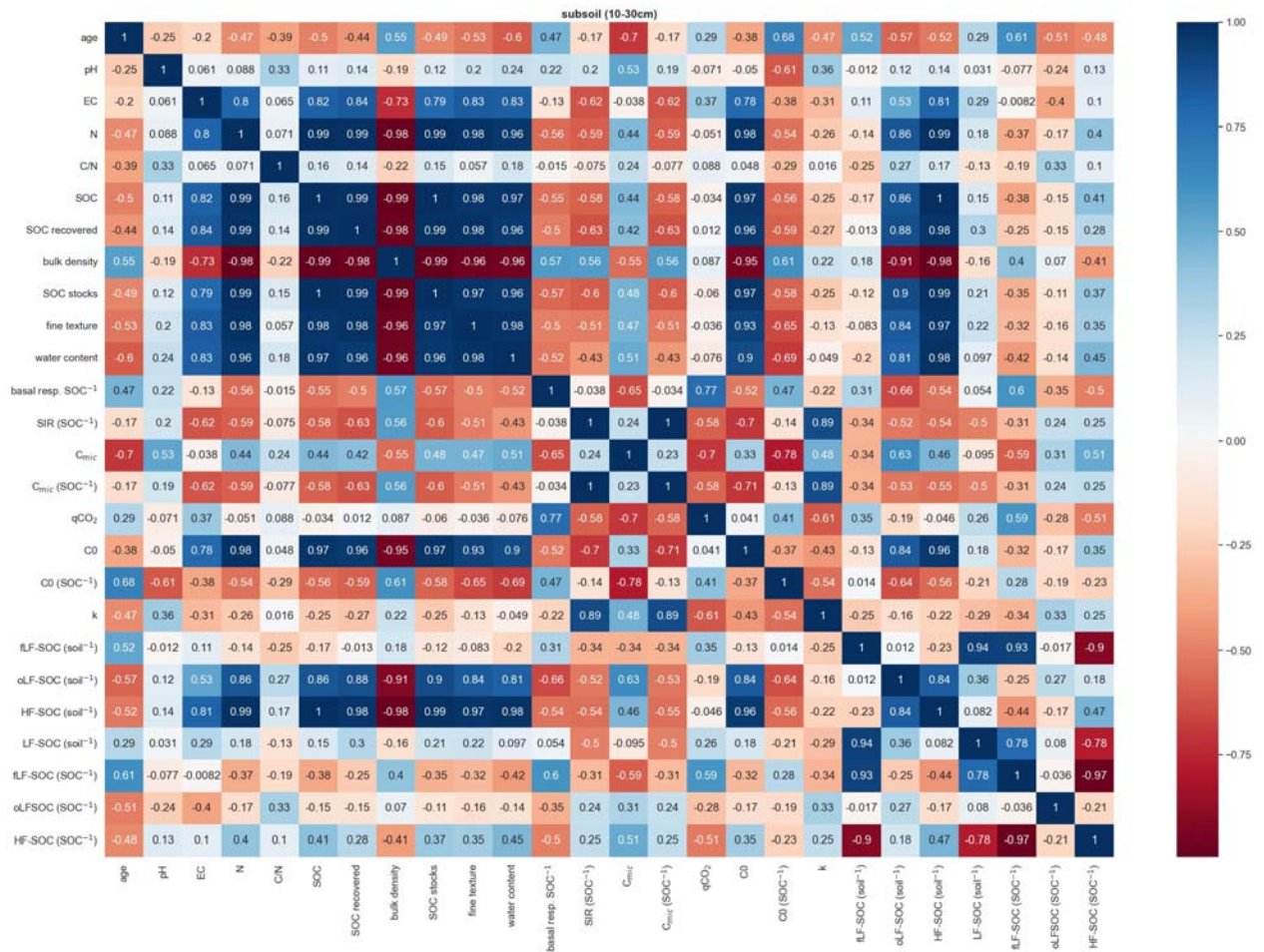| Site	ID	Soil Profile	RSG	Land use	Latitude (E)	Longitude (N)
Active low forest I	JB1	P1	Gleyic Fluvic Cambisol	forest	53.16446	11.14227
		P2	Fluvic Gleysol	forest	53.16462	11.14238
		P3	Fluvic Gleysol	forest	53.16458	11.14235
Active high forest II	JB3	P1	Gleyic Cambisol	plantation	53.15955	11.13163
		P2	Gleyic Cambisol	plantation	53.159519	11.131546
		P3	Fluvic Gleysol	plantation	53.15959	11.13155
Active high forest I	JW1	P1	(Lamelli-)Fluvic Arenosol	forest	53.17972	11.00866
		P2	(Lamelli-)Fluvic Arenosol	forest	53.17977	11.00882
		P3	(Lamelli-)Fluvic Arenosol	forest	53.17983	11.00874
Active low forest II	LS1	P1	Fluvic Cambisol	forest	53.28766	11.29416
		P2	Fluvic Cambisol	forest	53.08777	11.29426
		P3	Fluvic Cambisol	forest	53.0877	11.29439
Former low forest I (seepage)	LE1	P1	Gleyic Fluvisol	forest	52.8865	11.97123
		P2	Gleyic Fluvisol	forest	52.88658	11.97147
		P3	Gleyic Fluvisol	forest	52.8866	11.97127
Former low forest II (dis-connected)	SU1	P1	Fluvic Gleysol (drainic)	forest	53.27289	10.89453
		P2	Gleyic Fluvic Cambisol (drainic)	forest	53.27302	10.89433
		P3	Fluvic Gleysol (drainic)	forest	53.27287	10.89433

References

Acosta, M., Darenova, E., Dušek, J., Pavelka, M., 2017. Soil carbon dioxide fluxes in a mixed floodplain forest in the Czech Republic. European Journal of Soil Biology 82, 35-42. https://doi.org/10.1016/j.ejsobi.2017.08.006

Ad-hoc-AG Boden, 2005. Bodenkundliche Kartieranleitung, (Vol. 5), Hannover.

Anderson, T.-H., Domsch, K. H., 1993. The metabolic quotient for CO2 (qCO2) as a specific activity parameter to assess the effects of environmental conditions, such as ph, on the microbial biomass of forest soils. Soil Biol. Biochem. 25 (3), 393-395. https://doi.org/10.1016/0038-0717(93)90140-7

Appling, A. P., Bernhardt, E. S., Stanford, J. A., 2014. Floodplain biogeochemical mosaics: A multidimensional view of alluvial soils. J. Geophys. Res. Biogeosci. 119 (8), 1538-1553. https://doi.org/10.1002/2013JG002543

Bai, J., Ouyang, H., Deng, W., Zhu, Y., Zhang, X., Wang, Q., 2005. Spatial distribution characteristics of organic matter and total nitrogen of marsh soils in river marginal wetlands. Geoderma 124 (1), 181-192. https://doi.org/10.1016/j.geoderma.2004.04.012

Baker III, T. T., Lockaby, B. G., Conner, W. H., Meier, C. E., Stanturf, J. A., Burke, M. K., 2001. Leaf Litter Decomposition and Nutrient Dynamics in Four Southern Forested Floodplain Communities. Soil Sci. Soc. Am. J. 65 (4), 1334-1347. https://doi.org/10.2136/sssaj2001.6541334x

Basile-Doelsch, I., Balesdent, J., Pellerin, S., 2020. Reviews and syntheses: The mechanisms underlying carbon storage in soil. Biogeosciences 17 (21), 5223-5242. 10.5194/bg-17-5223-2020

Bastviken, D., Sundgren, I., Natchimuthu, S., Reyier, H., Gålfalk, M., 2015. Cost-efficient approaches to measure carbon dioxide (CO2) fluxes and concentrations in terrestrial and aquatic environments using mini loggers. Biogeosciences 12 (12), 3849-3859.

Battin, T. J., Luyssaert, S., Kaplan, L. A., Aufdenkampe, A. K., Richter, A., Tranvik, L. J., 2009. The boundless carbon cycle. Nature Geoscience 2 (9), 598-600. https://doi.org/10.1038/ngeo618

Bechtold, J. S., Naiman, R. J., 2009. A Quantitative Model of Soil Organic Matter Accumulation During Floodplain Primary Succession. Ecosystems 12 (8), 1352-1368. https://doi.org/10.1007/s10021-009-9294-9

Bechtold, S. J., Naiman, R. J., 2006. Soil texture and nitrogen mineralization potential across a riparian toposequence in a semi-arid savanna. Soil Biol. Biochem. 38 (6), 1325-1333. https://doi.org/10.1016/j.soilbio.2005.09.028

Blosser, G. D. (2018). *Assessment of aboveground net primary productivity and carbon pools, detrital biomass, community structure, and species composition across a floodplain forest of the Congaree River.* (Doctoral dissertation). Clemson University, Clemson, South Carolina. Retrieved from https://tigerprints.clemson.edu/all_dissertations/2228

Boeing, F., Rakovech, O., Kumar, R., Samaniego, L., Schrön, M., Hildebrandt, A., Rebmann, C., Thober, S., Müller, S., Zacharias, S., Bogena, H., Schneider, K., Kiese, R., Marx, A., 2021. High-resolution drought simulations and comparison to soil moisture observations in Germany. Hydrol. Earth Syst. Sci. Discuss. 2021, 1-35. https://doi.org/10.5194/hess-2021-402

Bond-Lamberty, B., Thomson, A., 2010. A global database of soil respiration data. Biogeosciences 7 (6), https://doi.org/10.5194/bg-7-1915-2010

Boone, R. D., Nadelhoffer, K. J., Canary, J. D., Kaye, J. P., 1998. Roots exert a strong influence on the temperature sensitivity of soil respiration. Nature 396 (6711), 570-572. https://doi.org/10.1038/25119

Bossuyt, H., Six, J., Hendrix, P. F., 2005. Protection of soil carbon by microaggregates within earthworm casts. Soil Biol. Biochem. 37 (2), 251-258. https://doi.org/10.1016/j.soilbio.2004.07.035

Brunotte, E., Dister, E., Günther-Diringer, D., Koenzen, U., Mehl, D., 2009. Flussauen in Deutschland: Erfassung und Bewertung des Auenzustandes, (Vol. 87) BfN-Schriftenvertrieb.

Buck, A. L., 1981. New Equations for Computing Vapor Pressure and Enhancement Factor. Journal of Applied Meteorology and Climatology 20 (12), 1527-1532. 10.1175/1520-0450(1981)020<1527:Nefcvp>2.0.Co;2

Bullinger-Weber, G., Le Bayon, R. C., Thébault, A., Schlaepfer, R., Guenat, C., 2014. Carbon storage and soil organic matter stabilisation in near-natural, restored and embanked Swiss floodplains. Geoderma 228-229, 122-131.

Cao, H., Chen, R., Wang, L., Jiang, L., Yang, F., Zheng, S., Wang, G., Lin, X., 2016. Soil pH, total phosphorus, climate and distance are the major factors influencing microbial activity at a regional spatial scale. Sci. Rep. 6, https://doi.org/10.1038/srep25815

Cerli, C., Celi, L., Kalbitz, K., Guggenberger, G., Kaiser, K., 2012. Separation of light and heavy organic matter fractions in soil—Testing for proper density cut-off and dispersion level. Geoderma 170, 403-416.

Chen, C., Hall, S. J., Coward, E., Thompson, A., 2020. Iron-mediated organic matter decomposition in humid soils can counteract protection. Nat. Commun. 11 (1), 1-13.

Chen, S., Zou, J., Hu, Z., Chen, H., Lu, Y., 2014. Global annual soil respiration in relation to climate, soil properties and vegetation characteristics: Summary of available data. Agric. For. Meteorol. 198-199, 335-346. https://doi.org/10.1016/j.agrformet.2014.08.020

Cierjacks, A., Kleinschmit, B., Babinsky, M., Kleinschroth, F., Markert, A., Menzel, M., Ziechmann, U., Schiller, T., Graf, M., Lang, F., 2010. Carbon stocks of soil and vegetation on Danubian floodplains. J. Plant Nutr. Soil Sci. 173 (5), 644-653. https://doi.org/10.1002/jpln.200900209

Cierjacks, A., Kleinschmit, B., Kowarik, I., Graf, M., Lang, F., 2011. Organic matter distribution in floodplains can be predicted using spatial and vegetation structure data. River Res. Appl. 27 (8), 1048-1057. https://doi.org/10.1002/rra.1409

Cole, J. J., Prairie, Y. T., Caraco, N. F., McDowell, W. H., Tranvik, L. J., Striegl, R. G., Duarte, C. M., Kortelainen, P., Downing, J. A., Middelburg, J. J., Melack, J., 2007. Plumbing the Global Carbon Cycle: Integrating Inland Waters into the Terrestrial Carbon Budget. Ecosystems 10 (1), 172-185. https://doi.org/10.1007/s10021-006-9013-8

Craft, C., Seneca, E., Broome, S., 1991. Loss on ignition and Kjeldahl digestion for estimating organic carbon and total nitrogen in estuarine marsh soils: calibration with dry combustion. Estuaries 14 (2), 175-179.

Cressey, E. L., Dungait, J. A. J., Jones, D. L., Nicholas, A. P., Quine, T. A., 2018. Soil microbial populations in deep floodplain soils are adapted to infrequent but regular carbon substrate addition. Soil Biol. Biochem. 122, 60-70. https://doi.org/10.1016/j.soilbio.2018.04.001

Curtis, P. S., Vogel, C. S., Gough, C. M., Schmid, H. P., Su, H. B., Bovard, B. D., 2005. Respiratory carbon losses and the carbon-use efficiency of a northern hardwood forest, 1999–2003. New Phytol. 167 (2), 437-456. https://doi.org/10.1111/j.1469-8137.2005.01438.x

D'Elia, A. H., Liles, G. C., Viers, J. H., Smart, D. R., 2017. Deep carbon storage potential of buried floodplain soils. Sci. Rep. 7 (1), 1-7.

Davidson, E. A., Belk, E., Boone, R. D., 1998. Soil water content and temperature as independent or confounded factors controlling soil respiration in a temperate mixed hardwood forest. Global Change Biol. 4 (2), 217-227. https://doi.org/10.1046/j.1365-2486.1998.00128.x

Davidson, E. A., Verchot, L. V., Cattânio, J. H., Ackerman, I. L., Carvalho, J. E. M., 2000. Effects of soil water content on soil respiration in forests and cattle pastures of eastern Amazonia. Biogeochemistry 48 (1), 53-69. https://doi.org/10.1023/A:1006204113917

Davis, M. R., Condron, L. M., 2002. Impact of grassland afforestation on soil carbon in New Zealand: a review of paired-site studies. Soil Research 40 (4), 675-690.

De Vos, B., Van Meirvenne, M., Quataert, P., Deckers, J., Muys, B., 2005. Predictive quality of pedotransfer functions for estimating bulk density of forest soils. Soil Sci. Soc. Am. J. 69 (2), 500-510.

Dee, M. M., Tank, J. L., 2020. Inundation time mediates denitrification end products and carbon limitation in constructed floodplains of an agricultural stream. Biogeochemistry 149 (2), 141-158. https://doi.org/10.1007/s10533-020-00670-x

Deiss, L., Franzluebbers, A. J., Amoozegar, A., Hesterberg, D., Polizzotto, M., Cubbage, F. W., 2017. Soil carbon fractions from an alluvial soil texture gradient in North Carolina. Soil Sci. Soc. Am. J. 81 (5), 1096-1106. https://doi.org/10.2136/sssaj2016.09.0304

Deutscher Wetterdienst, 2022. Niederschlag 1991-2020, Lüchow. https://opendata.dwd.de/climate_environment/CDC/observations_germany/climate/multi_annual/mean_91-20/, access date: 20/01/2022

Doering, M., Uehlinger, U., Ackermann, T., Woodtli, M., Tockner, K., 2011. Spatiotemporal heterogeneity of soil and sediment respiration in a river-floodplain mosaic (Tagliamento, NE Italy). Freshwat. Biol. 56 (7), 1297-1311. https://doi.org/10.1111/j.1365-2427.2011.02569.x

Drouin, A., Saint-Laurent, D., Lavoie, L., Ouellet, C., 2011. High-Precision Elevation Model to Evaluate the Spatial Distribution of Soil Organic Carbon in Active Floodplains. Wetlands 31 (6), 1151-1164. https://doi.org/10.1007/s13157-011-0226-z

Dybala, K. E., Matzek, V., Gardali, T., Seavy, N. E., 2019. Carbon sequestration in riparian forests: A global synthesis and meta-analysis. Global Change Biol. 25 (1), 57-67. https://doi.org/10.1111/gcb.14475

Eccles, R., Zhang, H., Hamilton, D., Trancoso, R., Syktus, J., 2021. Impacts of climate change on streamflow and floodplain inundation in a coastal subtropical catchment. Advances in Water Resources 147, https://doi.org/10.1016/j.advwatres.2020.103825

Fan, L. C., Han, W. Y., 2018. Soil respiration in Chinese tea gardens: autotrophic and heterotrophic respiration. Eur. J. Soil Sci. 69 (4), 675-684. https://doi.org/10.1111/ejss.12670

Fang, C., Moncrieff, J. B., 2001. The dependence of soil CO_2 efflux on temperature. Soil Biol. Biochem. 33 (2), 155-165. https://doi.org/10.1016/S0038-0717(00)00125-5

Ferréa, C., Zenone, T., Comolli, R., Seufert, G., 2012. Estimating heterotrophic and autotrophic soil respiration in a semi-natural forest of Lombardy, Italy. Pedobiologia 55 (6), 285-294. https://doi.org/10.1016/j.pedobi.2012.05.001

Gallardo, A., 2003. Spatial Variability of Soil Properties in a Floodplain Forest in Northwest Spain. Ecosystems 6 (6), 564-576. https://doi.org/10.1007/s10021-003-0198-9

Gellens, D., Roulin, E., 1998. Streamflow response of Belgian catchments to IPCC climate change scenarios. Journal of Hydrology 210 (1), 242-258. https://doi.org/10.1016/S0022-1694(98)00192-9

Giese, L. A., Aust, W. M., Trettin, C. C., Kolka, R. K., 2000. Spatial and temporal patterns of carbon storage and species richness in three South Carolina coastal plain riparian forests. Ecol. Eng. 15, 157-170.

Giese, L. A. B., Aust, W. M., Kolka, R. K., Trettin, C. C., 2003. Biomass and carbon pools of disturbed riparian forests. For. Ecol. Manage. 180 (1-3), 493-508.

Goenster, S., Gründler, C., Buerkert, A., Joergensen, R. G., 2017. Soil microbial indicators across land use types in the river oasis Bulgan sum center, Western Mongolia. Ecol. Indicators 76, 111-118. https://doi.org/10.1016/j.ecolind.2017.01.002

Golchin, A., Oades, J. M., Skjemstad, J. O., Clarke, P., 1994. Study of free and occluded particulate organic matter in soils by solid state 13C Cp/MAS NMR spectroscopy and scanning electron microscopy. Soil Research 32 (2), 285-309.

Gomez, J., Vidon, P., Gross, J., Beier, C., Caputo, J., Mitchell, M., 2016. Estimating greenhouse gas emissions at the soil–atmosphere interface in forested watersheds of the US Northeast. Environ. Monit. Assess. 188 (5), 295. https://doi.org/10.1007/s10661-016-5297-0

González, E., Cabezas, Á., Corenblit, D., Steiger, J., 2014. Autochthonous versus allochthonous organic matter in recent soil C accumulation along a floodplain

biogeomorphic gradient: an exploratory study. Journal of Environmental Geography 7 (1-2), 29-38. https://doi.org/10.2478/jengeo-2014-0004

Good, B. J., Patrick, W. H., 1987. Gas composition and respiration of water oak (Quercus nigra L.) and green ash (Fraxinus pennsylvanica Marsh.) roots after prolonged flooding. Plant Soil 97 (3), 419-427. https://doi.org/10.1007/BF02383232

Graf-Rosenfellner, M., Cierjacks, A., Kleinschmit, B., Lang, F., 2016. Soil formation and its implications for stabilization of soil organic matter in the riparian zone. Catena 139, 9-18. http://dx.doi.org/10.1016/j.catena.2015.11.010

Griepentrog, M., Bodé, S., Boeckx, P., Hagedorn, F., Heim, A., Schmidt, M. W., 2014. Nitrogen deposition promotes the production of new fungal residues but retards the decomposition of old residues in forest soil fractions. Global Change Biol. 20 (1), 327-340.

Guo, L. B., Gifford, R. M., 2002. Soil carbon stocks and land use change: a meta analysis. Global Change Biol. 8 (4), 345-360. https://doi.org/10.1046/j.1354-1013.2002.00486.x

Gurwick, N. P., Groffman, P. M., Yavitt, J. B., Gold, A. J., Blazejewski, G., Stolt, M., 2008. Microbially available carbon in buried riparian soils in a glaciated landscape. Soil Biol. Biochem. 40 (1), 85-96.

Hamarashid, N. H., Othman, M. A., Hussain, M.-A. H., 2010. Effects of soil texture on chemical compositions, microbial populations and carbon mineralization in soil. Egypt. J. Exp. Biol. (Bot.) 6 (1), 59-64.

Härdtle, W., von Oheimb, G., Friedel, A., Meyer, H., Westphal, C., 2004. Relationship between pH-values and nutrient availability in forest soils – the consequences for the use of ecograms in forest ecology. Flora - Morphology, Distribution, Functional Ecology of Plants 199 (2), 134-142. https://doi.org/10.1078/0367-2530-00142

Harmon, T. C., Dierick, D., Trahan, N., Allen, M. F., Rundel, P. W., Oberbauer, S. F., Schwendenmann, L., Zelikova, T. J., 2015. Low-cost soil CO 2 efflux and point concentration sensing systems for terrestrial ecology applications. Methods in Ecology and Evolution 6 (11), 1358-1362.

Heger, A., Becker, J. N., Vásconez Navas, L. K., Eschenbach, A., 2021. Factors controlling soil organic carbon stocks in hardwood floodplain forests of the lower middle Elbe River. Geoderma 404, https://doi.org/10.1016/j.geoderma.2021.115389

Heger, A., Kleinschmidt, V., Gröngröft, A., Kutzbach, L., Eschenbach, A., 2020. Application of a low-cost NDIR sensor module for continuous measurements of in situ soil CO2 concentration. J. Plant Nutr. Soil Sci. 183, 557–561. https://doi.org/10.1002/jpln.201900493

Hennings, N., Becker, J. N., Guillaume, T., Damris, M., Dippold, M. A., Kuzyakov, Y., 2021. Riparian wetland properties counter the effect of land-use change on soil carbon stocks after rainforest conversion to plantations. Catena 196, https://doi.org/10.1016/j.catena.2020.104941

Hiederer, R., Köchy, M., 2011. Global soil organic carbon estimates and the harmonized world soil database. Publication Office of the European Union EUR 25225 EN, https://doi.org/10.2788/13267

Hirano, T., Kim, H., Tanaka, Y., 2003. Long-term half-hourly measurement of soil CO2 concentration and soil respiration in a temperate deciduous forest. J. Geophys. Res. 108 (D20),

Hoffmann, T., Erkens, G., Cohen, K., Houben, P., Seidel, J., Dikau, R., 2007. Holocene floodplain sediment storage and hillslope erosion within the Rhine catchment. The Holocene 17 (1), 105-118.

Hoffmann, T., Glatzel, S., Dikau, R., 2009. A carbon storage perspective on alluvial sediment storage in the Rhine catchment. Geomorphology 108 (1-2), 127-137.

Hornung, L. K., Podschun, S. A., Pusch, M., 2019. Linking ecosystem services and measures in river and floodplain management. Ecosystems and People 15 (1), 214-231. 10.1080/26395916.2019.1656287

Huang, N., Wang, L., Song, X.-P., Black, T. A., Jassal, R. S., Myneni, R. B., Wu, C., Wang, L., Song, W., Ji, D., Yu, S., Niu, Z., 2020. Spatial and temporal variations in global

soil respiration and their relationships with climate and land cover. Science Advances 6 (41), eabb8508. 10.1126/sciadv.abb8508

Hughes, F. M. R., 1997. Floodplain biogeomorphology. Prog. Phys. Geogr. 21 (4), 501-529. https://doi.org/10.1177/030913339702100402

Hupp, J., 2011. The importance of water vapor measurements and corrections. LI-COR Biosciences Inc. Application Note 129, 8.

Iqbal, M. T., Joergensen, R. G., Knoblauch, C., Lucassen, R., Singh, Y., Watson, C., Wichern, F., 2016. Rice straw addition does not substantially alter microbial properties under hypersaline soil conditions. Biol. Fertility Soils 52 (6), 867-877. 10.1007/s00374-016-1126-4

IUSS Working Group WRB, 2015. World Reference Base for Soil Resources 2014, Update 2015: International soil classification system for naming soils and creating legends for soil maps, (Vol. 106) FAO, Rome.

Janssens, I. A., Pilegaard, K. I. M., 2003. Large seasonal changes in Q10 of soil respiration in a beech forest. Global Change Biol. 9 (6), 911-918. https://doi.org/10.1046/j.1365-2486.2003.00636.x

Jobbágy, E. G., Jackson, R. B., 2000. The vertical distribution of soil organic carbon and its relation to climate and vegetation. Ecol. Appl. 10 (2), 423-436. https://doi.org/10.1890/1051-0761(2000)010[0423:Tvdoso]2.0.Co;2

Jungmann, S., Luberichs, J., Roger, M., Schwarzer, O., Niermann, I., Tüngler, N., Valdeig, S., Engehausen, B., Hollenbach, M. (2009). *Biosphärenreservatsplan mit integriertem Umweltbericht – Biosphärenreservat „Niedersächsische Elbtalaue".* Retrieved from Hitzacker:

Kaiser, E. A., Mueller, T., Joergensen, R. G., Insam, H., Heinemeyer, O., 1992. Evaluation of methods to estimate the soil microbial biomass and the relationship with soil texture and organic matter. Soil Biol. Biochem. 24 (7), 675-683. https://doi.org/10.1016/0038-0717(92)90046-Z

Keimel, A. (2019). *Comparison of Low-Cost CO2 Non-Dispersive Infrared (NDIR) Sensors for Ambient Greenhouse Gas Monitoring.* (Undergraduate Theses). University of Vermont, Vermont.

Kobal, M., Urbančić, M., Potočić, N., De Vos, B., Simončić, P., 2011. Pedotransfer functions for bulk density estimation of forest soils. Šumarski list 135 (1-2), 19-27.

Kohavi, R., 1995. A study of cross-validation and bootstrap for accuracy estimation and model selection. Paper presented at the International Joint Conference on Artificial Intelligence.

Korol, A. R., Noe, G. B., Ahn, C., 2019. Controls of the spatial variability of denitrification potential in nontidal floodplains of the Chesapeake Bay watershed, USA. Geoderma 338, 14-29. https://doi.org/10.1016/j.geoderma.2018.11.015

Kreyling, O., Kölbl, A., Spielvogel, S., Rennert, T., Kaiser, K., Kögel-Knabner, I., 2013. Density fractionation of organic matter in dolomite-derived soils. J. Plant Nutr. Soil Sci. 176 (4), 509-519. https://doi.org/10.1002/jpln.201200276

Krishna, M. P., Mohan, M., 2017. Litter decomposition in forest ecosystems: a review. Energy, Ecology and Environment 2 (4), 236-249. 10.1007/s40974-017-0064-9

Lai, L., Zhao, X., Jiang, L., Wang, Y., Luo, L., Zheng, Y., Chen, X., Rimmington, G. M., 2012. Soil Respiration in Different Agricultural and Natural Ecosystems in an Arid Region. PLOS ONE 7 (10), e48011. 10.1371/journal.pone.0048011

Lal, R., 2005. Forest soils and carbon sequestration. For. Ecol. Manage. 220 (1-3), 242-258.

Lininger, K. B., Wohl, E., Rose, J. R., 2018. Geomorphic Controls on Floodplain Soil Organic Carbon in the Yukon Flats, Interior Alaska, From Reach to River Basin Scales. Water Resour. Res. 54 (3), 1934-1951. https://doi.org/10.1002/2017WR022042

Liu, X., Chen, S., Yang, Z., Lin, C., Xiong, D., Lin, W., Xu, C., Chen, G., Xie, J., Li, Y., Yang, Y., 2019. Will heterotrophic soil respiration be more sensitive to warming than autotrophic respiration in subtropical forests? Eur. J. Soil Sci. 70 (3), 655-663. https://doi.org/10.1111/ejss.12758

Lloyd, J., Taylor, J., 1994. On the temperature dependence of soil respiration. Funct. Ecol., 315-323.

References
___

Lorencová, H., 2007. Decomposition dynamics and biological activity in a floodplain forest. Folia Oecologica 34 (2), 116.

Luo, Y., Zhou, X., 2006. Soil respiration and the environment, Elsevier.

Luther-Mosebach, J., Kalinski, K., Gröngröft, A., Eschenbach, A., 2018. CO2 fluxes in subtropical dryland soils—a comparison of the gradient and the closed-chamber method. J. Plant Nutr. Soil Sci. 181 (1), 21-30.

Madsen, R., Xu, L., Mcdermitt, D. (2010). *Considerations for making chamber-based soil CO2 flux measurements.* Paper presented at the Proceedings of the 19th World Congress of Soil Science: Soil solutions for a changing world, Brisbane, Australia.

Maier, M., Schack-Kirchner, H., 2014. Using the gradient method to determine soil gas flux: A review. Agric. For. Meteorol. 192, 78-95.

Marks, C. O., Yellen, B. C., Wood, S. A., Martin, E. H., Nislow, K. H., 2020. Variation in Tree Growth along Soil Formation and Microtopographic Gradients in Riparian Forests. Wetlands 40 (6), 1909-1922. https://doi.org/10.1007/s13157-020-01363-9

Martin, C. R., Zeng, N., Karion, A., Dickerson, R. R., Ren, X., Turpie, B. N., Weber, K. J., 2017. Evaluation and environmental correction of ambient CO2 measurements from a low-cost NDIR sensor. Atmospheric measurement techniques 10,

Marttila, H., Kløve, B., 2015. Spatial and temporal variation in particle size and particulate organic matter content in suspended particulate matter from peatland-dominated catchments in Finland. Hydrological Processes 29 (6), 1069-1079. https://doi.org/10.1002/hyp.10221

Mayer, S., Kölbl, A., Völkel, J., Kögel-Knabner, I., 2019. Organic matter in temperate cultivated floodplain soils: Light fractions highly contribute to subsoil organic carbon. Geoderma 337, 679-690. https://doi.org/10.1016/j.geoderma.2018.10.014

McClaugherty, C. A., Pastor, J., Aber, J. D., Melillo, J. M., 1985. Forest Litter Decomposition in Relation to Soil Nitrogen Dynamics and Litter Quality. Ecology 66 (1), 266-275. https://doi.org/10.2307/1941327

McMurray, A., Pearson, T., Casarim, F., 2017. Guidance on applying the Monte Carlo approach to uncertainty analyses in forestry and greenhouse gas accounting. Winrock International: Arlington, VA, USA, 26.

Meesenburg, H., Riek, W., Ahrends, B., Eickenscheidt, N., Grüneberg, E., Evers, J., Fortmann H., König, N., Lauer, A., Meiwes, K. J., Nagel, H.-D., Schimming, C.-G., Wellbrock, N., 2019. Soil acidification in German forest soils, in Wellbrock N., A. Bolte (Eds.), Status and Dynamics of Forests in Germany. Springer, pp. 93-121.

Melack, J. M., Engle, D. L., 2009. An organic carbon budget for an Amazon floodplain lake. Internationale Vereinigung für theoretische und angewandte Limnologie: Verhandlungen 30 (8), 1179-1182.

Mendonça Santos, M. L., Guenat, C., Bouzelboudjen, M., Golay, F., 2000. Three-dimensional GIS cartography applied to the study of the spatial variation of soil horizons in a Swiss floodplain. Geoderma 97 (3), 351-366. https://doi.org/10.1016/S0016-7061(00)00045-8

Meyer, N., Welp, G., Amelung, W., 2018. The Temperature Sensitivity (Q10) of Soil Respiration: Controlling Factors and Spatial Prediction at Regional Scale Based on Environmental Soil Classes. Global Biogeochem. Cycles 32 (2), 306-323. https://doi.org/10.1002/2017GB005644

Middelkoop, H., Daamen, K., Gellens, D., Grabs, W., Kwadijk, J. C. J., Lang, H., Parmet, B. W. A. H., Schädler, B., Schulla, J., Wilke, K., 2001. Impact of Climate Change on Hydrological Regimes and Water Resources Management in the Rhine Basin. Clim. Change 49 (1), 105-128. 10.1023/A:1010784727448

Mielnick, P. C., Dugas, W. A., 2000. Soil CO2 flux in a tallgrass prairie. Soil Biol. Biochem. 32 (2), 221-228. https://doi.org/10.1016/S0038-0717(99)00150-9

Mitra, S., Wassmann, R., Vlek, P. L., 2005. An appraisal of global wetland area and its organic carbon stock. Curr. Sci. 88 (1), 25-35.

Moore, B., Kaur, G., Motavalli, P., Zurweller, B., Svoma, B., 2018. Soil greenhouse gas emissions from agroforestry and other land uses under different moisture regimes in

lower Missouri River Floodplain soils: a laboratory approach. Agrofor. Syst. 92 (2), 335-348. https://doi.org/10.1007/s10457-017-0083-8

Myklebust, M., Hipps, L., Ryel, R. J., 2008. Comparison of eddy covariance, chamber, and gradient methods of measuring soil CO2 efflux in an annual semi-arid grass, Bromus tectorum. Agric. For. Meteorol. 148 (11), 1894-1907.

Naiman, R. J., Bechtold, J. S., Beechie, T. J., Latterell, J. J., Van Pelt, R., 2010. A process-based view of floodplain forest patterns in coastal river valleys of the Pacific Northwest. Ecosystems 13 (1), 1-31.

Patzner, M. S., Mueller, C. W., Malusova, M., Baur, M., Nikeleit, V., Scholten, T., Hoeschen, C., Byrne, J. M., Borch, T., Kappler, A., 2020. Iron mineral dissolution releases iron and associated organic carbon during permafrost thaw. Nat. Commun. 11 (1), 1-11.

Pérez-Priego, O., López-Ballesteros, A., Sánchez-Cañete, E. P., Serrano-Ortiz, P., Kutzbach, L., Domingo, F., Eugster, W., Kowalski, A. S., 2015. Analysing uncertainties in the calculation of fluxes using whole-plant chambers: random and systematic errors. Plant Soil 393 (1-2), 229-244.

Pfeiffer, E.-M., Eschenbach, A., Munch, J. C., 2017. Boden, in G. P. Brasseur, D. Jacob, S. Schuck-Zöller (Eds.), Klimawandel in Deutschland: Entwicklung, Folgen, Risiken und Perspektiven. Springer, Berlin, Heidelberg, pp. 203-213.

Pfister, L., Kwadijk, J., Musy, A., Bronstert, A., Hoffmann, L., 2004. Climate change, land use change and runoff prediction in the Rhine–Meuse basins. River Res. Appl. 20 (3), 229-241. https://doi.org/10.1002/rra.775

Pinay, G., Fabre, A., Vervier, P., Gazelle, F., 1992. Control of C, N, P distribution in soils of riparian forests. Landscape Ecol. 6 (3), 121-132.

Pumpanen, J., Kulmala, L., Lindén, A., Kolari, P., Nikinmaa, E., Hari, P., 2015. Seasonal dynamics of autotrophic respiration in boreal forest soil estimated by continuous chamber measurements. Boreal Environ. Res. 20, 637-650.

R Core Team, 2020. R: A Language and Environment for Statistical Computing. https://www.R-project.org/,

R Core Team, 2021. R: A Language and Environment for Statistical Computing. https://www.R-project.org/, access date: 25/02/2022

Rasse, D. P., Rumpel, C., Dignac, M.-F., 2005. Is soil carbon mostly root carbon? Mechanisms for a specific stabilisation. Plant Soil 269 (1), 341-356. https://doi.org/10.1007/s11104-004-0907-y

Rennert, T., Georgiadis, A., Ghong, N. P., Rinklebe, J., 2018. Compositional variety of soil organic matter in mollic floodplain-soil profiles-Also an indicator of pedogenesis. Geoderma 311, 15-24.

Richter, A., Huallacháin, D. Ó., Doyle, E., Clipson, N., Van Leeuwen, J. P., Heuvelink, G. B., Creamer, R. E., 2018. Linking diagnostic features to soil microbial biomass and respiration in agricultural grassland soil: a large-scale study in Ireland. Eur. J. Soil Sci. 69 (3), 414-428. https://doi.org/10.1111/ejss.12551

Ricker, M. C., Donohue, S. W., Stolt, M. H., Zavada, M. S., 2012. Development and application of multi-proxy indices of land use change for riparian soils in southern New England, USA. Ecol. Appl. 22 (2), 487-501. https://doi.org/10.1890/11-1640.1

Ricker, M. C., Lockaby, B. G., 2015. Soil organic carbon stocks in a large eutrophic floodplain forest of the southeastern Atlantic Coastal Plain, USA. Wetlands 35 (2), 291-301. https://doi.org/10.1007/s13157-014-0618-y

Rieger, I., Lang, F., Kleinschmit, B., Kowarik, I., Cierjacks, A., 2013. Fine root and aboveground carbon stocks in riparian forests: the roles of diking and environmental gradients. Plant Soil 370 (1-2), 497-509. https://doi.org/10.1007/s11104-013-1638-8

Rieger, I., Lang, F., Kowarik, I., Cierjacks, A., 2014. The interplay of sedimentation and carbon accretion in riparian forests. Geomorphology 214, 157-167.

Rinklebe, J., Langer, U., 2006. Microbial diversity in three floodplain soils at the Elbe River (Germany). Soil Biol. Biochem. 38 (8), 2144-2151.

Rumpel, C., Kögel-Knabner, I., 2011. Deep soil organic matter—a key but poorly understood component of terrestrial C cycle. Plant Soil 338 (1), 143-158. https://doi.org/10.1007/s11104-010-0391-5

Sander, R., 2015. Compilation of Henry's law constants (version 4.0) for water as solvent. Atmos. Chem. Phys. 15 (8), 4399-4981. 10.5194/acp-15-4399-2015

Sardinha, M., Müller, T., Schmeisky, H., Joergensen, R. G., 2003. Microbial performance in soils along a salinity gradient under acidic conditions. Applied Soil Ecology 23 (3), 237-244. https://doi.org/10.1016/S0929-1393(03)00027-1

Schaaf-Titel, S. (2019). *Water availability and soil growth conditions of roadside trees in Hamburg.* (Doctoral dissertation). Universität Hamburg, Hamburg.

Scharlemann, J. P., Tanner, E. V., Hiederer, R., Kapos, V., 2014. Global soil carbon: understanding and managing the largest terrestrial carbon pool. Carbon Management 5 (1), 81-91.

Schindler, M., Donath, T. W., Terwei, A., Ludewig, K., 2021. Effects of flooding duration on the occurrence of three hardwood floodplain forest species inside and outside a dike relocation area at the Elbe River. Int. Rev. Hydrobiol., https://doi.org/10.1002/iroh.202002078

Schindler, T., Mander, Ü., Machacova, K., Espenberg, M., Krasnov, D., Escuer-Gatius, J., Veber, G., Pärn, J., Soosaar, K., 2020. Short-term flooding increases CH 4 and N 2 O emissions from trees in a riparian forest soil-stem continuum. Sci. Rep. 10 (1), 1-10.

Scholz, M., Mehl, D., Schulz-Zunkel, C., Kasperidus, H. D., Born, W., Henle, K. (Eds.), 2012. Ökosystemfunktionen von Flussauen: Analyse und Bewertung von Hochwasserretention, Nährstoffrückhalt, Kohlenstoffvorrat, Treibhausgasemissionen und Habitatfunktion. Münster: BfN-Schriftenvertrieb im Landwirtschaftsverlag.

Schröder, P., 1988. Aufbau und Untergliederung des Niederterrassenkörpers der Unterelbe. Mitteilungen aus dem Geologischen Institut der Universität Hannover 27, 1-120.

Schrumpf, M., Kaiser, K., Guggenberger, G., Persson, T., Kögel-Knabner, I., Schulze, E.-D., 2013. Storage and stability of organic carbon in soils as related to depth, occlusion within aggregates, and attachment to minerals. Biogeosciences 10, 1675-1691. https://doi.org/10.5194/bg-10-1675-2013

Schwartz, R., Gröngröft, A., Miehlich, G., 2003. Pore Water Composition as Device for the Detection of Origin and Flow Direction of Soil Water in Alluvial Soils of the Middle Elbe River. Acta Hydrochim. Hydrobiol. 31 (4-5), 423-435. https://doi.org/10.1002/aheh.200300498

Shupe, H. A., Hartmann, T., Scholz, M., Jensen, K., Ludewig, K., 2021. Carbon Stocks of Hardwood Floodplain Forests along the Middle Elbe: The Influence of Forest Age, Structure, Species, and Hydrological Conditions. Water 13 (5), 670. https://doi.org/10.3390/w13050670

Sieczko, A., Peduzzi, P., 2014. Origin, enzymatic response and fate of dissolved organic matter during flood and non-flood conditions in a river-floodplain system of the Danube (Austria). Aquat. Sci. 76 (1), 115-129. https://doi.org/10.1007/s00027-013-0318-3

Skjemstad, J. O., Janik, L. J., Head, M. J., McClure, S. G., 1993. High energy ultraviolet photo-oxidation: a novel technique for studying physically protected organic matter in clay- and silt-sized aggregates. J. Soil Sci. 44 (3), 485-499. https://doi.org/10.1111/j.1365-2389.1993.tb00471.x

Sollins, P., Homann, P., Caldwell, B. A., 1996. Stabilization and destabilization of soil organic matter: mechanisms and controls. Geoderma 74 (1), 65-105. https://doi.org/10.1016/S0016-7061(96)00036-5

Song, X., Zhu, Y., Chen, W., 2021. Dynamics of the soil respiration response to soil reclamation in a coastal wetland. Sci. Rep. 11 (1), 2911. 10.1038/s41598-021-82376-0

Steinicke, C., Köhler, M., Ahrends, B., Wellbrock, N., Evers, J., Hilbrig, L., Meesenburg, H., 2016. Pedotransferfunktionen zur Abschätzung der Trockenrohdichte von Waldböden in Deutschland. Waldökologie, Landschaftsforschung und Naturschutz 16, 95–107.

Stoyan, H., De-Polli, H., Böhm, S., Robertson, G. P., Paul, E. A., 2000. Spatial heterogeneity of soil respiration and related properties at the plant scale. Plant Soil 222 (1), 203-214. 10.1023/A:1004757405147

Sutfin, N. A., Wohl, E. E., Dwire, K. A., 2016. Banking carbon: a review of organic carbon storage and physical factors influencing retention in floodplains and riparian ecosystems. Earth Surf. Process. Landf. 41 (1), 38-60.

Swinnen, W., Daniëls, T., Maurer, E., Broothaerts, N., Verstraeten, G., 2020. Geomorphic controls on floodplain sediment and soil organic carbon storage in a Scottish mountain river. Earth Surf. Process. Landf. 45 (1), 207-223. https://doi.org/10.1002/esp.4729

Tamminen, P., Starr, M., 1994. Bulk density of forested mineral soils.

Tang, J., Baldocchi, D. D., 2005. Spatial–temporal variation in soil respiration in an oak–grass savanna ecosystem in California and its partitioning into autotrophic and heterotrophic components. Biogeochemistry 73 (1), 183-207. 10.1007/s10533-004-5889-6

Tang, X., Pei, X., Lei, N., Luo, X., Liu, L., Shi, L., Chen, G., Liang, J., 2020. Global patterns of soil autotrophic respiration and its relation to climate, soil and vegetation characteristics. Geoderma 369, 114339. https://doi.org/10.1016/j.geoderma.2020.114339

Valett, H. M., Baker, M. A., Morrice, J. A., Crawford, C. S., Molles Jr, M. C., Dahm, C. N., Moyer, D. L., Thibault, J. R., Ellis, L. M., 2005. Biogechemical and metabolic responses to the flood pulse in a semiarid floodplain. Ecology 86 (1), 220-234. https://doi.org/10.1890/03-4091

Van Den Heuvel, R. N., Bakker, S. E., Jetten, M. S. M., Hefting, M. M., 2011. Decreased N2O reduction by low soil pH causes high N2O emissions in a riparian ecosystem. Geobiology 9 (3), 294-300. https://doi.org/10.1111/j.1472-4669.2011.00276.x

Van Rossum, G., Drake, F. L., 2009. Python 3 Reference Manual, CreateSpace, Scotts Valley, CA.

Viret, F., Grand, S., 2019. Combined Size and Density Fractionation of Soils for Investigations of Organo-Mineral Interactions. JoVE (144), e58927. https://doi.org/doi:10.3791/58927

Wagai, R., Mayer, L. M., Kitayama, K., 2009. Nature of the "occluded" low-density fraction in soil organic matter studies: a critical review. Soil Sci. Plant Nutr. 55 (1), 13-25.

Wang, Y., Wang, H., He, J.-S., Feng, X., 2017. Iron-mediated soil carbon response to water-table decline in an alpine wetland. Nat. Commun. 8, https://doi.org/10.1038/ncomms15972

Wardle, D. A., Ghani, A., 1995. A critique of the microbial metabolic quotient (qCO2) as a bioindicator of disturbance and ecosystem development. Soil Biol. Biochem. 27 (12), 1601-1610. https://doi.org/10.1016/0038-0717(95)00093-T

Weber, A., Hatz, M., 2020. Hyd1d - Algorithms to compute 1D water levels along German federal waterways Elbe and Rhine. Journal of Ecohydraulics,

Weber, A., Rosenzweig, S., 2020. Hydflood - algorythms to compute flood extent and duration along german federal waterways elbe and rhine. Journal of Ecohydraulics,

Webster, K. L., Creed, I. F., Skowronski, M. D., Kaheil, Y. H., 2009. Comparison of the Performance of Statistical Models that Predict Soil Respiration from Forests. Soil Sci. Soc. Am. J. 73 (4), 1157-1167. https://doi.org/10.2136/sssaj2008.0310

Wei, L., Ge, T., Zhu, Z., Ye, R., Penuelas, J., Li, Y., Lynn, T. M., Jones, D. L., Wu, J., Kuzyakov, Y., 2022. Paddy soils have a much higher microbial biomass content than upland soils: A review of the origin, mechanisms, and drivers. Agric., Ecosyst. Environ. 326, 107798.

Wellbrock, N., Grüneberg, E., Riedel, T., Polley, H., 2017. Carbon stocks in tree biomass and soils of German forests. Central European Forestry Journal 63 (2-3), 105-112.

Welles, J. M., Demetriades-Shah, T. H., McDermitt, D. K., 2001. Considerations for measuring ground CO2 effluxes with chambers. Chem. Geol. 177 (1), 3-13. https://doi.org/10.1016/S0009-2541(00)00388-0

Wigginton, J. D., Lockaby, B. G., Trettin, C. C., 2000. Soil organic matter formation and sequestration across a forested floodplain chronosequence. Ecol. Eng. 15, 141-155.

Wildung, R. E., Garland, T. R., Buschbom, R. L., 1975. The interdependent effects of soil temperature and water content on soil respiration rate and plant root decomposition in

arid grassland soils. Soil Biol. Biochem. 7 (6), 373-378. https://doi.org/10.1016/0038-0717(75)90052-8

Wilson, J. S., Baldwin, D. S., Rees, G. N., Wilson, B. P., 2011. The effects of short-term inundation on carbon dynamics, microbial community structure and microbial activity in floodplain soil. River Res. Appl. 27 (2), 213-225. https://doi.org/10.1002/rra.1352

Xu, M., Qi, Y., 2001. Soil-surface CO_2 efflux and its spatial and temporal variations in a young ponderosa pine plantation in northern California. Global Change Biol. 7 (6), 667-677. https://doi.org/10.1046/j.1354-1013.2001.00435.x

Yasuda, T., Yonemura, S., Tani, A., 2012. Comparison of the characteristics of small commercial NDIR CO_2 sensor models and development of a portable CO_2 measurement device. Sensors 12 (3), 3641-3655.

Yin, S., Bai, J., Wang, W., Zhang, G., Jia, J., Cui, B., Liu, X., 2019. Effects of soil moisture on carbon mineralization in floodplain wetlands with different flooding frequencies. Journal of Hydrology 574, 1074-1084. https://doi.org/10.1016/j.jhydrol.2019.05.007

Yoon, T. K., Noh, N. J., Han, S., Lee, J., Son, Y., 2014. Soil moisture effects on leaf litter decomposition and soil carbon dioxide efflux in wetland and upland forests. Soil Sci. Soc. Am. J. 78 (5), 1804-1816. https://doi.org/10.2136/sssaj2014.03.0094

Yuste, J. C., Janssens, I. A., Carrara, A., Ceulemans, R., 2004. Annual Q10 of soil respiration reflects plant phenological patterns as well as temperature sensitivity. Global Change Biol. 10 (2), 161-169. https://doi.org/10.1111/j.1529-8817.2003.00727.x

Zehetner, F., Lair, G. J., Gerzabek, M. H., 2009. Rapid carbon accretion and organic matter pool stabilization in riverine floodplain soils. Global Biogeochem. Cycles 23 (4), https://doi.org/10.1029/2009gb003481

Zhang, H., Zhou, Z., 2018. Recalcitrant carbon controls the magnitude of soil organic matter mineralization in temperate forests of northern China. Forest Ecosystems 5 (1), 17. 10.1186/s40663-018-0137-z

Zhang, Q., Katul, G. G., Oren, R., Daly, E., Manzoni, S., Yang, D., 2015. The hysteresis response of soil CO_2 concentration and soil respiration to soil temperature. J. Geophys. Res. Biogeosci. 120 (8), 1605-1618.

Zhou, W., Han, G., Liu, M., Li, X., 2019. Effects of soil pH and texture on soil carbon and nitrogen in soil profiles under different land uses in Mun River Basin, Northeast Thailand. PeerJ 7:e7880, https://doi.org/10.7717/peerj.7880

Danksagung

Während meiner Doktorarbeit gab es schöne und schwierige Phasen. Ich möchte mich hiermit bei den Menschen bedanken, die mich in diesen Phasen teilnehmend, professionell, sachlich und emotional begleitet haben.

Zuerst möchte ich mich bei meiner Frau, Hanne, bedanken. Durch die Corona-Pandemie war Hanne nicht nur nach Feierabend für mich da, sondern hat mich auch, Homeoffice bedingt, den gesamten Arbeitsalltag begleitet. Ich möchte mich für ihr Aufbauen, in emotionalen Tiefpunkten, aber auch bei sachlichen Fragen, bedanken. Wir sind das perfekte Team und das hat sich auch während der gesamten Zeit, zusammen mit unserer Tochter Liv, gezeigt. Vielen Dank dafür. Ich liebe dich.

Ein ganz großer Dank geht an meine Vorgesetzte, Annette Eschenbach. In jeder Phase meiner Doktorarbeit hat Annette mich begleitet und auch in schwierigen Phasen ihre Zeit aufgewendet, um mich zu beraten und komplexe Ergebnisse zu diskutieren. Besonders möchte ich mich auch für ihre Unterstützung und Beratung meiner weiteren beruflichen Laufbahn bedanken. Mit Annette war die Beziehung nicht nur auf einer professionellen Ebene, sondern auch auf einer sehr empathisch kollegialen, vertrauten. Dafür bedanke ich mich und hoffe, dass wir uns in unseren Leben weiterhin oft begegnen werden.

Ich möchte mich bei Joscha Becker für die ständige Bereitschaft, meine Studien von Anfang bis zum Schluss zu begleiten, bedanken. Obwohl Joscha erst seit 2019 in meiner Arbeitsgruppe ist, hat sich eine sehr enge und gute Zusammenarbeit gebildet.

Ich möchte mich bei meiner Kollegin Lizeth Vásconez bedanken, mit der ich von Anfang an die meiste Zeit verbracht habe. Ich werde nie die ersten beiden Jahre vergessen, in denen wir viel Zeit in der Elbauenstation Pevestorf verbracht haben. Diese Zeit hat uns zusammengeschweißt.

Ich bedanke mich bei meinem Zweitgutachter Lars Kutzbach für Konzeptionierung und Diskussion meiner Ergebnisse. Lars hat vor dieser Doktorarbeit meinen Weg für die

Wissenschaft geebnet und ich bin froh, dass wir auch während dieser Zeit zusammengearbeitet haben.

Weiterhin bedanke ich mich bei meinen Kollegen Alexander Gröngröft und Volker Kleinschmidt, die mich immer mit wunderbaren Ideen und offenem Ohr für Fragen voran brachten.

Ich bedanke mich bei Deborah Harms, Sumita Rui und Birgit Grabellus für die stetige Unterstützung im Labor. Für weitere Unterstützung im Labor aber auch im Feld bedanke ich mich ebenfalls bei Niklas Pollex, Jana Bräuner, Tiffanie Sarino, Christina Moor, Simone Koller, Jessica Hamm, Lewis Sauerland und vielen weiteren studentischen Hilfskräften und Kolleg:innen aus dem Institut, die ich bereits dankend in meinen Publikationen erwähnt habe.

Ich bedanke mich bei meinen MediAN-Projekt-Kolleg:innen Heather Shupe, Anastasia Leonova, Kristin Ludewig, Simon Thomsen, Timo Hartmann, Nicole Scheunemann, David Russel, Sonja Biwer, Mathias Scholz, Meike Kleinwächter, Paula Höpfner, Christoph Reisdorff und Kai Jensen, für die sympathische und professionelle Zusammenarbeit. Weiterhin bedanke ich mich bei den Kolleg:innen Miriam Fuß, Mathias Spieckermann, David Holl, Kira Kalinski, Alexander Schütt, u. A. für tolle Mittagspausen und Feierabend-Bierchen.

Zum Schluss möchte ich mich bei meiner weiteren Familie und vielen Freund:innen bedanken, da sie mich stetig begleitet und motiviert haben.